ORNL/TM-2020/1829

# Review of Advanced Manufacturing Techniques and Qualification Processes for Light-Water Reactors: Laser-Directed Energy Deposition Additive Manufacturing


James Haley
Kevin Faraone
Brian Gibson
Joseph Simpson
Ryan Dehoff

**September 2021**

OAK RIDGE National Laboratory

ORNL IS MANAGED BY UT-BATTELLE LLC FOR THE US DEPARTMENT OF ENERGY

**ORNL/TM-2020/1829**

MANUFACTURING DEMONSTRATION FACILITY
Materials Science and Technology Division

# REVIEW OF ADVANCED MANUFACTURING TECHNIQUES AND QUALIFICATION PROCESSES FOR LIGHT WATER REACTORS: LASER-DIRECTED ENERGY DEPOSITION ADDITIVE MANUFACTURING

James Haley
Kevin Faraone
Brian Gibson
Joseph Simpson
Ryan Dehoff

September 2021

Prepared by
OAK RIDGE NATIONAL LABORATORY
Oak Ridge, TN 37831-6283
managed by
UT-BATTELLE, LLC
for the
US DEPARTMENT OF ENERGY
under contract DE-AC05-00OR22725

## CONTENTS

## LIST OF FIGURES

## LIST OF TABLES

## ABBREVIATIONS

| | |
|---|---|
| 2D | two-dimensional |
| 3D | three-dimensional |
| AAMI | Association for the Advancement of Medical Instrumentation |
| AI | artificial intelligence |
| AM | additive manufacturing |
| AMM | advanced manufacturing method |
| AMSC | Additive Manufacturing Standardization Collaborative |
| AMT | advanced manufacturing technology |
| AN | annealed |
| ANSI | American National Standards Institute |
| ASME | American Society of Mechanical Engineers |
| ASTM | ASTM International (formerly American Society for Testing and Materials) |
| AWS | American Welding Society |
| CAD | computer-aided design |
| CAM | computer-aided manufacturing |
| CASE | criticality, achievability, scope, effect |
| CCD | charged coupled device |
| CFD | computational fluid dynamics |
| CNC | computer numerical control |
| CT | computed tomography |
| DAS | dendrite arm spacing |
| DED | directed energy deposition |
| DICOM | Digital Imaging and Communications in Medicine |
| DOE | US Department of Energy |
| EBM | electron beam melting |
| EBSD | electron backscatter diffraction |
| EBW | electron beam–welded |
| EDM | electrical discharge machining |
| EDS | energy-dispersive x-ray spectroscopy |
| FAIR | findable, accessible, interoperable, and reusable |
| FEA | finite element analysis |
| FGM | functionally graded material |
| FVM | finite volume method |
| GA | gas atomization |
| GE | General Electric |
| GND | geometrically necessary dislocation |
| HAZ | heat-affected zone |
| HIP | hot isostatic pressing |
| HT | heat-treated |
| HV | Vickers hardness scale |
| IASCC | irradiation-assisted stress corrosion cracking |
| IEEE | Institute for Electronic and Electronics Engineers |
| IPC | Association Connecting Electronics Industries |
| ISO | International Organization for Standardization |
| LED | linear energy density |
| LENS | laser-engineered net shaping |
| L-DED | laser-directed energy deposition |
| LMD-w | laser metal deposition with wire |

| | |
|---|---|
| LPBF | laser powder bed fusion |
| LP-DED | laser powder-directed energy deposition |
| LWAM | laser wire additive manufacturing |
| LW-DED | laser wire-directed energy deposition |
| LWR | light water reactor |
| mBAAM | metal Big Area Additive Manufacturing |
| MIG | metal inert gas |
| MITA | Medical Imaging & Technology Alliance |
| μLMWD | micro laser metal wire deposition |
| MPIF | Metal Powder Industries Federation |
| NASA | National Aeronautics and Space Administration |
| NC | numerical control |
| NDE | nondestructive examination |
| Nd:YAG | neodymium-doped yttrium aluminum garnet |
| NEMA | National Electrical Manufacturers Association |
| NIST | National Institute of Standards and Technology |
| NPP | nuclear power plant |
| NRC | US Nuclear Regulatory Commission |
| ODS | oxide-dispersion-strengthened |
| ORNL | Oak Ridge National Laboratory |
| PBF | powder bed fusion |
| PID | proportional–integral–derivative |
| PM-HIP | powder metallurgically based hot isostatic pressing |
| PREP | plasma rotating electrode process |
| PSM | primary solidification mode |
| QA | quality assurance |
| QC | quality control |
| SCC | stress corrosion cracking |
| SEM | scanning electron microscopy |
| SH | strain hardened |
| STEM | scanning transmission electron microscopy |
| STL | stereolithography |
| TEM | transmission electron microscopy |
| UTS | ultimate tensile strength |
| VED | volumetric energy density |
| YS | yield strength |

## EXECUTIVE SUMMARY

Additive manufacturing (AM), specifically laser-directed energy deposition (L-DED), is being explored by academic, industrial, and regulatory entities for technical feasibility, cost effectiveness, and safety for fabricating components to be used in nuclear power plant (NPP) applications. L-DED can be used to fabricate complex geometries, and in some applications, assemblies with tens-to-hundreds of parts can be reduced to a single, as-fabricated component. In addition to providing geometric design freedom, L-DED allows for an advanced degree of composition design freedom, as the feedstock material can be mixed dynamically to locally tune portions of a particular component. However, these high degrees of design freedom create a corresponding burden to characterize and control material properties.

In general, L-DED is a repeatable process, with material properties equivalent, if not superior, to conventional manufacturing, if the appropriate calibration, technician training, and feedstock tracking processes are applied. However, quantitative data on part-to-part variability in a production setting, powder or wire feedstock lot-to-lot variability, and machine-to-machine variability are not readily available because of corporate confidentiality. Academic studies have attempted to address the knowledge gap in property variability, but these efforts are often impeded by incomplete reporting, narrow focus, and lack of replicated specimens. As a result, reported material property values for L-DED components vary widely in common measurements such as yield strength (YS) and ultimate tensile strength (UTS). For example, there may only be a few published journal articles on specific properties such as irradiation-assisted stress corrosion cracking (IASCC) and crack growth rates.

Some of the codes and standards indirectly supporting L-DED are well established (e.g., wire conformance, powder measurement, laser calibration). More codes and standards are targeted toward the similar technology of laser powder bed fusion (LPBF); however, the subject matter in several documents overlaps for metal additive manufacturing (AM) in general (e.g., destructive and nondestructive characterization), and standards or subsections of standards are being developed specifically for L-DED. Published codes and standards vary widely in quality. The National Aeronautics and Space Administration (NASA) published a standard (MSFC-STD-3716 [1]) which provides a statistically rigorous framework for determining material properties and design values in the context of an LPBF production setting. American Welding Society (AWS) specification D20.1/D20.1M [2] and American Society for Testing and Materials (ASTM) International standard 52904 on LPBF require that material property data be collected from simplified geometries such as cylinders and bars. However, it is the authors’ recommendation that material properties not be initially evaluated from simplified geometries, but instead, from sectioned, end-use geometry components whenever possible. Material properties are a function of geometry in L-DED, and the use of simplified geometries may give nonrepresentative results and encourage erroneous confidence. Because of the breadth of material chemistries and processing parameters used within L-DED 316L, as well as the breadth of environmental considerations associated with NPP use, data to predict all the potential effects associated with NPP applications are inadequate. Some codes and standards details must be resolved empirically as production data become available, and additional studies on the microstructure and welding of L-DED 316L are important in this regard.

Early studies indicate that L-DED 316L can offer equivalent or superior performance compared to conventional 316L with the appropriate processing, and it can also improve cost effectiveness and reduce assembly complexity. Compared to LPBF, L-DED has the comparative advantages of higher deposition speed, larger possible build volumes, and the option for direct integration with subtractive machining tools; however, L-DED minimum feature size resolution and microstructures are coarser than those of LPBF. The US Nuclear Regulatory Commission (NRC) has developed a companion document to this report (ML21292A188) that (1) provides context regarding the gaps identified herein from a regulatory

perspective and (2) highlights key technical information related to L-DED fabricated components in NPPs.

# 1. INTRODUCTION

Nuclear energy supplies approximately 18% of the US electrical power supply and the majority of carbon-free electricity [3]. Nuclear energy is a critical component of reliable domestically sourced power. To lower construction and maintenance costs associated with nuclear energy, innovations are being considered [3] [4], and multiple advanced manufacturing methods (AMMs) are being evaluated by academic, industrial, and regulatory bodies for cost effectiveness, technical feasibility, and safety [4]. The US Nuclear Regulatory Commission (NRC) is the federal agency responsible for regulating nuclear power plant (NPP) operation and ensuring public safety. Therefore, the NRC has a vested interest in surveying current scientific literature on AMMs. The objective of this report is to document the current state of a specific AMM—laser-directed energy deposition (L-DED)—with respect to material, microstructures, and properties relative to conventional manufacturing, technical gaps in ensuring repeatability, and standards and regulatory gaps in machine calibration, minimum requirements, and inspection practices. This report is motivated by the potential use of L-DED in fabricating components for new NPPs, as well as replacing components that are no longer commercially available for use in existing NPPs. The NRC has developed a companion document to this report (ML21292A188) that (1) provides context to the gaps identified herein from a regulatory perspective, and (2) highlights key technical information related to L-DED fabricated components in NPPs.

# 2. LASER-DIRECTED ENERGY DEPOSITION TECHNICAL REVIEW

Multiple additive manufacturing (AM) technologies have been developed in recent years and are poised to fundamentally alter the way components are designed and manufactured. AM is a process for producing components through layer-by-layer deposition of material. This is in direct contrast to conventional subtractive manufacturing. AM is progressing rapidly from its origins of rapid prototyping with polymers to scale production of metal components. Boeing has reduced the weight of the 787 Dreamliner with DED using plasma arc and titanium wire [5], and GE has fabricated fuel injection nozzles using laser powder bed fusion (LPBF) AM technologies [6]. The most common form of AM is powder bed fabrication, consisting of LPBF and electron beam melting (EBM) [7]–[9]. Key AM technologies that can be used to fabricate nuclear reactor components are LPBF and DED, including L-DED using powder or wire as feedstock. These technologies are not currently in widespread use for fabrication of NPP service components, but they have the potential to drastically reduce fabrication costs and timelines, to combine multiple systems and assembled components into single parts, and to increase safety and performance by tailoring local material properties and redesigning geometries for optimal performance. Terminology within the L-DED industry is highly unstructured and frequently trademarked; Table 1 contains a list of common terminology for the family of DED technologies. Throughout this report, the term *L-DED* is used to discuss *laser-directed energy deposition* processes, whereas *laser powder directed energy deposition* (LP-DED) refers to L-DED with blown powder deposition, and *laser wire directed energy deposition* (LW-DED) refers to L-DED with wire fed consumables.

**Table 1. Common synonyms for laser-directed energy deposition**

| Terminology | Corporate owner and/or user |
|---|---|
| Direct/laser metal deposition (DMD, LMD, DLD) | - |
| Laser metal deposition with wire (LMD-w) | - |
| Laser wire additive manufacturing (LWAM) | GKN Aerospace |
| Metal big area additive manufacturing (mBAAM) | - |
| Laser-directed energy deposition (L-DED) | - |
| Laser powder-directed energy deposition (LP-DED) | - |
| Laser wire-directed energy deposition with Wire (LW-DED) | - |
| Laser freeform manufacturing technology (LFMT) | - |
| Laser-engineered net shaping (LENS) | Optomec |
| Laser freeform fabrication ($LF^3$) | - |
| Laser cladding* | - |

*Although technologically similar, the term *cladding* is commonly used for applications that deposit a single layer of a different material to prevent wear and/or corrosion or to provide other performance benefits.

The review provided herein represents the current state of literature on the selected AM technology of L-DED, with an emphasis on quality control, material performance, repeatability, and component performance compared to conventionally manufactured materials. Research and standards published by government entities such as the National Institute of Standards and Technology (NIST) and the US Department of Energy (DOE) are included where applicable. In light of the rapid pace of advancements in AM and associated industries, literature must be reviewed frequently, and new knowledge must be integrated often. AM presents unique challenges for certification of NPP applications, such as anisotropic material properties, porosity, underdeveloped process control feedback systems, and reproducibility. This review begins with an overview of the selected AM technology of L-DED, with specific considerations for LP-DED and LW-DED, followed by a systematic review of literature to detail the fabrication process and difficulties when consistently fabricating fully dense, geometrically accurate components with repeatable material properties.

## 2.1 MANUFACTURING METHOD OVERVIEW

L-DED fabrication is accomplished by injecting feedstock material into a weld bead generated from a laser moving through a sequence of programmed scanning motions. This process sequentially adds material in the correct positions to create the specified geometry. As shown in Figure 1, the process begins with the user creating a 3-dimensional (3D) computer-aided design (CAD) model of the component in an engineering design software package such as Solidworks, AutoDesk, or AutoCad. The CAD model is then loaded into a separate computer-aided machining (CAM) software package specific for L-DED processing, this process is commonly referred to as *slicing*.

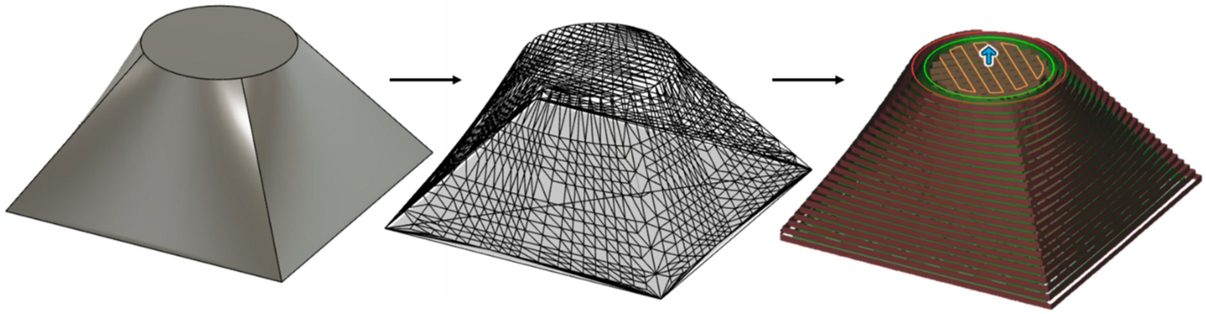

**Figure 1. AM software preparation workflow, from computer design to a triangulated mesh representation, to a sliced sequence of toolpath vectors (sample generated using Autodesk Fusion 360®).**

Depending on the component and machine specifics, slicing can be performed in one of two ways—with 3 axis motions, as done in the process used for LPBF, or with 5+ axis motions that allow for control of tool orientation relative to the built component, thus providing more design freedom. In 3-axis slicing, the original CAD model is separated into multiple layers that are vertically stacked and manufactured in sequential, uniformly spaced layers, as illustrated in **Error! Reference source not found.** [10]. Each layer is then treated as a 2D area which can be filled with a sequence of tool motions or *toolpath*, by tracing the outline of the area and then rastering the laser back and forth over the body of the area in a serpentine pattern. This slicing process is typically not proprietary and can be implemented using open-source and free software. The process is very similar across L-DED machine manufacturers.

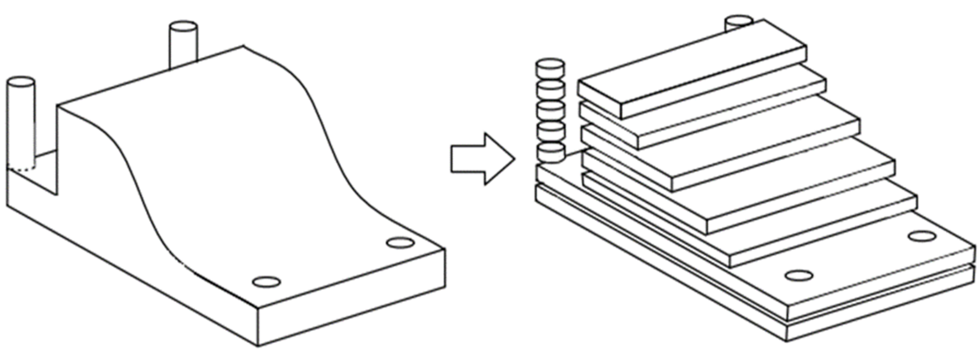

**Figure 2. Example of 3-axis slicing before (left) and after (right) slicing** [11].

In 5+ axis slicing, it is programmatically much more complicated to construct the toolpath. Both the tool position and the angle through time must be defined, and the slice surface can be reoriented. The CAD geometry can be sliced into sequential layers as shown in **Error! Reference source not found.**; however, the planes can be oriented in any direction, which is commonly referred to in the milling industry as *3+2 axis*. More complicated geometries can split the built parts into multiple subparts with different layer orientations. In even more complicated geometries, the slice surfaces are not even necessarily planar; instead, they follow the contours of the desired CAD geometry to produce desirable deposition orientations. Several commercial CAM software packages offer 5+ axis AM toolpath generation—such as Autodesk Powermill, Openmind Hypermill, and GibbsCAM. All of these software packages were originally built for advanced multiaxis subtractive machining and have been modified for the specific requirements of L-DED.

Once a CAD model has been sliced in a CAM software and the toolpath has been generated, the file is transferred to the L-DED controller, and the machine is prepared. The L-DED machine setup includes cleaning the machine, installing a substrate upon which the component is fabricated, and loading sieved metal powder for powder-based DED equipment and wire for wire-based DED equipment. Substrates can be either simple metal plates or previously fabricated components that are being added to or repaired. Figure 3 [11] provides a system schematic representative of many powder-based L-DED machines. For powder-based machines, powder is dispensed into a carrier gas stream which transports it through tubes to the deposition head. The powder is then sprayed through a nozzle toward the substrate, and the laser is then activated, forming the weld pool. The nozzle and laser delivery system, referred to as the *deposition head*, is then moved through the programmed toolpath to weld on the feedstock material and to fabricate the component. For wire-based systems, the deposition head includes a wire-feeder system which properly locates and orients the wire so that it feeds into the weld pool. The weld pool is formed on the substrate by the laser at a prescribed and often variable feed-rate: one of the primary process variables for wire-based L-DED. Figure 3 also includes a schematic of a representative wire-based L-DED process. The DED and LPBF processes have numerous advantages and disadvantages, as presented in Table 2.

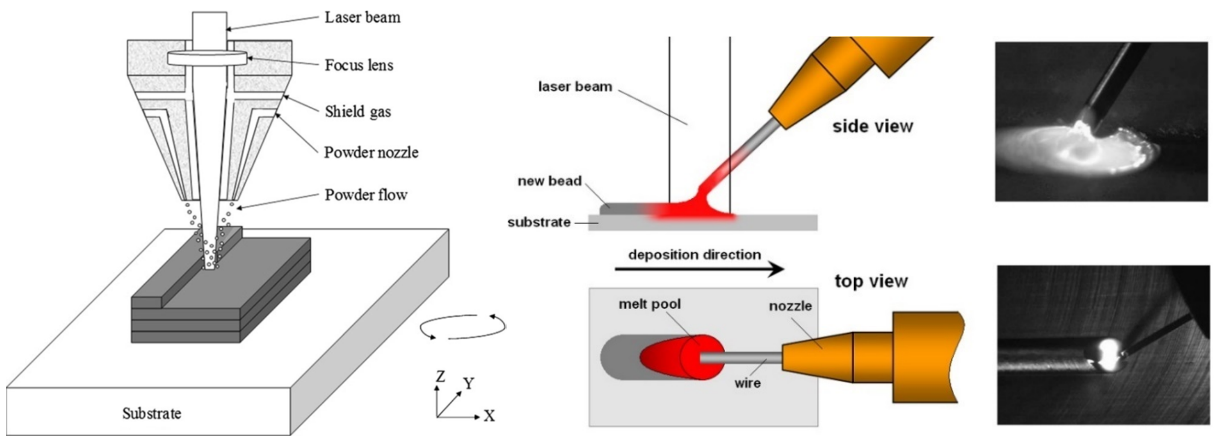


**Figure 3. Schematics of L-DED deposition setups common to many machines; Powder-based process (left) [11] and wire-based process (right).** [Image courtesy of GKN Aerospace].

While the term *directed energy deposition* is frequently intended to refer to a single technology, the method is better described as a suite of related AM methods share the common features of having a point heat source that forms a weld pool which is scanned relative to a substrate while material is continuously fed into the melt pool. This can be achieved with a laser, an electron beam, or a plasma welding arc, and the feedstock material can be either a sprayed powder or a wire. Some of the differences in machines made with these different techniques are summarized in Table 2. Note that the values presented in Table 2 primarily represent the more common design choices, but many systems are more specialized in order to remove certain limitations or to increase performance. For comparison purposes, electron beam with wire (e beam wire), Arc-DED, and LPBF are included in Table 2. E beam wire additions have been used to produce DED components, representing a process similar to L-DED; however e beam wire requires a vacuum chamber to operate the electron beam source. Arc-DED is a wire deposition process using traditional arc welding sources such as gas metal arc, plasma arc, or gas tungsten arc heat sources.

LP-DED and LW-DED are discussed in this report. In general, LP-DED has been reported more extensively in the context of AM and likewise is primarily discussed in this report. L-DED covers a wide range of deposition rates, as shown in Table 2, ranging from as low as 0.1 kg/hr for powder and up to 10 kg/hr using wire. Smaller, more complex items may be benefited through the use of powder, and larger, less complex parts may benefit from using wire. Substantial overlap between the materials, heat input, build volume, and melt pool size exist and are discussed in general as L-DED, and when necessary, they are specified for LP-DED or LW-DED.

DED is often utilized for fabricating new components; however, numerous variations and potential applications exist, such as alternating DED material deposition with machining (hybrid AM), building on top of components fabricated by other AM methods, or repairing existing components. These applications are mentioned for the reader's awareness, but they are outside the scope of this document and therefore are not described further.

**Table 2. Comparison of common DED methods, with comparison to LPBF for reference**

| Feature | Laser Powder | Laser Wire | E Beam Wire | Arc-DED | LPBF | Comment |
|---|---|---|---|---|---|---|
| Deposition rate | 0.1–5 kg/hr | 1–10 kg/hr | 1–10 kg/hr | 5–10 kg/hr | 10–100 g/hr | Typical deposition rates reported by process |
| Deposition volume linear scale | 0.3–1.5 m | 0.5–2 m | 1–5+ m | 1–5+ m | 0.1–0.5 m | Larger build dimensions trade off with tool rigidity (accuracy/acceleration). |
| Melt pool size/ Minimum feature size | ~ 500 µm – 1 cm | ~2 mm – 3 cm | ~2 mm – 3 cm | ~1–3 cm | ~100 µm | Grain structure and properties are highly affected by choice of melt pool size. |
| Feedstock efficiency | 30–90+% | >95% | >95% | >95% | >50% (with recycling) | Powder efficiency depends on melt size. Wire systems lose minor amounts of feedstock |
| Feedstock cost | Med-high | Low-med | Low-med | Low-med | Med-high | |
| Atmosphere options | Glovebox, flowing shield gas | Glovebox, flowing shield gas | Vacuum | Glovebox, flowing shield gas | Glovebox | Flowing gas is more economical, but imperfectly shields the melt pool |
| Surface roughness | Medium | Low-med. | Low-med. | High | Low | Roughness is due to layer line ‘scalloping’, and is attached powder or spatter/oxidation |
| Energy source to feedstock orientations | Coaxial, 1, 3, or 4 nozzles | Off axis | Off axis | Combined | Not applicable | Omnidirectionality of toolpath direction eases programming and process control |
| Resistive energy injection | Not applicable | Available | Not applicable | Available | Not applicable | To offset high required beam energies, Joule heating can preheat wire feedstock |
| Hybrid CNC milling integration | Available | Available | Not available | Available | Not applicable | |
| Graded material deposition | Implemented, 5+ powder compositions | Possible | Possible | Not Applicable | Not applicable | Graded material deposition allows for smoother compositional transitions between components. |
| Other limitations | | | Larger interaction volume allows higher powers | Fume generation can be substantial | More tolerant of overhanging geometry (45°) | |
| Capital expense | Med | Med | High | Low | High | Price varies greatly based on features, but E-Beam requires a vacuum chamber, and laser systems require special optics. |

*Values chosen to represent common capabilities, and not specific manufacturer designs or ultimate technology limitations.*

### 2.1.1 Feedstock Choice and Characterization

Feedstock must be evaluated and carefully selected based on several factors in both LP-DED and LW-DED. For powders, these factors include elemental composition, flowability, internal porosity, particle geometry, size distribution, and surface features to minimize or eliminate fabrication issues such as uneven powder spreading and feedstock-induced porosity [12]. Many powder manufacturers publish information on the sieve sizes used in production or the mean particle size. However, the D10, D50, and D90 (particle sizes at which 10, 50, and 90% of particles are of equal or lesser size, respectively) of a particle size distribution should be documented. Two methods of determining powder characteristics are *scanning electron microscopy* (SEM) and *energy dispersive x-ray spectroscopy* (EDS) [13]. SEM can be used to image dispersed samples of metal powder, typically against highly contrasting, conductive backgrounds such as carbon, to identify individual particles and particle size distribution. SEM can simultaneously provide qualitative information on particle shape and the presence of satellites. EDS is a well-established method for determining rough elemental composition, and if particles are sufficiently well dispersed during imaging, then it is possible to determine the composition of the overall sample and of individual particles. Analysis of powder characteristics and their measurement are described in the literature [14], [15].

Feedstock wire for LW-DED must be evaluated and selected with the same care as that used when selecting powders. In general, there are fewer metrics for characterizing the quality of feedstock wire compared to powders, and there is a long-established history of ensuring that welding consumables conform to applicable standards for industrial welding applications. The wire chemistry and processing path must be tightly controlled, and for LW-DED applications, it is common practice to make use of welding wire feedstock that is certified by the manufacturer to conform to AWS or International Organization of Standardization (ISO) standards for the specific alloy and wire product in question.

Welding consumable wire diameters range from 0.6 to 2.4 mm, with the most common diameters being 1.2 and 1.6 mm [16]. Smaller diameter wire can be procured and is discussed in research literature. The smaller diameter permits a smaller melt pool diameter and minimum feature size at the expense of material deposition speed, and sometimes reliability, of wire feeding mechanisms. Micro wire feeders have been used for laser welding with recent AM application by Demir to study the use of 0.3 and 0.5 mm wire in a process termed *micro laser metal wire deposition* (μLMWD) [17]. Demir used smaller wire to further increase the resolution of the deposited metal and to reduce heat input for the deposited layer.

#### 2.1.1.1 Elemental composition

In both LP-DED and LW-DED, control over the elemental composition of metal AM components is critical for ensuring quality control and predictable properties. As a result, most systems utilize pre-alloyed powders or commercially available wire to achieve high elemental control and homogeneity [18]. The elemental composition of LP-DED–fabricated components may deviate from that of the feedstock as a result of four primary causes: powder cross contamination, melt pool vaporization, oxidation of feedstock, and oxidation of the melt pool. Melt pool oxidation can be minimized by operating in a high-purity inert gas environment for LP-DED [19]. It can also be minimized by introducing a constant flow of inert gas through the deposition head to shield the melt pool. Powder cross contamination is known to be a serious area of concern and can only be solved by either dedicating machines to a single feedstock or meticulously cleaning the machines during powder changeovers. Metal vaporization may be a concern for elements with high vapor pressures [20], but the high travel speed of the melt pool helps to ensure that any location on the build surface is only momentarily molten before it solidifies. A study conducted on Ti6Al4V demonstrated the ability to numerically predict the vaporization mass loss for selected elements in an Arcam melt pool, and it also experimentally demonstrated a mean aluminum loss of 0.12 wt% per melt cycle over five melt cycles [21] [22]. Contamination and composition concerns with LW-DED are well understood based on welding literature. LW-DED shares the control issues of elemental vaporization and oxidation of the melt pool, but notably, it does not have the large surface area of powder which can oxidize or adsorb contaminants.

The cost of LP-DED components can be reduced by recycling the powder. Depending on the nozzle geometry, which shapes the trajectories of the powder particles, only a fraction of the powder sprayed is successfully delivered to the melt pool. Larger melt pool sizes can achieve powder use efficiency over 90%, obviating the need for powder recycling. However, the finer melt pool sizes required for depositing thin features have a limited surface area as a target for sprayed powder and can have capture efficiency less than 10% [23], [24]. Although powder recycling is not necessary, it can be economically attractive. Most studies on powder reuse focus on powder bed techniques, but some research results are available on powder reuse for LP-DED [25]. Several factors must be considered for recycled powders, as shown in Figure 4. First, some fraction of the sprayed powder will travel through the laser's path, which will heat and can melt the powder. This can cause oxidation and loss of elements with high vapor pressures. Second, these molten powders can impact and agglomerate with other powders before they solidify, as shown in Figure 4. Resolidified powders have a different microstructure than the original atomized powders; however, this is not necessarily a problem, because the powders will be remelted when used in further recycled feedstock. Finally, even in the absence of laser heating, recycled powders will collect and agglomerate with any other particulates or contaminants in the chamber. Vaporized metals from the melt pool condense as a fine soot, which can adhere strongly to available free surfaces and may not be removable with conventional sieving practices. This alters the powder's chemical purity, size distribution, and flowability [25].

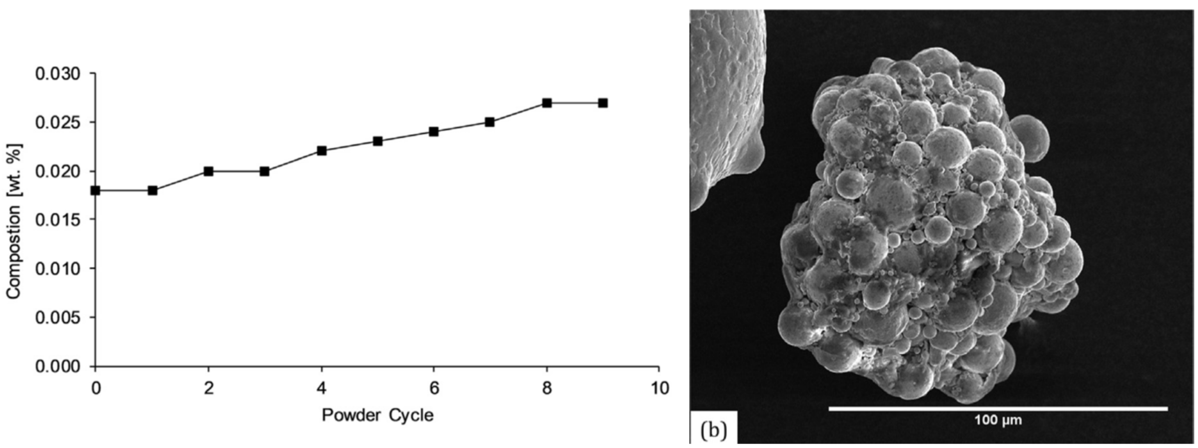


**Figure 4. Powder reuse in LP-DED can affect elemental composition of powders, as shown in oxygen content increase in SS316L (left), partly due to agglomeration and contaminant pickup (right)** [25].

Heiden et al. [26] also report the presence of nanoscale $SiO_2$ surface growths on virgin powder and larger $SiO_2$ and $MnCr_2O_4$ growths on recycled powder, as shown in **Error! Reference source not found.**. Although the powder production method was not specified, preferential oxygen scavenging by Si is likely the root cause of the oxide growths in virgin powder. Oxygen scavenging during the LPBF process is also the likely cause of the $MnCr_2O_4$ growths and enlarged $SiO_2$ inclusions. $SiO_2$ inclusions in LPBF 316L fabricated components have been correlated to accelerated stress corrosion cracking (SCC) growth rates; this topic is discussed in depth in Section 2.2.1. Taken as a whole, powder recycling appears to have mixed beneficial and detrimental effects on the quality control of the fabrication process and on fabricated component material properties. However, quantitative standards must be developed to determine when powder can no longer be recycled.

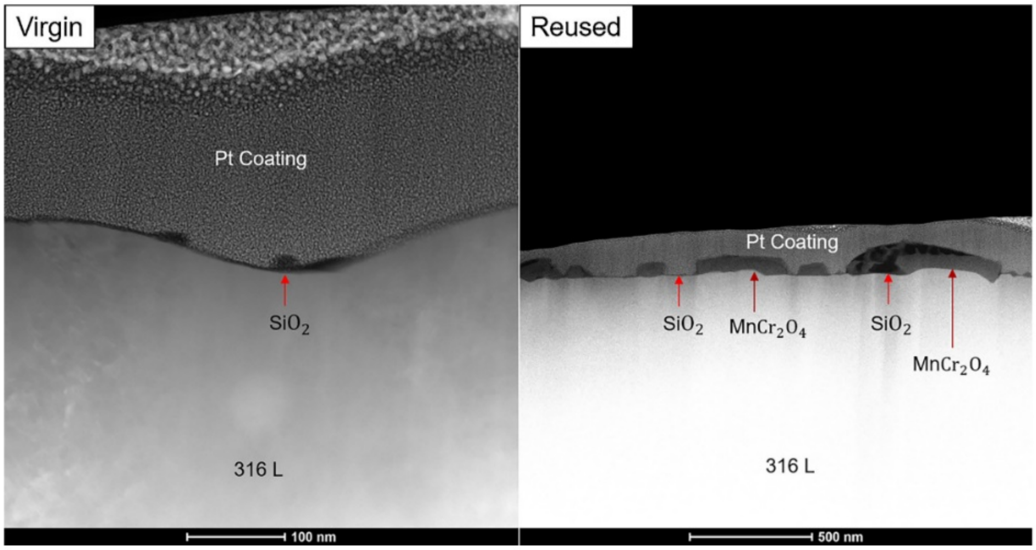


**Figure 5. Observation of oxides on 316L feedstock particle surfaces** [27].

#### 2.1.1.2 Powder porosity

Internal porosity and trapped gas in powders can result in porosity in metal AM-fabricated components [27] and are two of several porosity sources in LP-DED. Therefore, it is typically desirable to minimize internal porosity in feedstocks. Porosity in components resulting from gas entrapped in powder can be recognized by spherical voids, whereas porosity induced by the fabrication process tends to exhibit irregular, elongated voids, as seen in Figure 6 [18] and Figure 7 [28]. Powder porosity is largely dependent on the production technology used. Powders produced via plasma atomization or the plasma rotating electrode process (PREP) have been shown to eliminate voids resulting from gas entrapped in powder [27]–[29], whereas gas atomization (GA) yields powder with significant quantities of entrapped gas, as seen in Figure 8 [28]. GA and rotary atomization yield powders with satellites and irregular shapes, respectively, adversely affecting flowability and powder packing density.

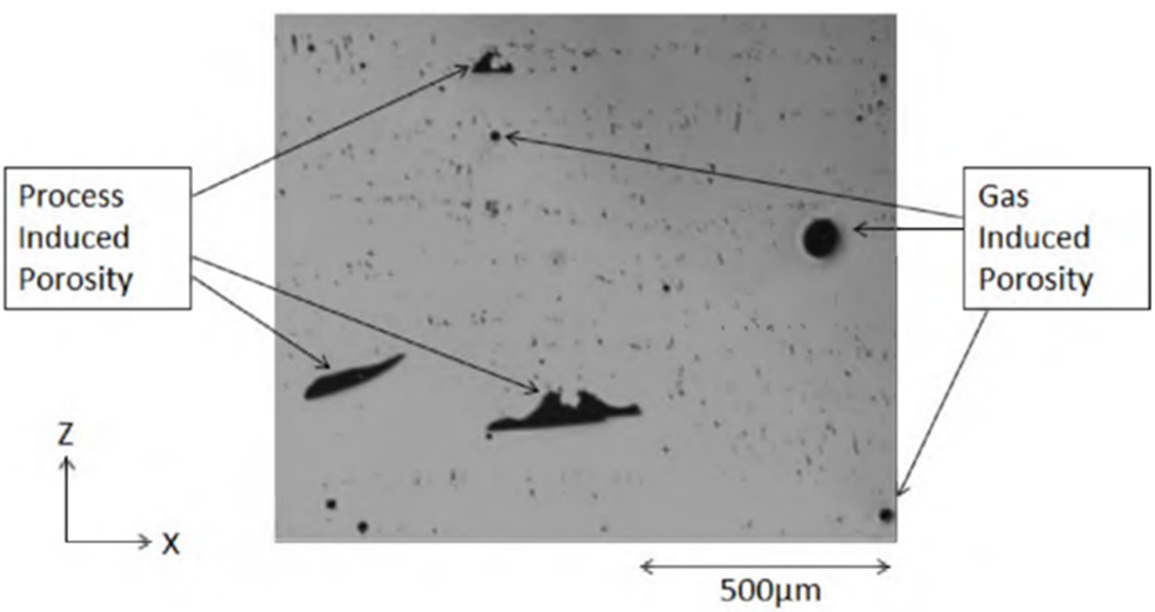


**Figure 6. Process-induced vs. gas-induced porosity** [18].

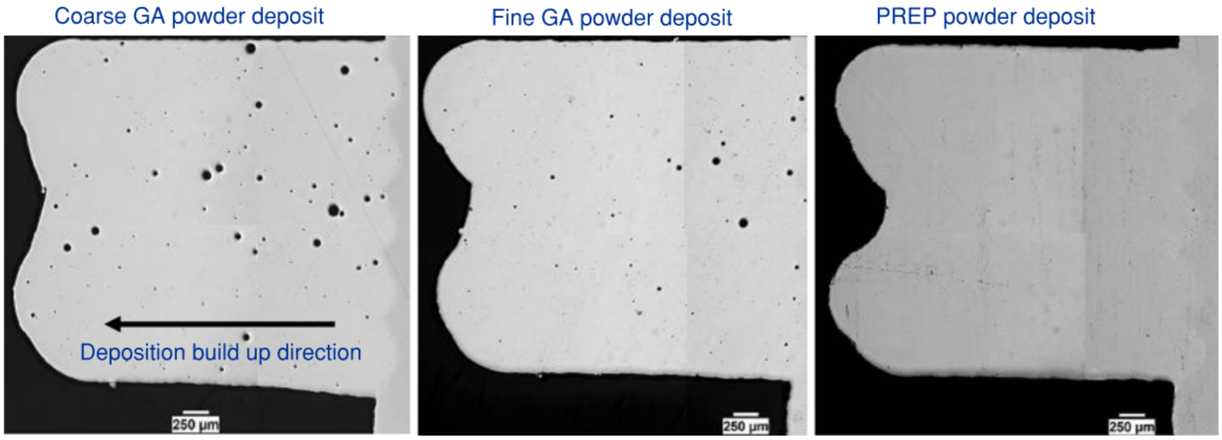


**Figure 7. Examples of powder-induced porosity in components** [28].

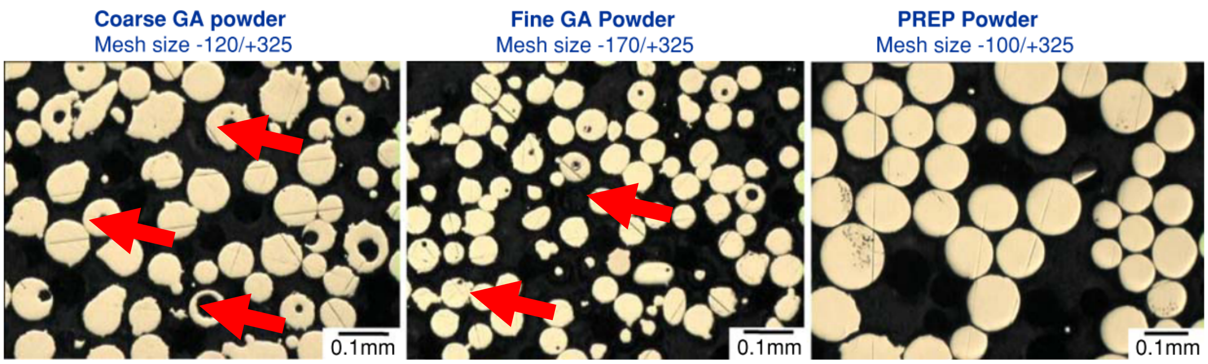


**Figure 8. Examples of Gas Atomized (GA) powder porosity** [28].

#### 2.1.1.3 Other powder properties

Beyond chemistry and porosity, a number of other powder characteristics influence the deposition process in LP-DED. The powder morphology and moisture content influence the consistency of dispensing devices such as rotating tables or vibratory hoppers. The powder size distribution, morphology, surface roughness, and density can affect the drag coefficient and flight trajectory of sprayed powder particles, which can change the amount of powder that is injected into the melt pool [30], [31]. The surface roughness, oxidation, and coating material on the particle can affect how well it wets to the liquid metal in the melt pool [32], [33] Simulation can be shown to alter the absorption of powder into the melt pool [34], [35]. Because the process is sensitive to the feedstock powder, the user must establish a set of powder handling and characterization practices, as discussed in Section 3.2.

### 2.1.2 File Preparation

In both LP-DED and LW-DED, file preparation consists of using the CAM software to program machine instructions to set the energy source scan path, the timing of switching the energy source on and off, the layer thickness, the energy source spot size, the laser energy output, and other environmental parameters. The machine parameters and scan strategy must ensure complete fusion while avoiding issues such as melt pool balling, delamination, porosity, warping, and unacceptable residual stresses. The term *contour* refers to the toolpath that follows the outside edge of a layer slice, and *infill* refers to the interior of a layer slice. *Scan strategy* in the context of L-DED refers to the path the laser travels during the melting process. Scan strategies in L-DED are generally more constrained than those used in LPBF, because the changes in scan direction require acceleration of a heavy nozzle and lens assembly instead of two small mirrors. For LW-DED in particular, the scan strategy can be even further constrained by bead ordering selections that prevent undesired wire interactions/collisions with previously deposited beads or features on the object under construction. A typical approach is illustrated in Figure 9. Scan strategy optimization depends on whether the objective is to minimize build time, reduce thermal gradient, mitigate residual stress, or maximize surface finish quality. Unlike in LPBF, a "chessboard" or "island" strategy of isolated patches of deposited material is less typical, because tool acceleration is slower, and additional dwell time at corners can lead to over-deposited material. The raster pattern is frequently rotated to minimize alignment between subsequent layers, which can cause patterned defects.

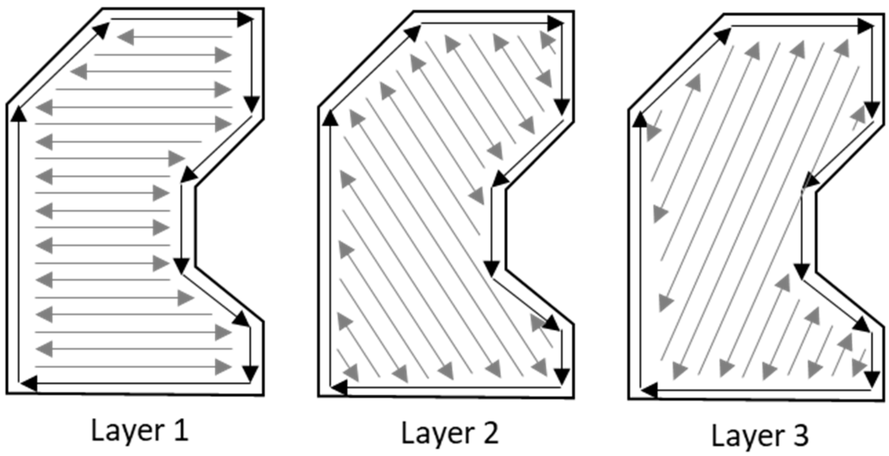


**Figure 9. Illustrated scan strategy, with a single contour pass and bi-directional infill, rotated 57° between layers.**

Many L-DED systems provide significant flexibility to operators in their choice of parameters. For example, operators may specify the scanning pattern used (e.g., unidirectional, bidirectional), whether contours will be melted before or after infill, inter-layer pattern rotation angles, laser power level, laser spot size, and travel speed, to name a few. These parameters directly affect the thermal history of a specific location within a component, as well as porosity, surface quality, yield, and tensile strength, and other qualitative and quantitative outcomes. Process parameters must be coordinated to control the critical relationship between thermal energy output and melt pool velocity. Scan strategy parameters are typically static and uniform. However, the way that scan strategies and heat transfer from the meltpool interact with component geometry is nonuniform throughout the component. Therefore, the microstructure and material properties change throughout the component because of varying local temperatures resulting from heat transfer. Controlling processing parameters to vary as a function of thermal conditions may be a possible route to compensate for the effect of geometry and to obtain uniform (if not isotropic) microstructures. The ability to control parameters and to incorporate closed-loop control systems may facilitate formation of uniform microstructures; therefore, real-time sensing and control for L-DED processes is an area of significant research [36]–[39]. Determining which parameter combination should be used at each point throughout a component is not trivial and will likely require advances in multiscale simulation techniques and computer processing power. These parameter control changes represent significant technological challenges, but they offer the possibility of solving AM issues such as intracomponent yield and tensile strength variation.

### 2.1.3 Laser-Directed Energy Deposition Design Considerations

L-DED AM has revolutionized the approach to component design: it does not require straight lines, conventional simple geometries, or direct lines of sight to create internal features. It opens new avenues for application of topology-optimized components, allowing for significant performance gains, as well as weight and cost reduction. However, the technique does impose its own set of constraints on manufacturability. Specifically, five major obstacles must be considered: build volume, build time, overhanging geometry, microstructural anisotropy, and surface roughness. These design considerations are shared by both LW-DED and LP-DED.

First, the size of components produced by L-DED is constrained by the machine's build volume. The size can typically be much larger than that for LPBF at a lower cost, because many L-DED machines leverage existing platforms such as a computer numerically controlled (CNC) subtractive milling machine, or for even larger components, a robotic arm is used. Due to gantry rigidity and mechanical constraints, there is a tradeoff between the size of the component that can be produced and the accuracy of the positioning system. Therefore, it is desirable to deposit components on an appropriately sized machine.

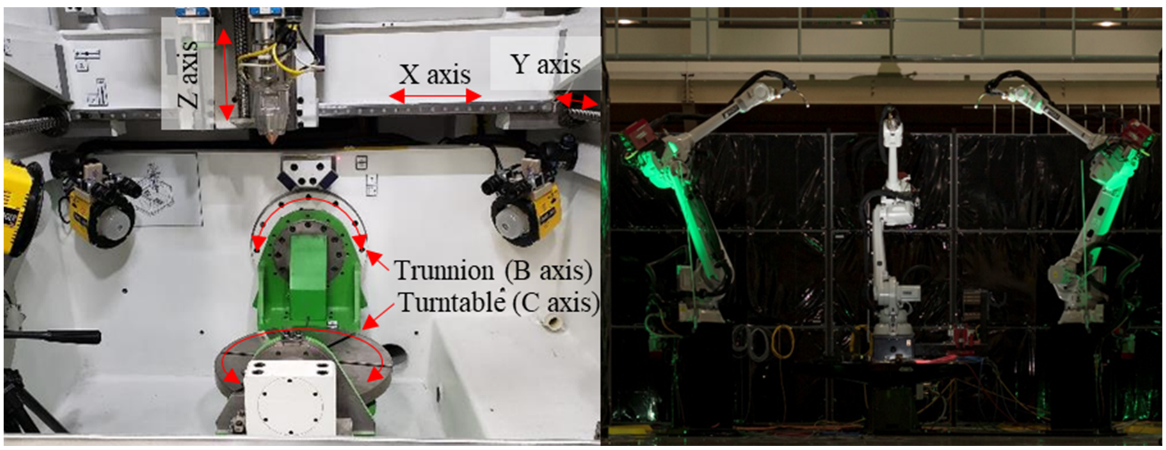


BeAM Modulo 400: high-accuracy CNC mill style for XYZ axis motion, plus a trunnion and turntable for B and C axis tilting

Lincoln Electric MedUSA system: 3 robotic arms and turntable for independent positioning of 3 separate metal inert gas (MIG) AM wire heads

**Figure 10. Two DED systems at the ORNL Manufacturing Demonstration Facility that use different positioning systems (deposition scales, speeds, and resolutions).**

Second, the amount of time required to deposit a component, scales with its physical volume and can become unacceptably slow for very large components. To combat this and to increase process speed, L-DED typically has a significantly larger melt pool than that of LPBF that is on the order of 1–20 mm wide, depending on system design. Larger melt pool sizes reduce the ability to print thin or small features, and they also lower the surface quality that can be achieved. Some machine manufacturers are moving toward a multiresolution approach in which different nozzle assemblies are used to produce a large roughing melt pool for large volumes, whereas a smaller, fine melt pool is used to add important details or surfaces. This approach is analogous to the conventional subtractive CNC approach, in which several different tools are available for specific jobs. The importance of net-shape deposition to the designer may ultimately dictate the method chosen, be it faster bulk deposition, slower fine deposition, or a combination of these techniques. Feedstock cost is often a driving factor in this decision as well, because material lost due to post-deposition machining can generate a costly waste stream as characterized by the aerospace industry's use of the "buy-to-fly" ratio [40].

Third, when designing components for manufacture with L-DED, it is important to consider unsupported or overhanging geometries. Unlike the LPBF process, the L-DED process does not have a bed of powder, so the melt pool must be supported by underlying material. Under certain processing conditions, the surface tension of the melt pool can allow for building geometries with some overhang—in some cases up to 60° [41], as shown in Figure 11. Alternatively, this limitation in L-DED can be overcome through leveraging 5+ axis deposition, in which the tool or the part is reoriented to align the deposition axis to be parallel to the side of the deposited geometry. While this has been mechanically implemented in multiple L-DED systems, as discussed in Section 2.1, the software required to generate toolpaths for 5+ axis deposition is not robustly automated, so the user must be suitably experienced. Furthermore, when planning multiaxis motions, clearances are not necessarily guaranteed as they are in 3-axis deposition, which requires advanced simulation and re-routing capabilities in CAM software packages.

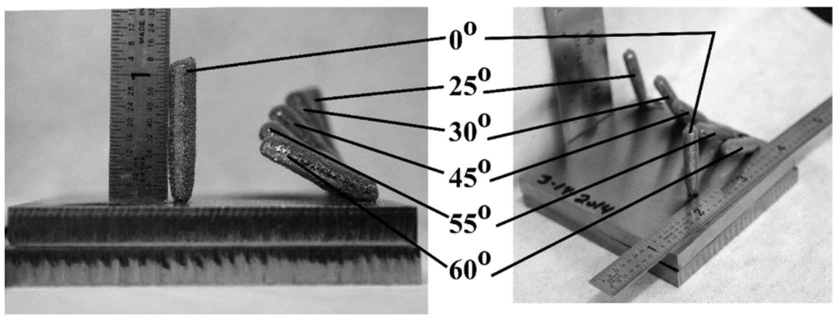


**Figure 11. Demonstration of printing of highly overhanging geometries ranging up to 60° with L-DED** [41].

Fourth, in L-DED, the material solidifies in a trail behind the melt pool, which forms a highly anisotropic microstructure for many material systems. It is well documented that grain structures tend to be columnar, and dendritic solidification structures can form. These structures tend to follow the build direction. In other AM systems such as E-beam powder bed fusion, the heat source can be moved fast enough to cause solidification to progress from the edges of the melt pool instead of from the bottom. This effect enables programmatic tailoring of microstructures and transitions between columnar and more equiaxed structures [42]. However, in L-DED, the beam typically moves too slowly to permit such transitions.

In addition to generating anisotropic microstructures, shrinkage following solidification from the coefficient of thermal expansion causes tensile residual stress to form along the weld track. These stresses build up with each subsequent layer and can lead to problems. The accumulated macroscopic deformations can cause the part to fail to meet dimensional tolerances. This can be corrected with machining rework operations, by reinforcing the printed structure with supporting structures that must be machined away after deposition, or by simulating the deformation with thermomechanical finite element analysis (FEA) and pre-deforming the structure so that it naturally bends into the correct shape during printing. Because accumulated stresses also affect the mechanical performance, parts are frequently subjected to a heat treatment to alleviate these stresses and achieve the desired microstructure.

Fifth, in L-DED, the surface finish can be of fairly poor quality. This occurs for two reasons. The shape of the weld bead, which is the fundamental building block of AM, is controlled by surface tension, so it forms a track of material with an oval cross section that cannot precisely conform to the original intended geometry. This results in each layer having a scalloped appearance. A poor quality surface finish in LP-DED can also be caused by powder particles becoming trapped on the surface of the melt pool. These particles may not completely melt before the laser has moved on, resulting in numerous partially welded-on powder particles "decorating" the component. For these reasons, L-DED is sometimes referred to as a *near-net shape* process that requires additional machining to meet design tolerances.

A different, relatively new approach to address the problems of surface finish and dimensional tolerances is to incorporate both additive and subtractive manufacturing into one hybrid machine which allows for fast, low-resolution printing, followed by high-precision machining [43]. This approach includes the advantages of AM's geometric design flexibility, but it also compensates for many of its drawbacks through the use of conventional, established machining methods.

### 2.1.4 Substrate, Support Structure and Powder Removal

In both LP-DED and LW-DED, components must undergo additional preparation after fabrication prior to use. First, for LP-DED excess powder must be cleaned off and removed from any cavities. This is typically done using a wire brush and by vacuuming. Second, the substrate must be cut off. This can be done using wire electrical discharge machining (EDM) or a bandsaw. One issue that can arise is that induced residual stresses from the uneven thermal field during solidification can significantly deform the fabricated component and the substrate onto which it is deposited, so process optimization may be needed to ensure that the part can maintain dimensional tolerances. Finally, overhanging geometries are frequently supported with structures that are not part of the intended design, so these must be removed. Because minimum feature sizes can be fairly large (~1 mm), support structures cannot typically be removed by hand, so they must be machined off. While these steps are not technologically challenging, there do point to an industry need for specialized support equipment to perform depowdering and build-plate removal.

## 2.2 PROCESSING OF L-DED 316L

Properties of additively manufactured metallic components are frequently comparable if not superior to those of conventionally manufactured parts. This is partially due to finer grain size [7]. As in LPBF, L-DED essentially welds layers together, and the small spot size of the energy source results in small melt pools and rapid cooling, which inhibits grain growth upon solidification. Columnar grain structures oriented lengthwise in the build direction (Z-axis) are frequently observed, and this grain structure has been reported in Ti-6Al-4V [44] and Inconel 718 [45]–[47]. Grain structures are primarily dependent on the temperature gradient and solidification interface velocity, and it is possible to selectively form columnar or equiaxed grains by varying the energy source power and scan speed [42]. For this reason, the typically larger melt pool sizes in LW-DED than in LP-DED result in microstructures more akin to traditional welding.

Many alloy groups have been successfully fabricated with L-DED to date [7], [48], [49], including the four primary structural alloy groups of titanium [7], [50]–[52], steels, nickel alloys [53], [54], and aluminum alloys [55], [56]. Numerous investigations are being conducted on the use of more specialized materials such as the new class of high-entropy alloys, metal matrix composites incorporating tungsten carbide [57] and other carbides, and numerous functional materials. For structural materials, the specific steel classes used in AM include austenitic stainless steels [58], tool steels [59], precipitation hardenable stainless steels [60], and maraging steels [61]. General reviews on the hardness [62] of AM metals, the effects of build orientation [63], and anisotropic material properties [64] have been published. The high number of combinations of processing methods and alloy designs has resulted in a fast field of research that encompasses the study, prediction, and control of the microstructure of metal AM processes. As such, the primary focus of material property review centers on 316L given its relevant application in NPP environments and the well-documented performance of conventionally manufactured 316L in irradiated environments.

While a significant amount of research has been performed to investigate the unique microstructures formed in LP-DED and LW-DED, meaningful comparison of literature results is complicated by the significant number of fabrication parameter variables, as well as incomplete reporting. For example, absorptivity of Fe varies from 0.12 at room temperature for a $CO_2$ laser to 0.25–0.32 for a Nd:YAG laser [65]. Therefore, it is necessary to report both applied power and laser wavelength to calculate absorbed energy, yet laser type is not consistently reported. Similarly, spot size, hatch spacing, layer thickness, build orientation, and material porosity are not consistently reported, yet their information is required for accurate parameter comparison and calculation of thermal history. Incomplete reporting can be partially attributed to three causes (1) nonstandardized terminology within the community, (2) inter-supplier variation in hardware and software, and (3) a lack of reporting standards not addressed by sufficient rigor in the peer review process. Uncertainty in interpretation of these results is further complicated by the influence of geometry as an independent variable. The lack of accepted standardized geometries frequently leads to unique geometries for each study. Therefore, the approach when interpreting quantitative results in L-DED material properties should be more skeptical than is typical for most scientific endeavors, and reliance on the data must account for the availability of contextual processing information.

Finally, although the current report is focused on the LP-DED and LW-DED process, a broader understanding of similar laser welding type processes such as LPBF can anchor expectations for material behavior given the imperfect literature coverage of available processing alternatives. As such, studies focused on LPBF are included in the following discussion for reference when LP-DED or LW-DED studies are incomplete or nonexistent.

### 2.2.1 Processing Parameters for L-DED

A review of the L-DED process would be incomplete without explaining the effects of the various available processing parameters. The microstructure and properties obtained are a direct consequence of these parameters. The parameters for L-DED can be understood by visualizing the melt pool in an equilibrium state, balancing energetic and mass inputs and outputs, as schematically shown in Figure 12 [66].

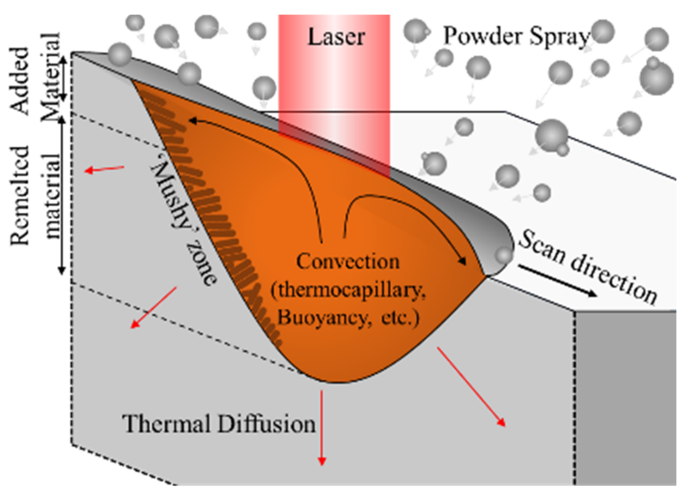


**Figure 12. The dynamic thermal equilibrium in LP-DED** [66].

An energy balance in the melt pool is formed between incoming incident laser energy and dissipation through thermal conduction into the substrate, convection with forced carrier gas, and radiation into the build chamber. Fluid convection of the molten metal can significantly contribute to the speed of thermal dissipation and is strongly affected by the thermocapillary effect, in which the gradient in temperature across the melt pool surface changes the surface tension of the melt locally. This in turn drives fluid flow along the melt pool's surface. As the melt pool solidifies, a two-phase region of liquid and solid appears, called the "mushy" zone. In particular, the mushy zone is studied in the analysis of solidification cracking [67]. Establishing these highly dynamic relationships for different material systems is currently the focus of intense academic research. This research uses tools such as high-speed visible imaging, synchrotron x-ray imaging, and computational fluid dynamics (CFD) numerical simulation.

The mass balance in the melt pool is established by incoming feedstock material, re-melted substrate material, and the deposited metal. Melt pool size can be controlled through processing parameters such as energy input and travel speed. In LP-DED, the amount of powder deposited into the melt pool surface is a function of the spray nozzle design, the powder characteristics, the standoff distance, and the size of the melt pool. Under ideal deposition conditions, all the impinging powder is molten, and it solidifies as part of the deposited layer. However, if the energy density of the laser is high enough, then metal will vaporize off the top surface of the melt pool and will then re-condense as fine soot elsewhere in the deposition chamber. In LW-DED, deposition parameters must be tuned such that the behavior of the wire as it enters the molten pool on the substrate is stable, thus avoiding frequent droplet transfer or "stubby" behavior. With stable wire feed behavior, there is generally very little spatter in LW-DED, and the mass transfer efficiency is high.

Generally, the available processing parameters and their effects on these equilibria are as follows. The laser power increases the energy available in the melt pool and generally increases the dimensions of the melt pool. Increasing the feedstock flow rate increases the amount of mass injected into the melt pool; this will cause the melt pool to be taller. The traverse speed of the laser and nozzle or wire feeder assembly, termed *scan speed*, reduces the residence time of the laser and feedstock injection and allows for more rapid heat dissipation, leading to smaller melt pool sizes and heights. The focus of the laser can concentrate or spread heat across the surface of the melt pool; if it is excessively concentrated, then metal will vaporize off the surface of the melt, and recoil pressure will force the liquid metal outward, forming an open cavity in the center of the melt pool. This cavity is termed a *keyhole*. This effect is generally associated with higher levels of porosity. The *hatch spacing* is the programmed distance between adjacent passes of the deposition head and is generally set to 60–80% of the weld track width. The *layer height* is the programmed distance that the deposition head moves upward to deposit the next layer. Together, the hatch spacing and layer height define the expected volume to be deposited per weld track. If the deposition conditions are such that significantly more volume is deposited than expected, then the part will over deposit and swell; if less material is deposited than expected, then the part will have significant porosity.

## 2.3 MICROSTRUCTURE AND MECHANICAL PROPERTIES OF L-DED 316L

While L-DED 316L is chemically very similar to a cast or wrought 316L, the LP-DED and LW-DED processes produce distinctly different microstructures that reflect the rapid directional solidification that is characteristic of the process. Several microstructural features are of note and have been the focus of numerous academic studies. This section provides a discussion of the phase content, grain structure, microsegregation, precipitation behavior, dislocation density, porosity, and heat treatment response of similar austenitic stainless steels (316, 316L, 304, 304L), drawing from both L-DED literature and LPBF for comparison when pertinent. These differences affect the mechanical, chemical, and environmental properties of the resulting material and are discussed in this section.

### 2.3.1 Equilibrium Phase Diagrams and Predictive Diagrams

The microstructure of welded austenitic stainless steels has been extensively studied and can be applied to understand the microstructural behavior of both LP-DED and LW-DED. Phase diagrams such as the Fe-Cr-Ni diagram in Figure 13 can be helpful in determining the stable phases in equilibrium conditions. As presented in Figure 13, 304L and 316L are noted to show the multiple phases of ferrite ($\delta$) and austenite ($\gamma$) that may be present for both alloys at temperatures up to the melting temperature. The sigma phase ($\sigma$), which is not shown, is an intermetallic phase that may form in austenitic stainless steels and is known for its very brittle characteristics at room temperature, which is to be avoided [68]. Higher levels of chromium (>17%) increase the rate of sigma phase nucleation, which normally occurs at ferrite-to-austenite grain boundaries. Intermediate temperatures >400°C may accelerate the formation of the sigma phase. However, welding of these alloys does not occur at equilibrium conditions, so more predictive diagrams are needed. Many of the weld metal constitution diagrams developed for stainless steels were primarily focused on arc welding. The WRC1992 and Shaeffler diagram are some of the most used. These diagrams rely on the balance of elements delineated between ferrite stabilizing elements such as Cr and austenite stabilizing elements such as Ni. A ratio of these elements is typically referenced as the Cr/Ni ratio and can be used to predict phase balance. Care must be taken to use the Cr/Ni equivalency values referenced by each diagram. These diagrams were developed mostly to predict residual ferrite content in weld metals.

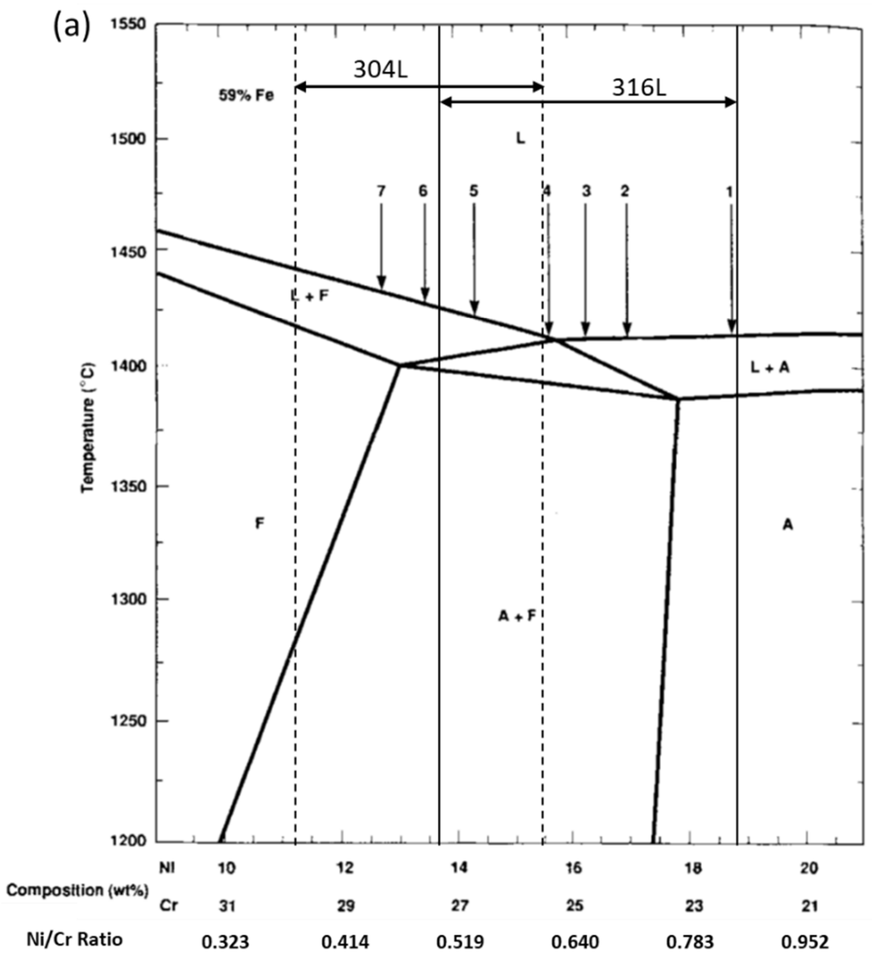


**Figure 13. Ternary phase diagram section for Fe-Cr-Ni from Elmer et al.** [69]. The ternary projection of the 304L and 316L austenitic stainless steel composition range are denoted.

The importance of this microstructural evolution was plotted by Suutala [70] and was plotted again later with a modified Suttala diagram created by Lienert (Figure 14) to predict the crack sensitivity of pulsed laser welds. Phosphorus and sulfur (P+S) are known as elements with low melting temperatures that segregate to grain boundaries and can cause cracking. The role of ferrite and austenite has been studied extensively and is widely accepted to be a significant factor in the weld material's susceptibility to cracking. The first phase to solidify, known as the *primary solidification mode* (PSM) was plotted by

Lienert and is a significant factor in the crack sensitivity of austenitic stainless steels. As shown in Figure 14, the PSM changes with material chemistry based on the Cr/Ni equivalency. Material chemistry therefore has a large influence on the solidification mode. Cracking can be nearly eliminated in the weld metal with primary ferrite solidification, as shown in Figure 14 [71]. Rapid solidification has been found to also influence the solidification mode. As shown in Figure 15, a transition from ferrite grain growth to austenite can occur at fast solidification rates. This is caused by dendrite tip undercooling, in which the phase with the highest dendrite tip temperature at the growth rate will be preferred. The transition from ferrite to austenite was estimated by Fukumoto through calculations to occur near $10^{-2}$ m/sec in growth velocity [72]. In 304L, these cellular dendritic structures are believed to contribute significantly to the yield strength (YS) of the as-deposited material and can increase the YS by up to 100 MPa [73]. Recommended $Cr/Ni_{eq}$ values >1.5 for arc welding (not shown, refer to Suutala diagram [70]) and >1.7 for laser welding have been used, as shown in Figure 14 [74].

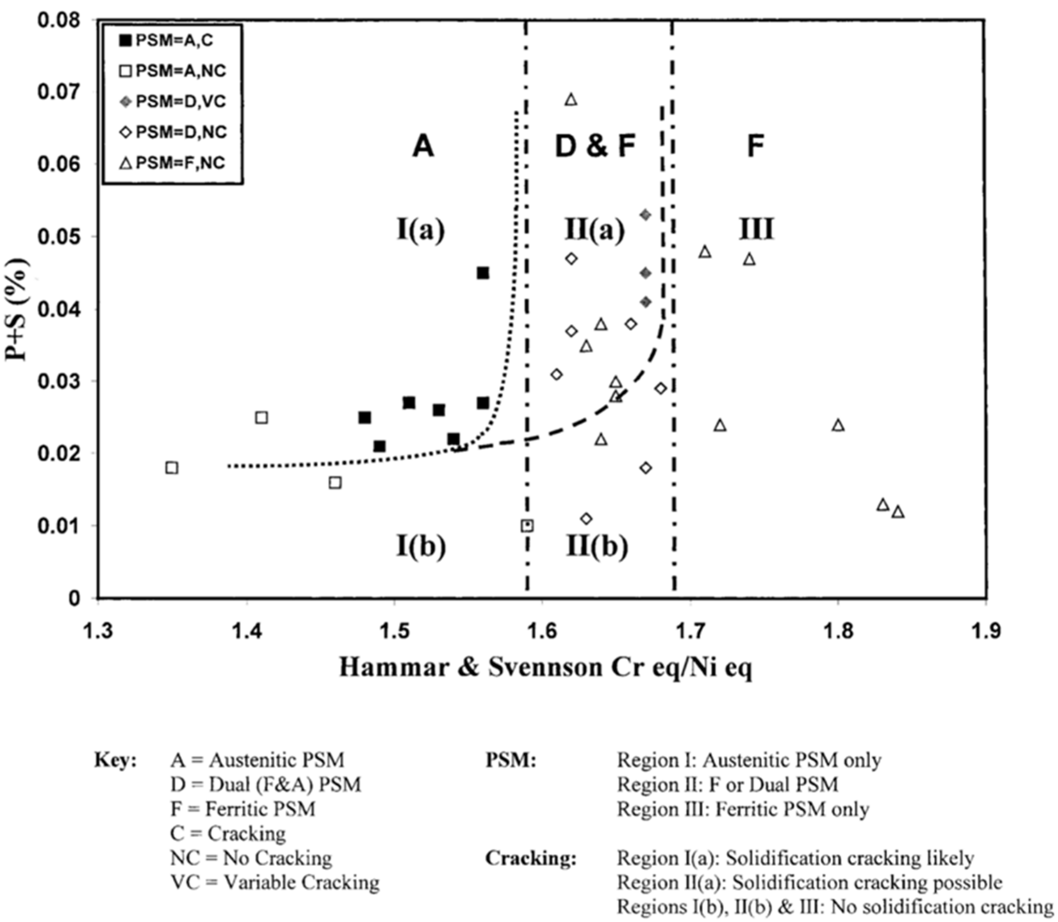


**Figure 14. Cracking susceptibility of pulsed laser austenitic stainless steel welds** [75].

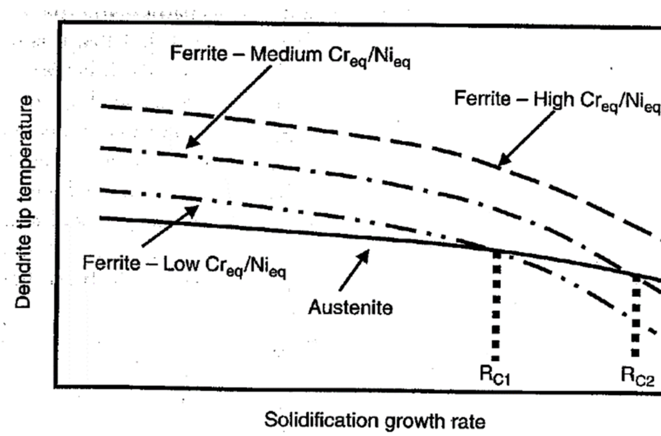


**Figure 15. Transition of solidification mode through rapid solidification** [74].

For L-DED, the solidification rates are faster than those for arc welding, so predictive diagrams for faster cooling rate processes are more suitable. Lippold and Elmer developed some of the most widely cited predictive diagrams incorporating solidification rate. These diagrams were originally produced for pulsed laser and electron beam welding applications, yet they have proven reliable for AM [76]. See Figure 16 and Figure 17 for Lippold and Elmer's predictive diagrams. Lippold uses the WRC 1992 equation, whereas Elmer uses the Hammer and Svensson equation.

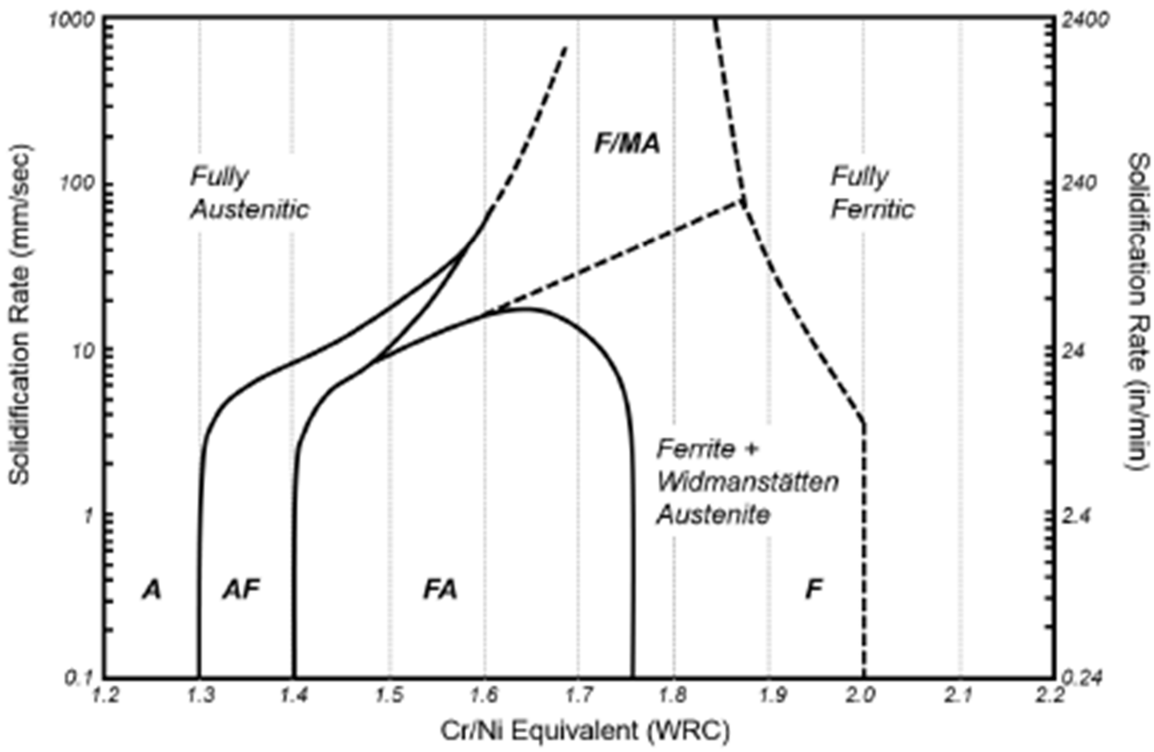


**Figure 16. Predictive morphologies developed by Lippold** [77].

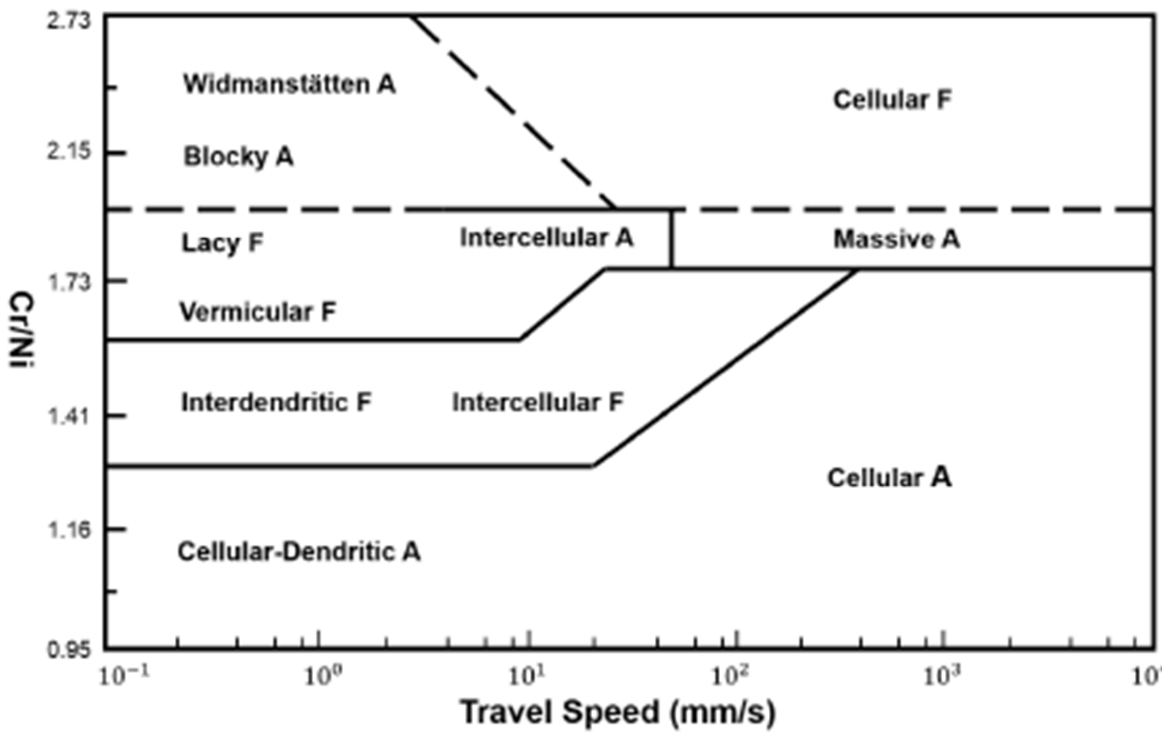


**Figure 17. Predicted morphologies developed by Elmer** [69].

### 2.3.2 Grain Structure and Texture

The mechanical and corrosion properties of a material are largely influenced by its grain structure (size and morphology) and texture. The grain structure of a material is highly contingent upon the chemical composition of the material, as well as the thermomechanical processing that subsequently takes place.

The as-built grain structure in L-DED 316L is typically columnar, anisotropic, and without strong orientation texture, as shown in Figure 18. LP-DED and LW-DED share similar heat inputs, so their resulting grain morphologies will be similar. Oxide inclusions, discussed in Section 2.3.4, will also act to restrict the grain growth of LP-DED deposited material. Grains grow in the direction of the thermal gradient at the trailing edge of the melt pool, and grains with a [100] orientation variant along this thermal gradient solidify fastest. As the heat source moves on, the boundary of the melt pool also moves, causing a change in the direction of solidification which yields the characteristic arced grains shown in Figure 18(a). Depending on the scan strategy selected, the microstructure will be partially re-melted on the next pass of the laser, leading to partial overwriting of the microstructure, and causing a repeating motif for some portions of the solidification pattern. In addition, grain growth is frequently seen to be partially epitaxial from the prior layer, which can yield highly elongated grains that cross several melt pool track boundaries. In this way, the melt pool size and shape directly influence the grain structure of the as-built component. This grain structure can be homogenized with heat treatment to obtain a more regular yet coarser grain structure, as shown in Figure 18 (b) and (d), if sufficient temperature and time is allowed. This is discussed further in Section 2.3.9. Competitive growth at the fusion boundary will prefer the grains closest to the easy growth direction with the highest directional alignment to the heat flow direction. Therefore, heat input parameters and build patterns affect the microstructure, texture, and properties of the component [78].

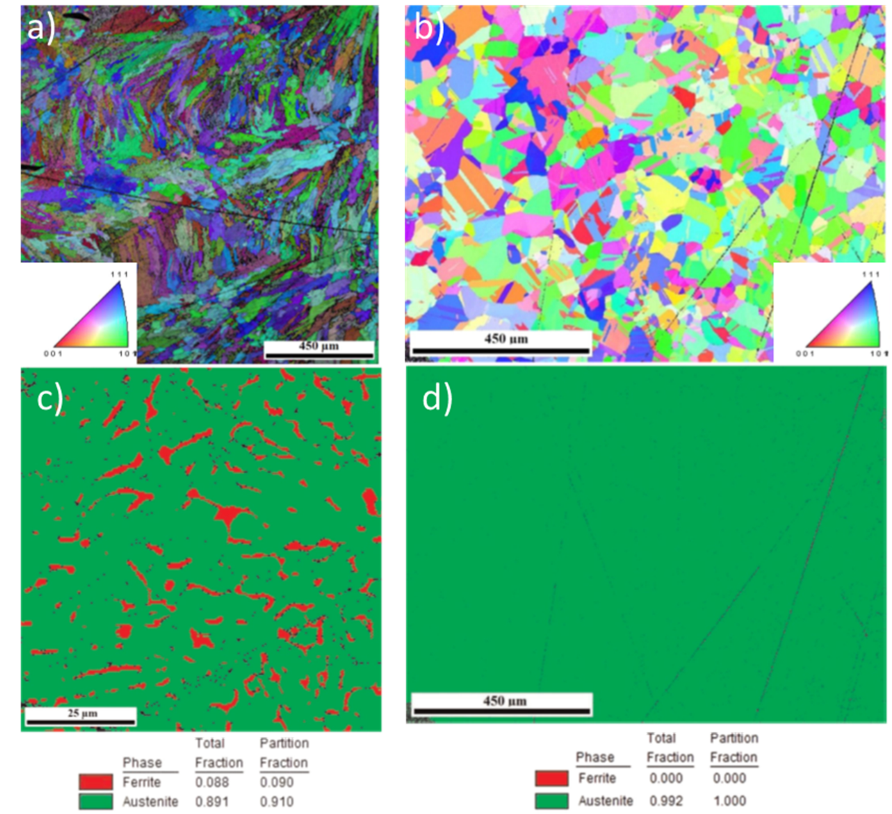


**Figure 18. Typical grain structure (a, b) and phase content (c, d) measured via electron backscatter diffraction (EBSD) for as-built (a, c) and heat-treated (b, d) L-DED 316L stainless steel.** Heat treatment was a homogenizing treatment for 2 h at 1,150 °C, air-cooled [79].

Under virtually all process conditions, L-DED and LPBF 316L form cellular solidification structures which are revealed through etching or from compositional analysis, as shown in Figure 19 [80]. For primary austenite formation in 316L, the cell core is enriched in Ni, and the boundaries of these solidification structures are enriched with Cr and Mo, as shown in Figure 20 [81]. For primary ferrite solidification, the cell core would be enriched with Cr, and the boundaries would be enriched with Ni. The respective 2 and 4 wt% margins for Cr and Ni content in these alloys can allow for differences in solidification structure based on the feedstock material.

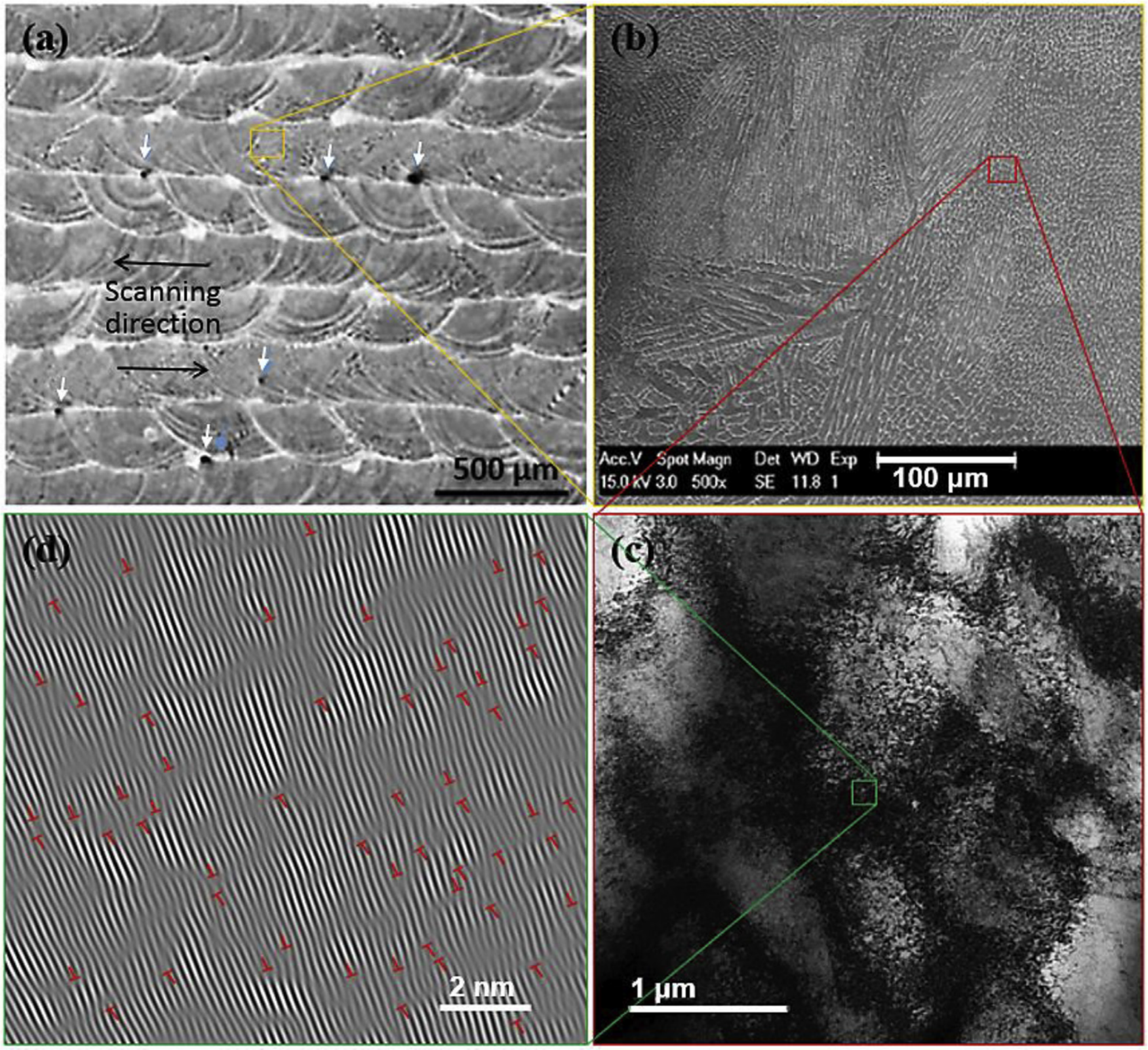


**Figure 19. Meso-to-nanoscale microstructure of L-DED 316L stainless steel [80].** (a) Individual melt pool tracks are evident from etched microstructures that highlight solute-enriched bottoms and sides of melt pool tracks. (b) Etching reveals cellular microstructure characteristic of AM 316L stainless steel. (c) Brightfield transmission electron microscopy (TEM) shows dislocation entanglements at cell wall boundaries, which are seen under high resolution dislocation mapping (d).

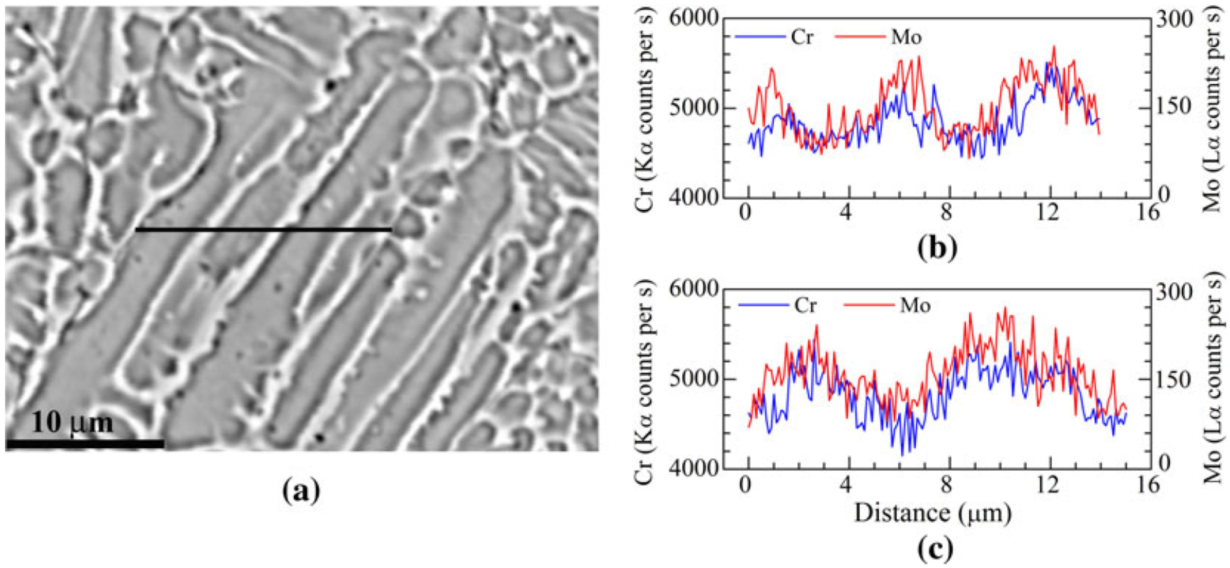


**Figure 20. (a) EPMA BSD image showing cellular dendritic structures within the first layer of a 316L L-DED deposited wall;** (b) and (c) Cr and Mo enrichment in cell boundaries in the first and ninth layers.

Using the same lot of powder material, a direct comparison of the microstructure and properties can be made. Calculations provided by Wilson on dendrite arm spacing exceed that reported in Table 2, in which LPBF is reported as having a cooling rate approximately two orders of magnitude faster than that of LP-DED. Wilson calculated rates of $10^5$ and $10^2$ °C/s for LPBF and LP-DED, respectively. Cooling rate curves calculated using Rosenthal's heat flow equation were completed and are shown in Figure 21. Three parameter sets are plotted: L-PBF minimum (dashed line), L-PBF maximum (solid line), and LP-DED (solid line). This difference in cooling rate influences the microstructure evolution and the resulting build properties. LW-DED and LP-DED largely overlap the same range of cooling rates. In general, LW-DED uses larger melt pools and greater deposition rates, leading to higher heat inputs which slow the cooling rate further. This would extend the cooling rate curve in Figure 21 further to the right because of slower cooling rates. Differences between cooling rates for L-PBF and LP-DED are accurate at the time of this report. For comparisons between LP-DED and LW-DED, heat input must be considered when comparing cooling rates [76].

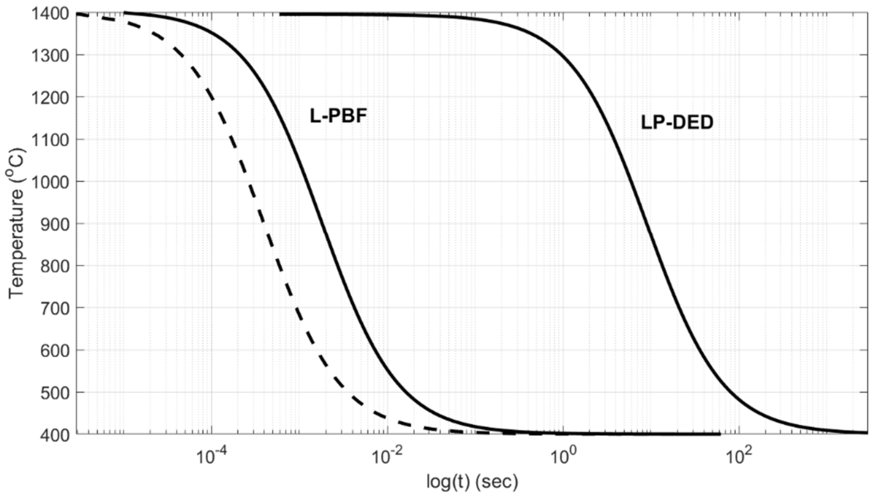


**Figure 21. Cooling rate curves calculated for LPBF minimum (dashed line), LPBF maximum (solid line) and LP-DED (solid line) [76].**

Superimposing the previously calculated solidification rates onto the predictive diagrams by Lippold and Elmer reveals the expected LPBF and L-DED microstructures of 316L components, as shown in Figure 22. A distinct microstructure evolution is expected between the two processes / heat inputs and is validated through metallography. A dual solidification mode of ferrite and austenite was seen in the LP-DED builds (Figure 23), whereas a diffusion-limited ferritic solidification and massive austenite transformation could be seen in the quickly solidifying LPBF builds (Figure 24). The heat-affected zone is not seen in the LPBF weld metallographs. LP-DED, with its higher heat input, did have a noticeable heat-affected zone, as reported by Wilson [76]. As predicted by both diagrams, the solidification mode of the LP-DED welds were of type FA, with a cellular austenite matrix and with retained ferrite between grains [76]. The LPBF welds show a distinct cellular austenite structure alongside the grains of massive austenite [76].

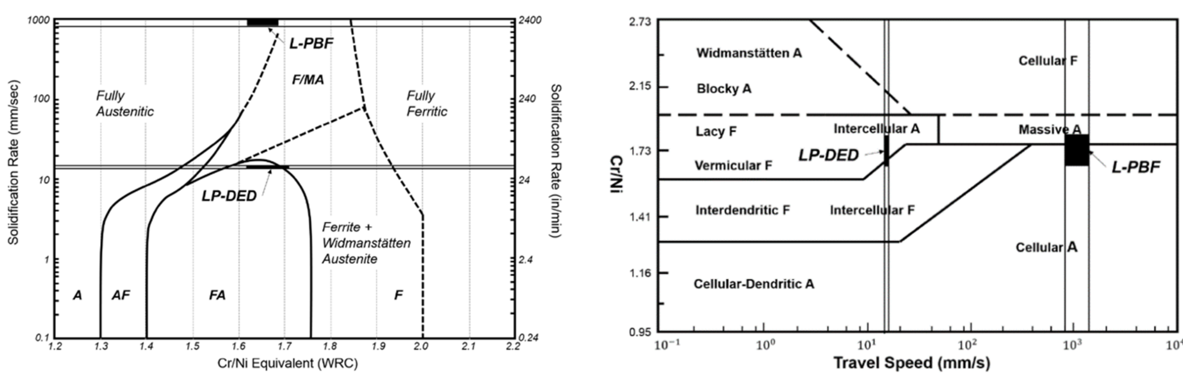


**Figure 22. Predictive diagram from Lippold [77] (left) and Elmer [69] (right), with superimposed LPBF and LP-DED transformation regions of 316L from Wilson [76].**

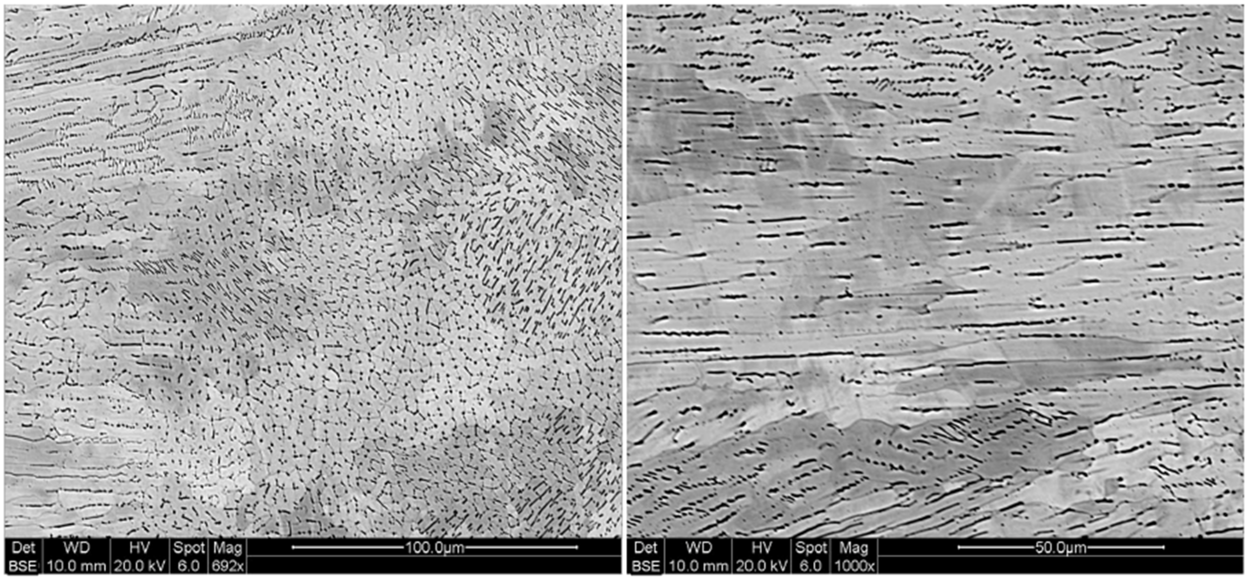


**Figure 23. LP-DED SEM images** [76].

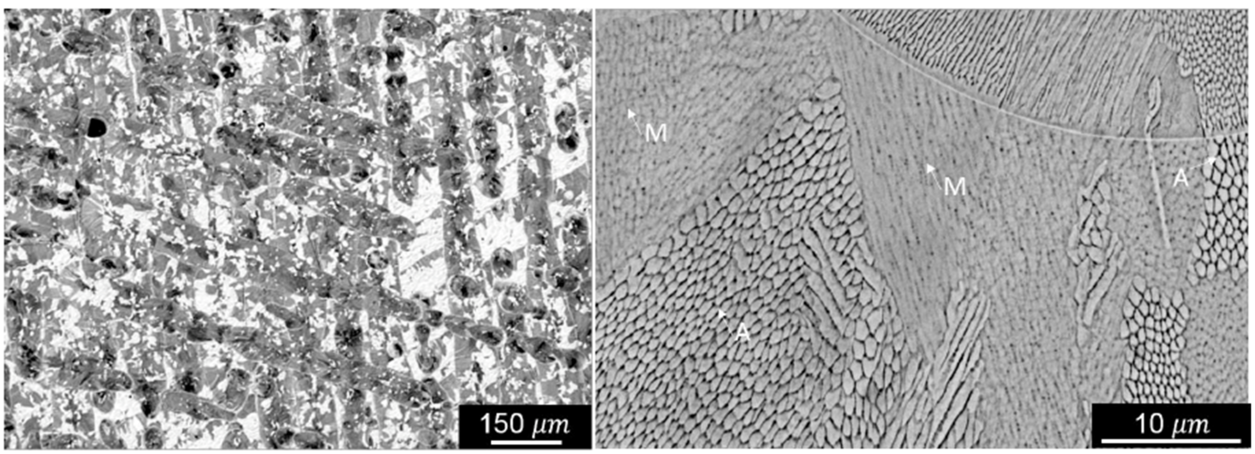


**Figure 24. 304L LPBF metallographs, XY plane (left), and ZY plane (right)** [76].

A comparison of 316L microstructures from the Zhang [82] and Scipioni Bertoli [83] was also completed by Wilson [76]. Cr/Ni ratios from each author were compared and plotted on the Lippold and Elmer diagrams to predict the resulting microstructures [76]. The authors evaluated multiple travel speeds for their respective AM processes. Zhang completed the welds using LP-DED, and Scipioni Bertoli using LPBF. Plotting the parameters according to the material $Cr/Ni_{eq}$ and the solidification rate / travel speeds reveal a result similar to the 304L plots shown in Figure 22. On the Elmer diagram presented in Figure 25, the faster LPBF scan speeds predict a fully austenitic microstructure, with only the slowest speed showing intercellular ferrite. As may be expected, the LP-DED parameters are deeper into the intercellular and interdendritic regions. As plotted on Lippold's diagram, the faster speeds for the LPBF are fully in the austenite region, with the slower speed close to the secondary ferrite phase region. The LP-DED welds straddle the interface between the fully austenitic to the secondary ferritic phase boundary [76].

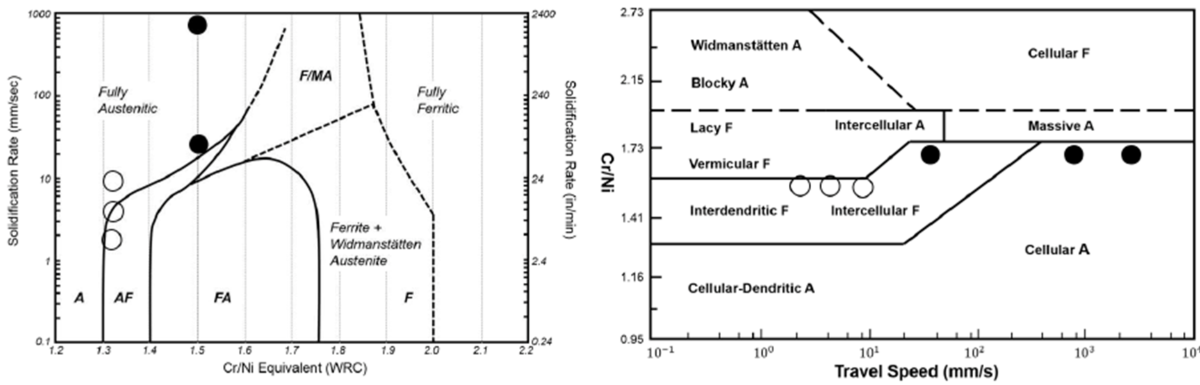


**Figure 25. Predictive diagrams for 316L builds from Zhang, LPBF, closed circles [82] and Scipioni Bertoli, LP-DED, open circles [83], as compiled by Wilson** [76].

Weld metallographs were prepared from each of the parameter sets, as shown in Figure 26. A cellular austenite solidification is evident in the predicted faster travel speeds. Scipioni Bertoli notes that a dendritic microstructure was not seen in the samples, and a determination of ferrite content was not mentioned and cannot be ascertained through the provided metallography [83]. Zhang using LP-DED metallographs at multiple speeds for cases in which secondary (intercellular and/or interdendritic) ferrite was predicted. In Figure 27, a dendritic microstructure can be seen. Neither author reports on the amount of ferrite, but it would be expected in the LP-DED samples. Dendrite arm spacing (DAS) is directly related to cooling rate, with an empirical relationship developed by Katayama [84]. As seen in Figure 26, and Figure 27, as travel speed / solidification rate increases, the grain size is inversely related. This leads to strengthening caused by a Hall-Petch relationship. Although ferrite content is not mentioned, a decrease in ferrite content associated with less partitioning is expected with increased travel speed. Greater heat input and slower cooling rates increase the deposited material grain size and allow for ferrite to form as a result of partitioning of the chemical elements. The presence of ferrite will affect the mechanical properties, cracking resistance, and corrosion behavior of the material (see Section 2.3.7).

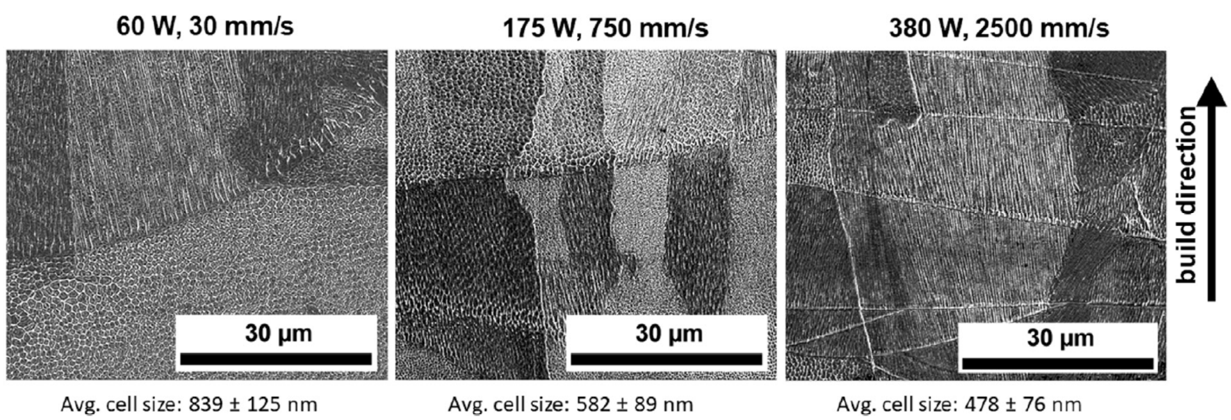


**Figure 26. Metallographs of 316L builds made by LPBF at various travel speeds** [83].

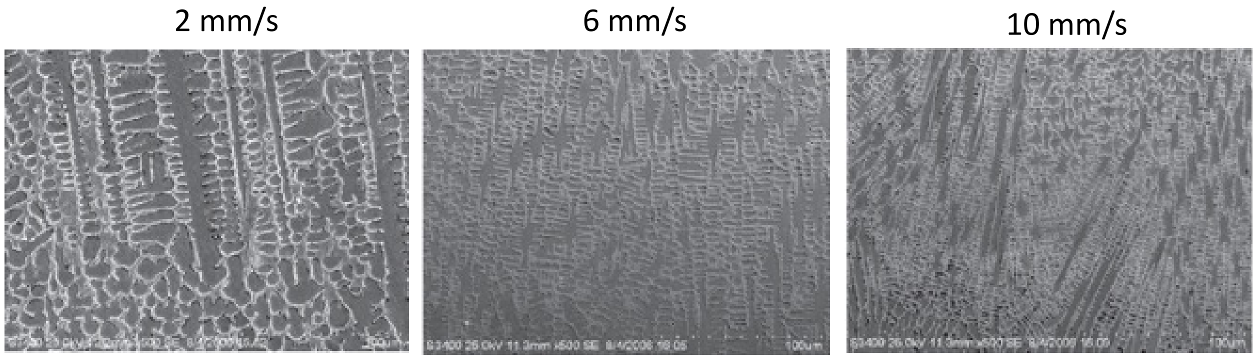


**Figure 27. Metallographs of 316L builds made using LP-DED at various travel speeds** [82].

### 2.3.3 Roles of Argon and Nitrogen

Because of iron's reactivity to oxygen, shielding gasses are used to protect the molten pool from air during LP-DED and LW-DED. Argon is generally used because of its inert nature and is not an active addition to stainless steels. Nitrogen is generally avoided in the conventional welding of stainless steels because of its effect on austenite stability, which may affect the crack susceptibility of the stainless steel. Nitrogen is a strong solid solution strengthener, increasing the 0.2% yield stress more than any other element, as illustrated in Figure 28 [85]. Nitrogen can improve the creep resistance, toughness, and corrosion resistance of stainless steels [85], [86]. Intergranular corrosion can be improved through the formation of $Cr_2N$ nitrides instead of the heavy chromium carbides ($Cr_{23}C_6$) that deplete the grain boundaries [85]. A class of stainless steels utilizes the beneficial aspects of nitrogen as a solid solution strengthener and was originally advertised as an improved 304L. These alloys are called by their tradenames of nitronic alloys, with Nitronic 40 being the most prevalent. Nitronic 40, also called, 21-6-9, contains 21 wt% Cr, 6 wt% Ni, and 9 wt% Mn, and it can have up to 0.40 wt% N per ASTM A276 [87]. Welding of these nitronic alloys depletes the fusion zone of nitrogen; therefore, additions by nitrogen gas shielding have been used.

Nitrogen is being used in the manufacture of powder through nitrogen gas atomization. The entrapment of some residual nitrogen in the powder is possible, but this has not been reported to have a significant impact on the nitrogen content of the build. The atomization gas has been shown to affect the powder size, shape, and flow characteristics, with argon shown to improve sphericity, increasing the flow properties of the powder particles [88].

Aversa studied the microstructure and mechanical properties of LP-DED 316L with the use of nitrogen as a shielding gas and in a nitrogen-filled build chamber [86]. Nitrogen-shielded 316L LP-DED builds were comparable to argon-shielded welds, with improved YSs and UTSs, but with lower elongations than wrought material. Because of the grain boundary pinning oxides in LP-DED builds, regardless of the shielding gas used, a small increase in strength was seen due to solid solution strengthening, with the majority of the strength provided by finely dispersed oxides and grain refinement [86].

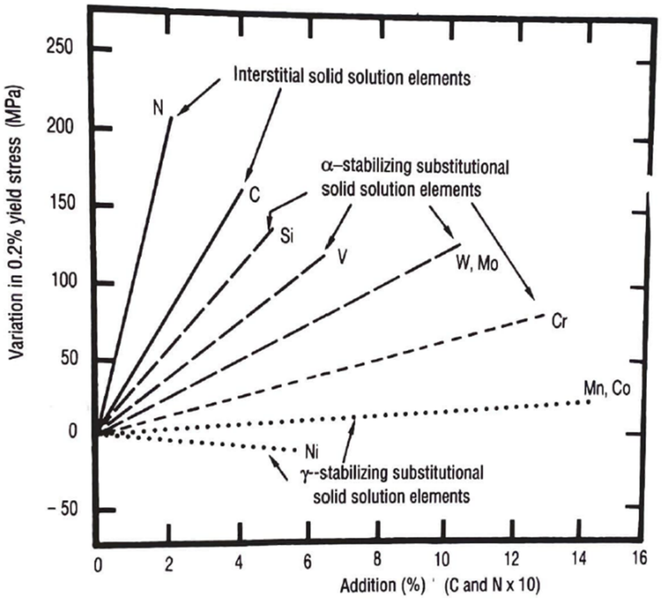


**Figure 28. Alloying element effects on yield strength** [85].

### 2.3.4 Fine Dispersed Oxides for LP-DED

Common to powder processing is the presence of fine, ~1–100 µm dispersed oxides, similar to those shown in Figure 29 [89]. Oxides and unconsumed powder are found in the builds using powder feed stock, with little-to-no oxides found in LW-DED processing. The presence of small oxides can relate to oxide-dispersion-strengthened (ODS) steels in which the incoherent, insoluble oxide is non-shearable by dislocations and leads to Orowan strengthening to elevated temperatures [90]. Eo reports (1) that YS is improved by 50 Mpa, with a higher number count density of oxide inclusions formed under different processing conditions and (2) the size of these inclusions can be maintained below several microns in diameter under the correct processing conditions [91]. Eo relates the increase in YS to the numerical density of finely dispersed oxides, consistent with precipitate strengthening [91]. A similar result is estimated by Smith et al., in which an increase in 20–28 MPa is estimated based on observation of 100–150 nm oxide precipitates. However, not all effects have been positive. Decreased toughness (Section 2.3.7.2), reduced ductility (Section 2.3.7.1), and increased SCC susceptibility (Section 2.3.7.4) are all negative effects of the dispersed oxides. Oxides have been reported to contain Si and Mn in the form of $SiO_2$, as well as $MnSiO_3$ [76], [86], [91], [92]. Heat treatments have been reported to be affected by oxides [93] because of their high melting temperatures. Heat treatments are discussed further in Section 2.3.9.

The oxide particles are remnants from the powder metallurgy process, or they are inherently picked up by the large surface area of the powder. Lou reports oxygen contents in LPBF 316L material (384 ppm) to be well above that of powder metallurgically based hot isostatic pressing (PM-HIP) material (190 ppm) and wrought material (23 ppm) [92]. Similar oxygen contents were found in LP-DED processes, with reported levels of 306 to 994 ppm [91].

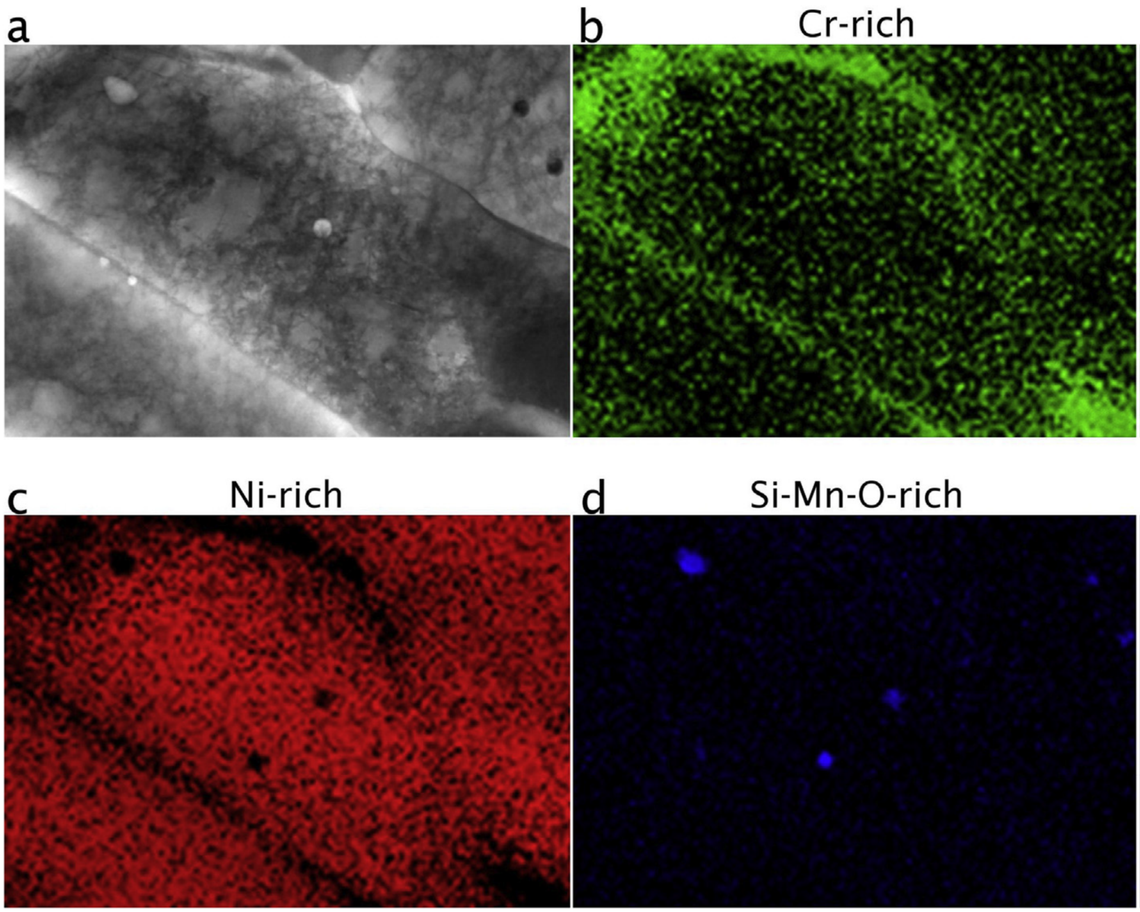


**Figure 29. Brightfield scanning transmission electron microscopy (STEM) and energy dispersive spectroscopy (EDS) of fine-scale microstructure in LP-DED 304L** showing (a) solidification structure, (b) Cr segregation to cellular solidification structure boundaries, (c) Ni depletion of these boundaries, and (d) fine Si-Mn rich oxides [89].

### 2.3.5 Dislocation Density

An additional favorable characteristic of L-DED and LPBF austenitic stainless steel microstructures is the presence of high dislocation densities in the as-built microstructures. These densities are on the order of 2–5 $10^{13}$ $m^{-2}$, which is lower than that of wrought material, but higher than that expected of cast or annealed material. As in the wrought materials, these densities can be annealed with heat treatment, but because of the oxide precipitates, recrystallization only occurs at higher temperatures, as shown in Figure 30 [94]. These high as-built dislocation densities significantly increase the YS of L-DED 316L, with a minor tradeoff with elongation, as discussed in Section 2.3.7.1.

No long-term thermal aging studies of LP-DED or LW-DED 316L or similar systems were found. Yin et al. studied thermal aging of LPBF 316L for up to 400 hours and found that the microstructure was stable at up to 600°C; at 700°C and beyond, the cellular substructure homogenized, and precipitates formed at high-angle grain boundaries [95]. Because the cellular structure and precipitation behavior is different for LP-DED and LW-DED than for LPBF, study of thermal aging effects is warranted.

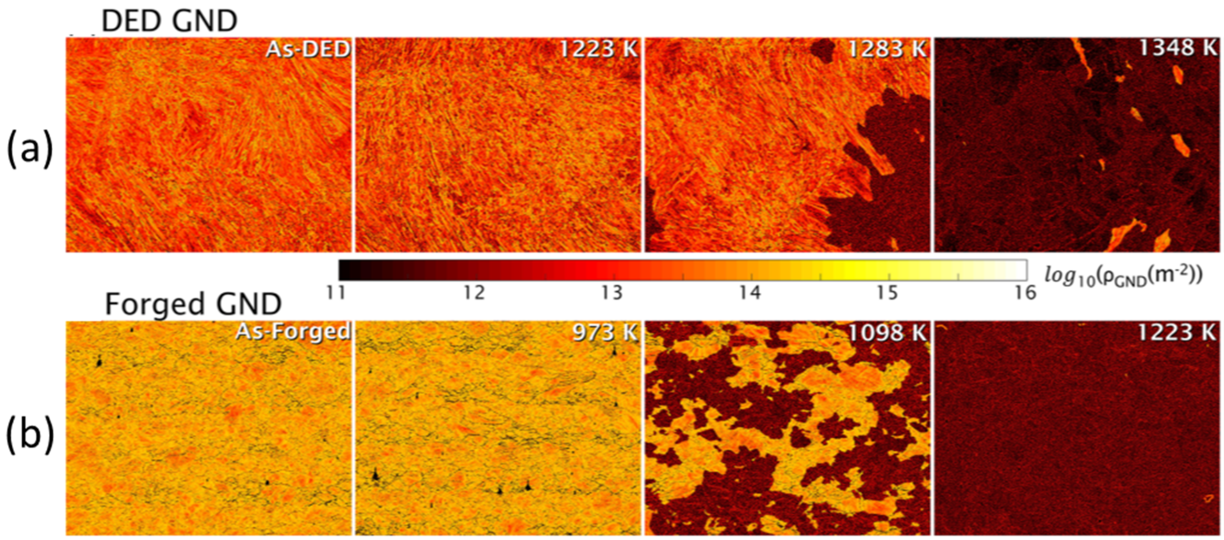


**Figure 30. Geometrically necessary dislocation (GND) concentration for AM (a) and forged (b) 316L over half-hour heat treatments at different temperatures.** LP-DED 316L recrystallizes and eliminates dislocation content at significantly higher temperatures as a result of oxide nanoprecipitates [94].

### 2.3.6 Porosity

One deleterious feature that is found to be extremely common in LP-DED and LW-DED microstructures is the presence of porosity. Porosity is more prevalent in LP-DED than in LW-DED; however, porosity is common to both laser processes. Three primary causes are cited—keyhole collapse, entrapped powder gas porosity, and lack of fusion. Keyhole collapse occurs when the cavity caused by vaporization from an excessively focused laser closes over, and a gas bubble is solidified in place. LP-DED and LW-DED utilize higher heat inputs, allowing greater time for gas bubbles to escape the melt pool with less turbulence. Entrapped powder gas porosity occurs when the feedstock powder has residual internal pores from the GA process; these gas pockets are released once the powder melts, but they do not always migrate to the melt pool surface before the melt pool solidifies and entraps them, as has been observed with synchrotron x-ray experiments [96]. This porosity can be avoided by using higher quality feedstock or powders created with a method such as PREP. Porosity can also be caused by lack of fusion, which occurs when the liquid melt pool does not possess sufficient energy to remelt a portion of the prior layer and instead simply solidifies on top of it. Such porosity is especially damaging to properties, as pores tend to be large and have sharp corners, thus concentrating stress. Proper development of the processing parameters with sufficient feedback using nondestructive examination (NDE) methods to characterize porosity can greatly reduce porosity formation.

### 2.3.7 Properties of L-DED 316L

Many studies have investigated the properties of L-DED manufactured 316L; however, because of the sensitivity of the microstructure to the processing parameters, reported results vary significantly.

Differences in processing conditions such as heat input, powder chemistry, powder re-use, wire size, and shielding gas affect the microstructural evolution of the component, which therefore results in varying chemical and mechanical properties. Reported results do not always contain all the information needed to fully recreate the test and are typically focused on a particular aspect of study. Some skepticism is required when approaching the reported properties of L-DED fabricated 316L, despite the apparent abundance of data in the literature. Properties achieved in one L-DED study may not transfer directly to another L-DED study because of different component histories.

Because of this large inter-study variability, this report does not comprehensively agglomerate all efforts that report L-DED 316L properties. Instead, this work focuses on literature that explains the mechanistic links between microstructure and observed properties. Five pertinent property families of L-DED fabricated 316L are discussed below: tensile properties, fracture toughness, hardness, fatigue strength, and corrosion. In this evaluation, L-DED builds are primarily reported with the use of powder, as in LP-DED processing. As mentioned in Section 2.1, there is significant overlap between the build volumes, melt pool size, and mechanical properties of LP-DED and LW-DED builds. In 316L, the two processes may share similar or equivalent properties, but similar properties should not be assumed for the full range of heat inputs or for other alloy systems. Because LW-DED has similarities to a multi-pass laser weld, its research can benefit from the large amount of laser welding literature available. LW-DED as an AM process is less developed than LP-DED, with limited 316L properties reported. The added oxides, porosity, and dislocation density of powder-based methods will affect the mechanical and chemical properties in different ways than in wrought materials, so these are the focus of the sections below.

#### 2.3.7.1 Tensile properties

Tensile properties of 316L manufactured by LP-DED and LPBF are reported numerous times in the literature under a large variety of manufacturing conditions. Some as-built (i.e., no post-processing) properties are summarized by DebRoy et al. [78] in Table 3 below. In general, austenitic stainless steels fabricated through both processes show some anisotropy in material properties, and elongated grains and dendrites oriented in the Z-axis are often observed [97]–[101]. L-DED has a higher sensitivity to geometry orientation than LPBF. This is attributed to incomplete thermal dissipation between layers, which can lead to a buildup of residual heat. This in turn affects the solidification and microstructure of the component and residual stresses present [102]. YS and UTS are often comparable or superior to that obtained using conventionally manufactured annealed austenitic stainless steels, while elongation at failure is decreased [98], [101], [103]–[105].

While there is no standard for L-DED 316L tensile properties, the values in Table 3 can be compared to the specifications for LPBF and rolled conditions. ASTM F3184-16, "Standard Specification for Additive Manufacturing Stainless Steel Alloy (UNS S31603) with Powder Bed Fusion" [106], specifies minimum requirements of 207 MPa for YS, 517 MPa for UTS, and 30% elongation at failure for LPBF 316L. ASTM A276-17, "Standard Specification for Stainless Steel Bars and Shapes," specifies 310–515 MPa for YS, 550–655 MPa for UTS, and 25–30% elongation at failure for conventionally manufactured cold rolled 316L, depending on size [107]. Lack of fusion defects are responsible for reduced elongation results in some builds, as reported by Wilson and Scipioni Bertoli [76], [83]. In Figure 31 and Figure 32, results for LP-DED and LPBF as collated by DebRoy are compared against annealed and cast conditions [78]. DebRoy generalizes the results in YS and UTS as equal or higher in the build layer (X-Y) compared to the build direction (Z). The variability in reported mechanical properties was attributed to differences in laser types, actual energy used, and scan strategy. As DebRoy points out, it is difficult to compare results because of the undisclosed hatch spacing, layer thickness, and limited data access to scan strategies of commercial AM systems [78].

Aversa reports higher TS and UTS results with smaller oxides and nitrogen content [86]. Wang compared 316L DED to wrought plate [108]. Grain size according to the Hall-Petch relationship, correlating small grains with increased strength, was valid for DED components, as well as the use of lower heat inputs to achieve a finer grain structure and resultant higher YS. Poor elongation of the DED material was attributed to the columnar elongated grains in the Z direction. Wang evaluated the presence of martensite using magnetic permeability and optical means. The presence of martensite was not detected in the DED material, whereas small amounts were detected in the deformed wrought material. Wang attributed the higher TS of the wrought material to the stress-induced martensite, which allowed higher strength with minimal loss in ductility. Using electron diffraction techniques, Shiau was able to detect the formation of strain-induced martensite around nanopores and at sub-grain boundaries of 316L DED material [109]. The martensite detected by Shiau was seen at around 200 nm pores, and a vol% value was not reported. It is unclear whether the amount of martensite seen by Shiau would be measurable using magnetic permeability, as done by Wang [108].

**Table 3. Tensile mechanical properties for LP-DED and LPBF as-built, as collated by DebRoy et al.** [78]

| Material | P (W) | V (mm/s) | ρ (%) | Orient. | $\sigma_y$ (MPa) | $\sigma_{UTS}$ (MPa) | El. (%) | HV |
|---|---|---|---|---|---|---|---|---|
| | | | | **DED – Powder Feedstock** | | | | |
| 304 | - | - | 100 | Long. | 448 | 710 | 59 | |
| | | | | Transv. | 324 | 655 | 70 | |
| 304L | 2,300 | 9. | >99.9 | Long. | 337 ± 29 | 609 ± 18 | 48.2 ± 2.5 | |
| | | | | Transv. | 314 ± 6 | 606 ± 13 | 56.4 ± 5.8 | |
| | 4,000 | 11 | | Long. | 277 ± 27 | 581 ± 20 | 41.8 ± 3.5 | - |
| | | | | Transv. | 274 ± 7 | 560 ± 12 | 50.5 ± 6.7 | - |
| 316 | | - | 100 | Long. | 593 | 807 | 33 | - |
| | | | | Transv. | 448 | 793 | 36-66 | - |
| 316 | | | 93.2–97.4 | Long. | 363-487 | 648–970 | 20-44 | |
| 316 | 600–1,400 | 2–10 | - | Long. | 558 | 639 | 21 | 310–350 |
| | | | | Transv. | 352 | 536 | 46 | |
| 316L | 570 | 13 | 100 | Long. | 490 ± 8 | 685 ± 5 | 51 ± 2 | 164–215 |
| | | | | Transv. | 280 ± 6 | 580 ± 10 | 62 ± 5 | - |
| 316L | 1,000 | 6 | - | Long. | - | 812–901 | 9-15 | 305 |
| 316L | 400 | 15 | 100 | Long. | 576 | 776 | 33 | 272 ± 35 |
| | | | | Transv. | 479 | 703 | 46 | 289 ± 16 |
| 316L | 1,650 | 23 | 98 | Transv. | 450 | 510 | 20 | 270 |
| | 1,450 | 20 | 97 | Transv. | 440 | 470 | 18 | 240 |
| | 1,150 | 17 | 97 | Transv. | 410 | 460 | 22 | 215 |
| | 1,000 | 13 | 96 | Transv. | 420 | 440 | 15 | 220 |
| | 800 | 10 | 96 | Transv. | 405 | 430 | 14 | 220 |
| | | | | **Powder Bed Fusion** | | | | |
| 304 | 200 | 25 | 100 | Long. | 520 | 710 | 38 | - |
| | | | | Transv. | 450 | 580 | 58 | - |
| 304L | 95 | 70 | - | Long. | 182 | 393 | 26 | 217 |
| | | 90 | - | | 156 | 389 | 22 | 209 |
| 316L | 200 | ≤1,000 | 100. | Long. | 602 ± 47 | 664 ± 7 | 30 ± 0 | 235 |
| | | | | Transv. | 557 ± 14 | 591 ± 12 | 42 ± 2 | - |
| 316L | 100 | 400 | 97.2 ± 1.2 | Long. | 438 ± 28 | 528 ± 23 | 10 ± 2 | - |
| | | | | Transv. | 435 ± 2 | 504 ± 12 | 16 ± 3 | - |
| | | 591 | 98.5± 1.4 | Long. | 379 ± 17 | 489 ± 28 | 23 ± 6 | - |
| | | | | Transv. | 287 ± 6 | 317 ± 11 | 7 ± 4 | - |
| | | 600 | 98 ± 1.0 | Long. | 399 ± 29 | 486 ± 40 | 9 ± 3 | |
| | | | | Transv. | 316 ± 6 | 367 ± 6 | 7 ± 1 | |
| 316L | 175 | 700 | 97.5 ± 1 | Long. | 534 ± 5.7 | 653 ± 3.4 | 16.2 ± 0.8 | |
| | | | 93.8 ± 2.6 | Transv. | 444 ± 26.5 | 567 ± 18.6 | 8 ± 2.9 | |
| 316L | 380 | 635–3,000 | >99 | - | - | - | - | 220–213 |
| 316L | 100 | 300 | 99. | - | - | 501.1 ± 8.3 | - | - |
| 316L | 103 | 425 | - | Transv. | 640 | 760 | 30 | - |
| | | | | **Traditionally processed** | | | | |
| 304L | Annealed | | | | 168 | 556 | 61 | 136 |
| 304L | Annealed | | | | 265 ± 9 | 722 ± 14 | 62.3 ± 2.6 | - |
| 316L | Cast | | | | 365 ± 22 | 596 ± 16 | 69 ± 9 | - |
| 316L | Annealed | | | | 241 | 586 | 50 | 215–225 |

P: laser power, S: scan speed, ρ: density, $\sigma_y$: YS, $\sigma_{UTS}$: ultimate strength, EL: elongation, HV: Vickers hardness

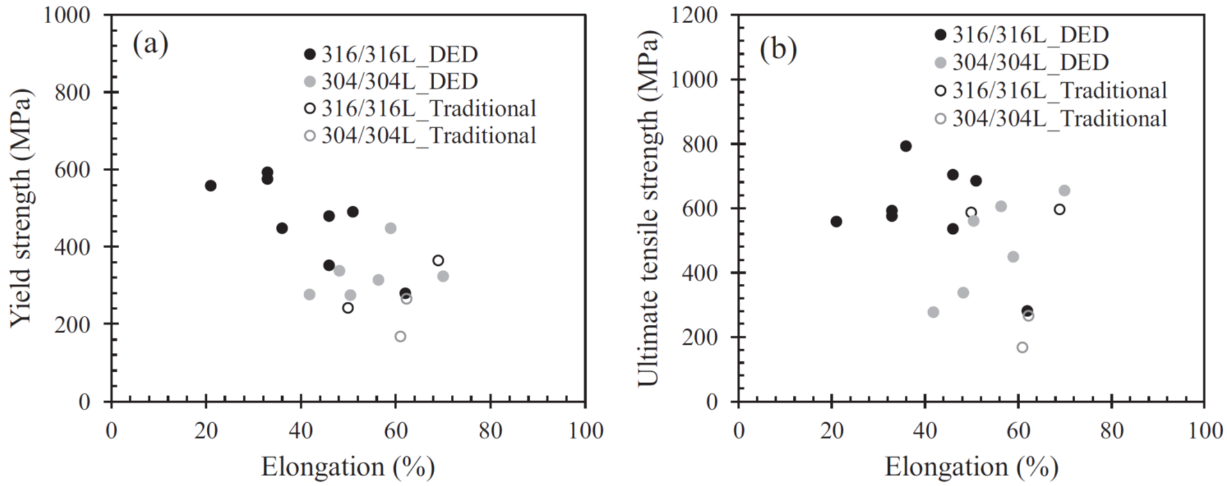


**Figure 31. Tensile mechanical properties from Table 3 of LP-DED austenitic stainless steel compared to that obtained using other manufacturing methods [78].**

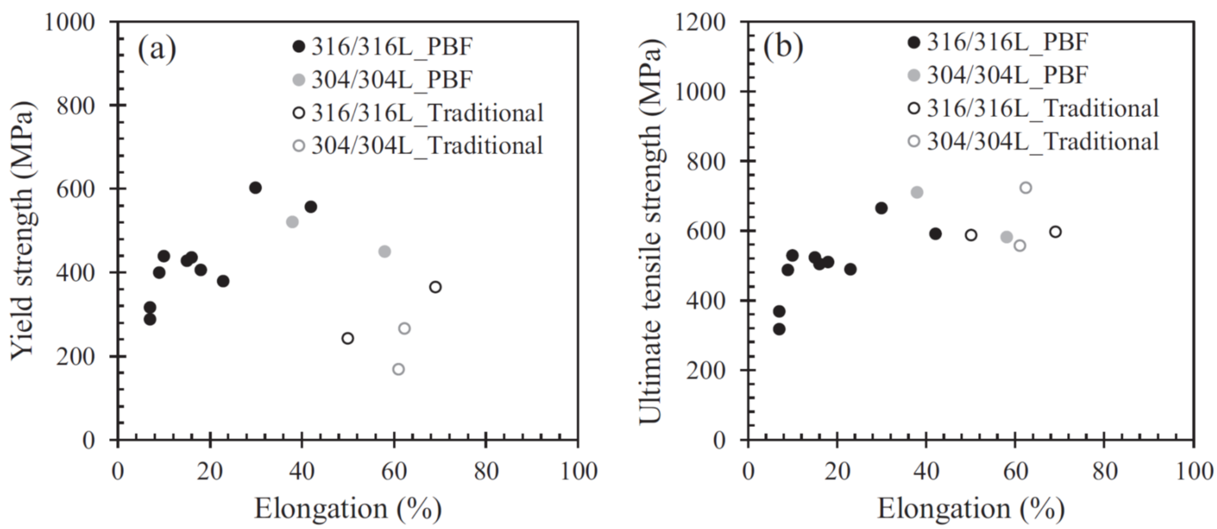


**Figure 32. Tensile mechanical properties from Table 3 of LPBF austenitic stainless steel compared to that obtained using other manufacturing methods [78].**

LW-DED tensile properties were reported by Akbari. As shown in Figure 33, two build configurations were made: a thin wall and a block. The geometry orientation affects the tensile strength of the material, as reported for LP-DED. Heat sinking between the two orientations provides a different thermal history to the melt, resulting in a difference in tensile strength. A larger difference in strength was seen between the thin wall and block orientations than in the tensile bar orientation. The tensile properties are shown in Table 4 [110].

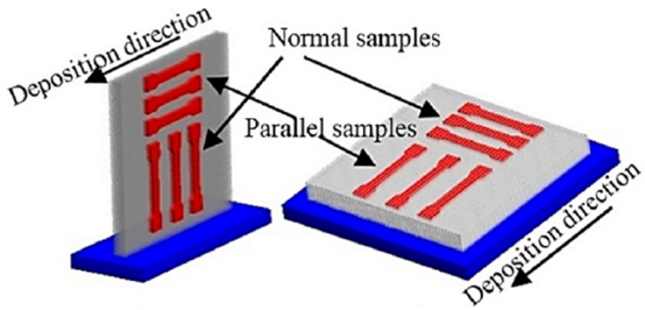


**Figure 33. LW-DED deposition orientations showing thin wall (left), and block (right)** [110].

**Table 4. Tensile mechanical properties for LW-DED** [110]

| Material | P (W) | V (mm/s) | Wire feed speed | Orientation | $\sigma_y$ (MPa) | $\sigma_{UTS}$ (MPa) | El. (%) | HV |
|---|---|---|---|---|---|---|---|---|
| | | | | **DED –wire feedstock** | | | | |
| 316LSi | 1,000 | 8 | 12 | Block parallel | 430–440 | 629–635 | 36–40 | 226 |
| | | | | Block perpendicular | 415–425 | 593–600 | 30–37 | 226 |
| | | | | Thin wall parallel | 260–300 | 516–546 | 39–42 | 216 |
| | | | | Thin wall perpendicular | 220–270 | 484–522 | 32–40 | 216 |

P: laser power, $\sigma_y$: YS, $\sigma_{UTS}$: ultimate strength, EL: elongation, HV: Vickers hardness

### 2.3.7.2 Fracture and impact toughness

According to powder metallurgy literature, impact toughness and fracture toughness are known to be sensitive to oxide precipitation, impurity content, and grain structure in 316L. As such, these properties are expected to be sensitive to any processing parameter that effects these microstructural features in both LP-DED and LW-DED. Literature examining crack propagation energy in 316L L-DED is sparser than that for tensile properties; however, several studies exemplify the relevant mechanisms.

The Charpy impact toughness of LP-DED 316L was studied as a function of scan strategy by Kono et al. [111]. The reported average for impact toughness was 112 J/cm$^2$, with a variation of less than 10% across the scan strategies evaluated. This can be compared to the Charpy impact toughness of LPBF, PM-HIP, and wrought 316L as investigated by Lou [92]. LPBF impact toughness was reported to 130–150 J/cm$^2$. Wrought material is generally considered to be greater than 200 J/cm$^2$ and was reported up to 350 J/cm$^2$. AM powder–based processes use similar powder as powder metallurgy, and oxide precipitates form in both. Cooper evaluated the fracture toughness of PM-HIP material and developed a correlation between impact energy and oxygen content. A reduction to 150 J was found, with an oxygen content of 190 ppm at room temperature [112]. A toughness of 335 J was reported, with 23 ppm oxygen. Expectations for LP-DED processes are expected to follow suit since oxidized content cannot be avoided when using powder, and its degradation of fracture toughness in stainless steels is well documented. Fracture toughness of 316L PM-HIP material vs. oxygen content was plotted by Cooper and is shown in Figure 34 [112]. For LP-DED, oxide inclusions and unconsumed powder act as early nucleation sites for microvoid coalescence, resulting in lower impact toughness [92]. Lou concludes that the reduced impact toughness was a result of the elevated oxygen level and oxide particles [92]. A value of 0.03 vol.% oxide inclusions is reported to reduce fracture toughness to less than 150 J [112].

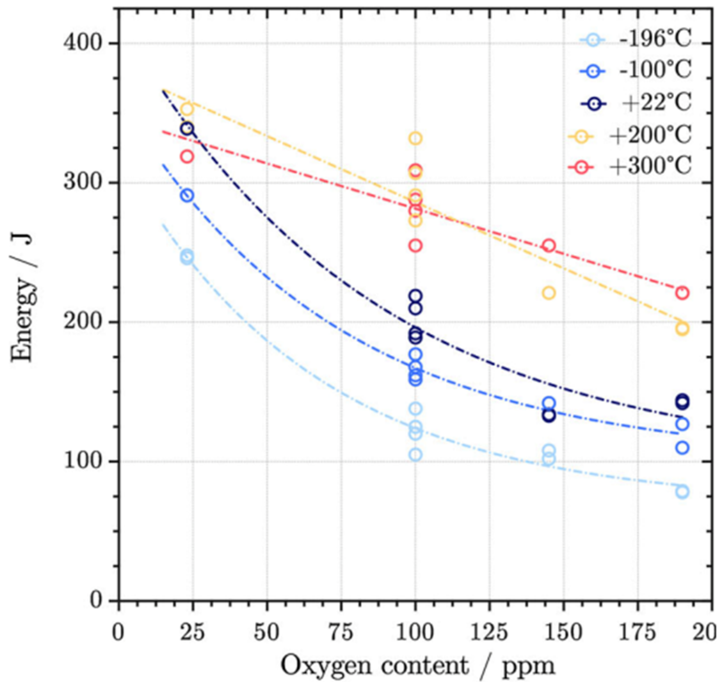


**Figure 34. Charpy impact energy vs. oxygen content (ppm) of PM-HIP material** [112].

McWilliams et al. [113] investigated LP-DED (via laser-engineered net shaping [LENS]®) 304L fracture toughness and the effect of hydrogen charging via the three-point bend technique. As shown in Figure 35 and Table 5, they found nearly identical to substantially lower toughness values for LP-DED, ranging from ~98 to ~46% that of forged samples, with a large dependence on orientation. Hydrogen charging further reduced the fracture toughness of both forged and LP-DED samples by approximately 60 and 70%, respectively, with LP-DED being somewhat more sensitive.

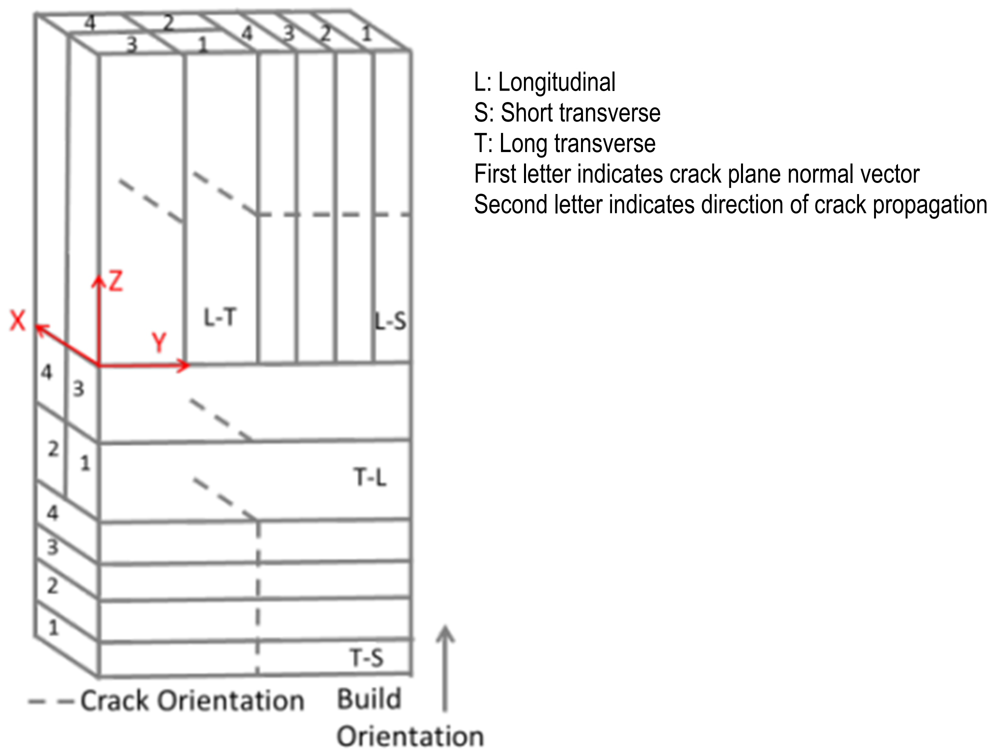


**Figure 35. Orientation schematic for fracture toughness specimens in Table 5 [113] using notation from ASTM E1823.**

The fracture surfaces evaluated by McWilliams showed a ductile failure with microvoid coalescence in the as-deposited state [113]. A fracture surface of an as-deposited sample is shown in Figure 36. McWilliams notes the high density of the material, as well as the presence of silica particles and unconsumed particles in the microvoids, which likely acted as nucleation sites [113].

**Table 5. Fracture toughness ($kJ/m^2$) of forged and L-DED 304L in as-built and hydrogen-charged conditions** [113]

| Direction | Forged (as-built) | Forged ($H_2$) | L-DED (as-built) | L-DED ($H_2$) | L-DED/ Forged (as-built) | L-DED/ Forged ($H_2$) |
|---|---|---|---|---|---|---|
| LS | 1,578 | 844 | 1,546 | 510 | 98% | 60% |
| LT | 2,088 | 831 | 1,538 | 461 | 74% | 55% |
| TL | 1,998 | 901 | 1,119 | 349 | 56% | 39% |
| TS | 2,096 | 815 | 967 | 360 | 46% | 44% |

L: Longitudinal, S: Short transverse, T: Long transverse
First letter indicates crack plane normal vector
Second letter indicates direction of crack propagation

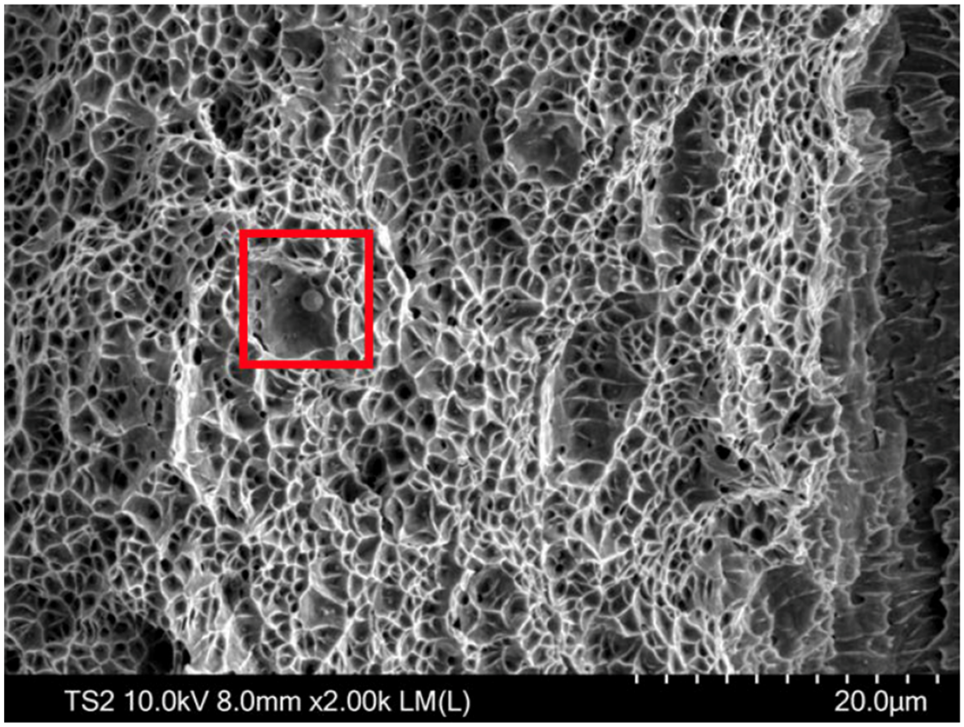


**Figure 36. Fracture surface of as-deposited LENS 304L sample showing unconsumed particle in void** [113].

Annealing and homogenization heat treatments have been shown to affect the oxide size and distribution, dislocation density, and grain structure of L-DED, which would be expected to influence fracture toughness. As shown in other fracture toughness studies of electron beam–welded (EBW) metal AM displayed in Figure 37 [114], exact test results depend strongly on the microstructure, porosity, and oxide content local to the crack.

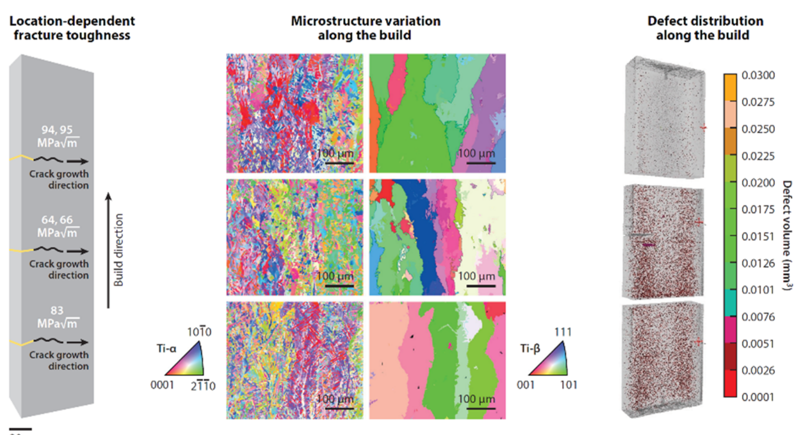


**Figure 37. Illustration of the nonhomogeneous microstructure effects on AM fracture toughness; sample is EBW Ti-6Al-4V [114].**

### 2.3.7.3 Fatigue properties

Fatigue properties of AM materials are generally poor in as-processed builds as a result of the surface roughness of unmachined surfaces, lack of fusion, porosity, and large irregular oxides [78]. Defects located near the surfaces of the samples tend to be more detrimental [115]. The fatigue lives of LPBF, LP-

DED, and LW-DED components share many of the same mechanistic features; therefore, the similar results can be expected. Feature sizes should be considered when comparing processes, but the same procedures used to improve fatigue will apply to both: surface machining, heat treatments, and hot isostatic pressing (HIP). The two most common defects found in AM—lack of fusion and porosity—have a significant effect on the fatigue life of AM components [78], [116]. Study results from Xu et al. [117] show fatigue crack growth in LENS LP-DED 316L, which provides mechanistic explanations of fatigue behavior. An interaction was observed between the elongated grain morphology, which causes some anisotropy in crack propagation along or across the build direction, as shown in Figure 38. As seen in the detail of subfigures b and c, as the crack propagates across layer interfacial boundaries, the growth rate is slowed. Sections 1 through 8 in subfigure C show positions of crack growth rate analysis. The dashed lines in subfigures c, d, and e are layer boundaries. The previously deposited layers will be subjected to additional thermal cycles from the subsequently deposited layers. Xu notes the drop in crack growth rate as the crack progressed through build layers. A change in the microstructure from coarsened grains, with fewer dislocations in the heat-affected zone of each layer to a finer grain structure with higher dislocation density, was observed. The coarsened grain structures show faster crack growth rates than the finer grain structures in subsequently deposited layer. Subfigures d and e show optical microscopy detail from the two interfaces denoted in c. No interaction with pores smaller than 1 μm was observed, and some interaction with the nanoscale precipitates was seen.

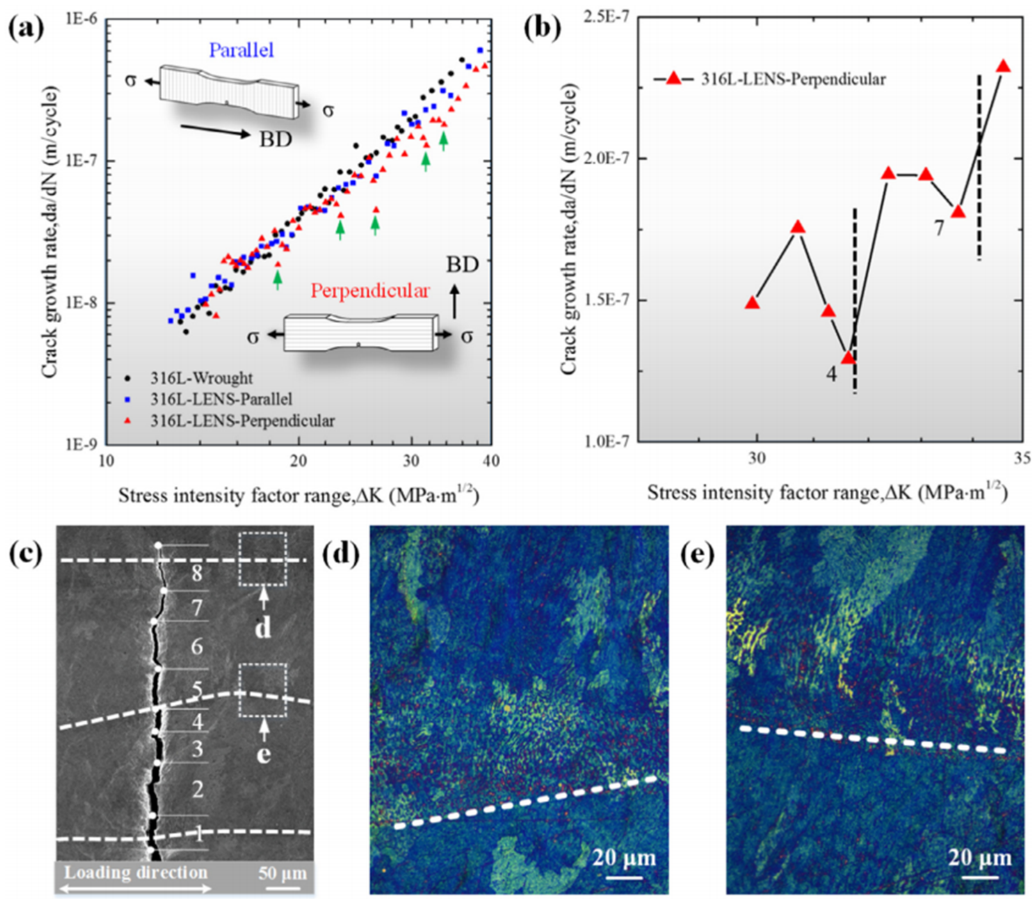


**Figure 38. Fatigue crack growth in LENS LP-DED 316L [117]: (a) crack growth rates (green arrows point to crack retardation regions of perpendicular sample); (b) magnified region of perpendicular sample; (c) metallograph showing build layers (dashed lines) and fatigue crack growth rate intervals (1–8); (d) and (e) metallographs at layer interfaces in (c).**

In another study, fatigue life of LP-DED 304L was explored as a function of porosity, as shown in Figure 39 [118]. Lower density samples demonstrated reduced fatigue life, and fractography showed interaction between larger lack of fusion defects and the propagating crack. Interestingly, the differences between the wrought and different LP-DED densities were well accounted for when normalizing by experimental UTS. This implies two things about LP-DED austenitic stainless steels: first, that when porosity is minimized through process optimization, the fatigue life will approach that of wrought performance, and second, other less time-consuming test methods that are sensitive to porosity such as tensile testing can provide more rapid, informative feedback for process optimization.

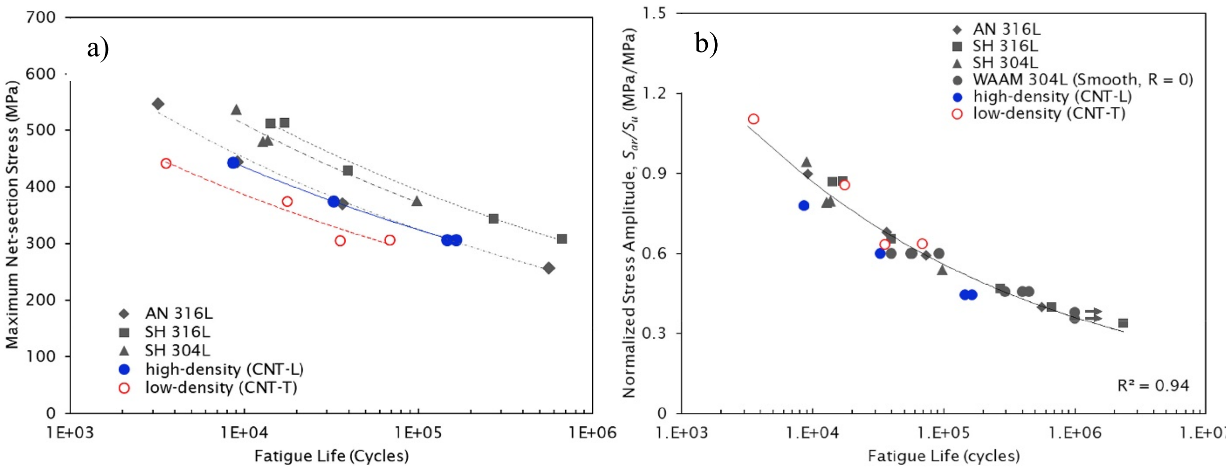


**Figure 39. (a) Fatigue life of annealed (AN) and strain hardened (SH), wrought 316L and 304L compared with LP-DED manufactured 304L samples with low and high (>98.5%) densities; (b) fatigue life with stress amplitude normalized by UTS, including effects from porosity [118].**

A comparison between LP-DED and LW-DED was conducted by Blinn [119]. The LW-DED process resulted in significantly higher fatigue strength than the LP-DED. Higher fatigue strength was attributed to a higher delta ferrite phase fraction and smaller grain size of the wire-based process [119].

In general, fatigue life of 316L AM builds can be improved from as-deposited levels below wrought materials to values that exceed the high cycle performance of wrought material. Processing parameters should be optimized to control heat input while minimizing internal defects such as irregular shaped oxides and large pores. Deposited builds can then be surface machined and/or polished to remove crack notch initiation sites [78], [115], [116].

### 2.3.7.4 Corrosion properties

The corrosion properties of stainless steel are well documented. Chromium depletion caused by the formation of chromium carbides in the heat-affected zones of welds are well documented and have led to the development of low carbon grades (304L). As discussed in this report, LP-DED and LW-DED result in microstructures very similar to welding, so it is likely that much of the established corrosion properties of austenitic stainless steel welds are valid. The corrosion potential depends upon a number of factors such as corrosion environment, degree of sensitization, grain structure, grain size, passive film stability, elemental segregation, and material composition [120]. The part's residual stress also plays a role, particularly in SCC. As discussed above, different DED processes/heat inputs will affect grain structure/size, elemental segregation, and sensitization. Cooling rate differences may shift the phase balance to result in higher volume fractions of austenite than in traditional arc welds, which may enhance corrosion resistance in some environments. Stull et al. [121] compared LP-DED 316L to wrought 316L under heat-treated and non–heat-treated conditions. Etched micrographs are shown in Figure 40; the LP-

DED 316L solidified with a primary ferrite cellular dendritic structure because of an out-of-spec chromium content. This caused chromium and molybdenum enrichment at the cell core, which is the inverse of other study results of 316L subjected to primary austenite solidification [81]. The out-of-spec chromium content  was found to increase sensitization as a result of chromium carbide precipitation, which depleted grain boundary chrome content. This in turn led to preferential breakdown of the passivation oxide layer, which is similar to what occurs in welded 316L. Potentiodynamic sweeps measuring activation potential showed that heat treatment decreased the sensitization of the LP-DED specimen, suggesting an increased resistance to intergranular corrosion and intergranular SCC. Heat treatment allowed for homogenization of the compositional segregation, as shown in Figure 40 (c) and (d), suggesting that further heat treatment optimization may allow L-DED 316L to reclaim more of its corrosion resistance. Differences in sensitization from chromium enrichment in primary austenite vs. primary ferrite solidification were not studied, but it is likely that heat treatment and homogenization would also improve the corrosion-resistance properties of primary austenite. The use of nitrogen to prevent the formation of chromium-rich $Cr_{23}C_6$ carbides, as discussed in Section 2.3.3, can also be used to prevent intergranular corrosion.

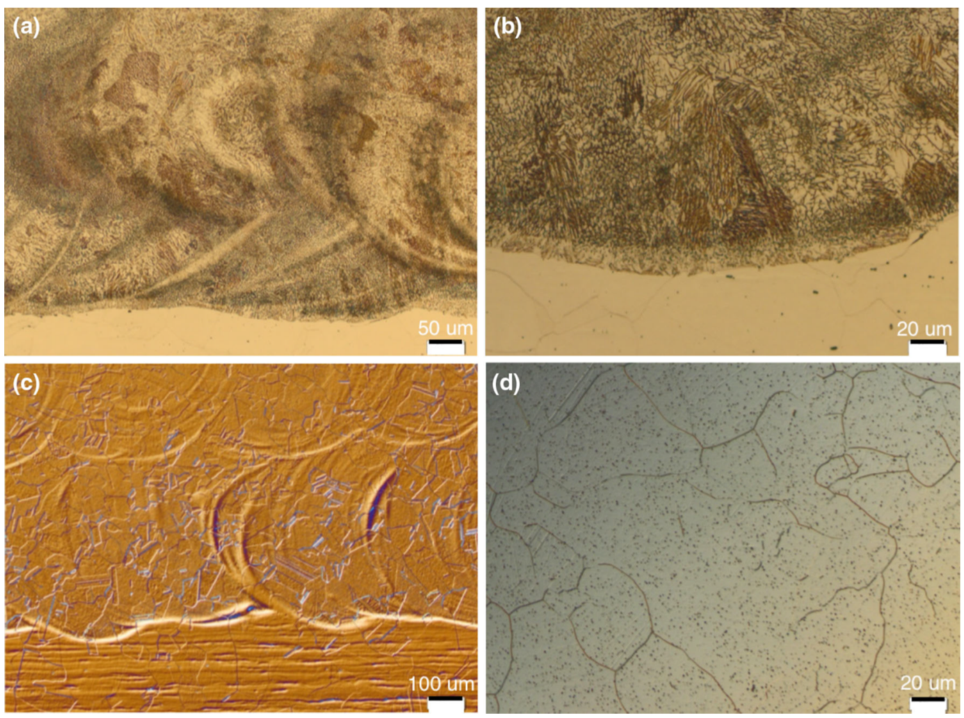


**Figure 40. Optical micrographs of LP-DED 316L, in non–heat-treated (a, b) and heat-treated (c, d) conditions [121].**

In a study of a similar 304L alloy deposited with LP-DED [122], Melia et al. contrasted the different active microstructural effects controlling electrochemical behavior. In order of importance, it was found that porosity, interdendritic delta ferrite, oxide inclusions, and preferential dissolution of gamma austenite surrounding the delta phase contributed to breakdown in corrosion resistance. The study also found that, although oxide precipitates were significantly refined from wrought components, the reduction in corrosion potential from that phenomenon was overshadowed by porosity and galvanic effects. As shown in Figure 41, the lack-of-fusion type (a, b and c) and gas pore (d, e, and f) in an LP-DED 304 sample were measured with profilometry and optical microscopy before and after polarization and electrochemical attack. The results clearly show that pore geometry can interact with and provide initiation sites for corrosion pit formation; this effect can confound electrochemical polarization results, which is expected to be true of LP-DED and LW-DED 316L, as well.

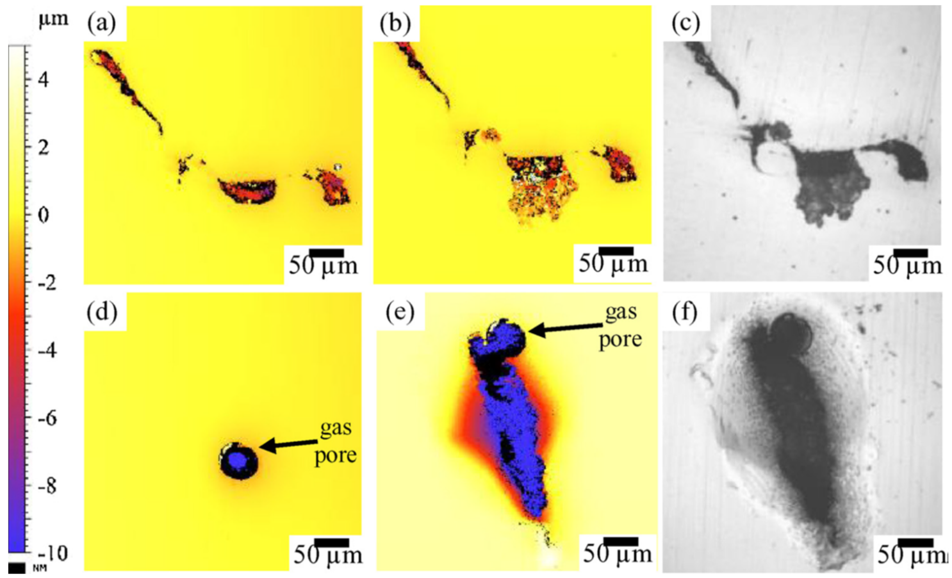


**Figure 41. Profilometry and optical microscopy showing preferential attack of pores: both lack of fusion type (a–c), and gas porosity (d–f) [122] for an LP-DED 304L sample.**

Results from Chen et al. show promise in processing 316L using hybrid manufacturing techniques incorporating LW-DED [123]. In this work, the poor surface finish of LW-DED 316L responsible for corrosion attack was machined using integrated subtractive tooling. The surface was then remelted using the AM laser, which formed high-phase fractions of delta phases and eliminated sigma phases, significantly increasing corrosion resistance.

Lou reports crack growth rates during SCC of LP-DED–produced 316L that are similar to those seen in wrought material [92]. Tests were conducted in boiling water reactor conditions at 288°C. Intergranular cracks were seen in the AM material, with levels of branching higher than those than seen in the wrought heats. Silicon oxides were completely dissolved along grain boundaries in the boiling water reactor conditions, thus allowing chromium-rich oxides to form around their original locations. The soluble silicas allowed for localized corrosion at the crack interfaces, which accelerated corrosion and provided a pathway for additional crack branching. The silicon oxides were reported to be detrimental to SCC because they reduced the protective oxide and increased oxidation susceptibility [92].

Research into the corrosion properties of AM 316L primarily showed corrosion resistance that was comparable-to-better than that of wrought material [92], [122]–[124]. However, the use of powder in DED processes may introduce the unconsumed powder, pores, and oxides often found at grain boundaries. These properties are seen in both LPBF and LP-DED materials. As described in this document's sister report by Simpson and Dehoff [22, Section 2.4.1] and the NRC's technical assessment [125], L-DED and LPBF 316L have similar microstructural features. Irradiation of LP-DED and LW-DED material may have an effect on corrosion resistance; see Section 2.3.8 for additional discussion.

### 2.3.8 Properties of Irradiated L-DED 316L

The majority of studies that evaluated irradiation of AM materials analyzed LPBF processes. As of this writing, there is insufficient information to determine if studies conducted on LPBF directly correlate to those on LP-DED. However, the AM field—specifically in the areas of LP-DED and LW-DED—is rapidly developing, and new literature is frequently being published. Because of the strong microstructural- and defect-sensitive nature of the irradiation response, further work is needed. LW-DED analysis will benefit from existing information on weld irradiation responses; however, microstructural and defect aspects specific to LW-DED should be evaluated.

Two papers developed by Idaho National Laboratory present evaluations of the irradiation response of LP-DED with blown powder from a LENS system [109], [126]. McMurtrey evaluated LP-DED of 316L by normalizing the microstructure through a solution anneal and HIP to achieve wrought-like microstructure. A solution heat treatment at 983°C for 45 minutes was used, although an equiaxed grain structure was not achieved. A cellular grain structure remained in the LP-DED samples, with large pores approximately 40 μm in diameter, and small pores approximately 400 nm in diameter, with lower dislocation density than wrought. Irradiation of the samples resulted in fewer void formations in the LP-DED samples, although those that existed were larger in size. TEM images of the post-irradiation voids in LP-DED and wrought material can be seen in Figure 43. The quantity of void formations is believed to relate closely to the irradiation-assisted SCC (IASCC) resistance. Comparing the number of cracks and total length of cracks in the LP-DED and wrought materials, the LP-DED material was found to have lower IASCC susceptibility [126]. Further analysis of as-processed LP-DED material by Shiau had similar results, with fewer but larger voids after irradiation in the LP-DED samples having a lower dislocation loop density. It is theorized that the nano-sized pores created during LP-DED processing act as irradiation-induced defect sinks [109], [126]. The accumulation of irradiation-induced voids at existing pore sites instead of the nucleation of new voids may reduce localized stresses. IASCC susceptibility is thereby reduced through a lower density of radiation defects [126].

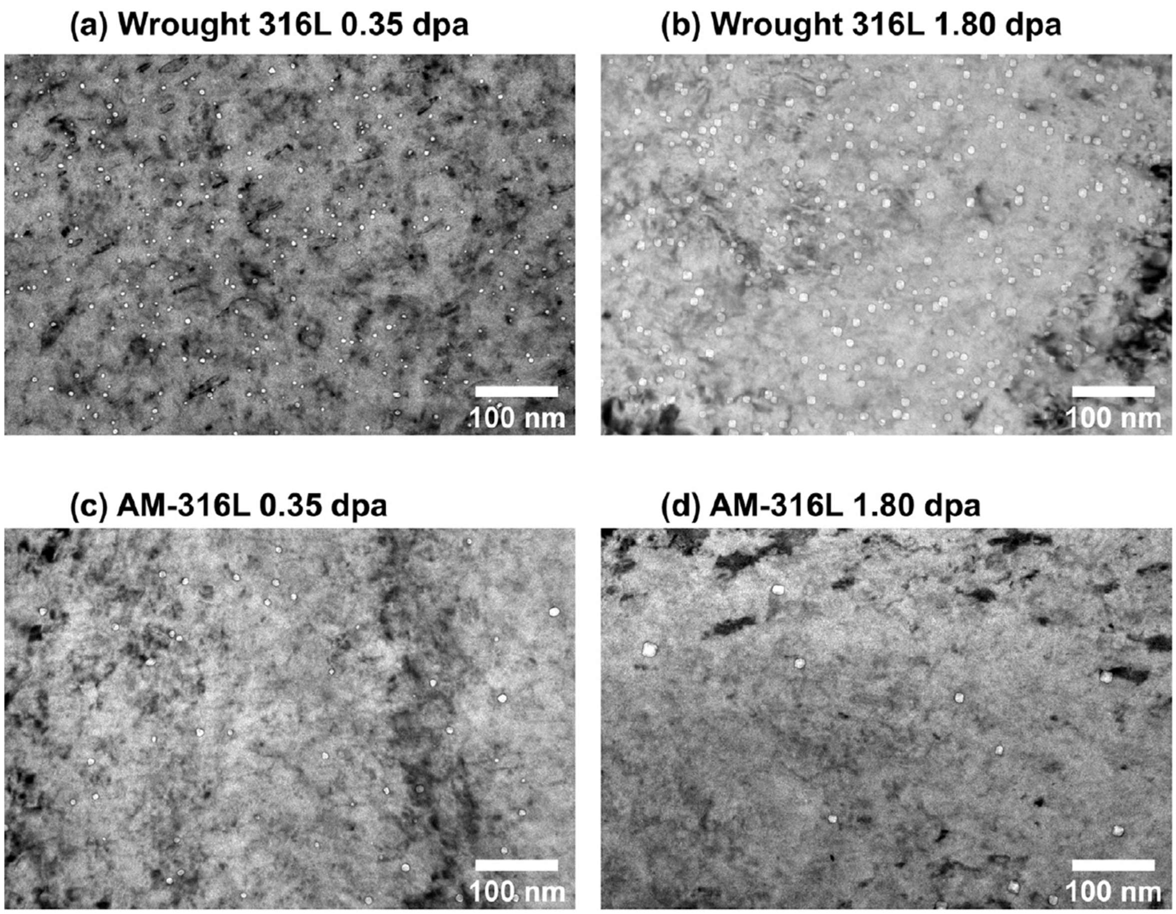


**Figure 42. TEM images of 316L LP-DED irradiation-induced void formation** [109].

### 2.3.9 Hot Isostatic Pressing and Heat Treatments

Hot isostatic pressing (HIP) is a method in which components are heated in the presence of a high-pressure inert gas environment to mitigate internal porosity [127]. Internal cracks may also be remediated by HIP, as demonstrated in LPBF-fabricated Ni superalloy components [128]. However, surface-connected cracks remain after HIP.

HIP is generally considered one of the most effective ways to mitigate the porosity defects characteristic of the AM processes, including LP-DED and LW-DED. However, like heat treatment, HIP induces microstructure changes similar to those that result from annealing, which can negate some of the beneficial features of the as-built structure.

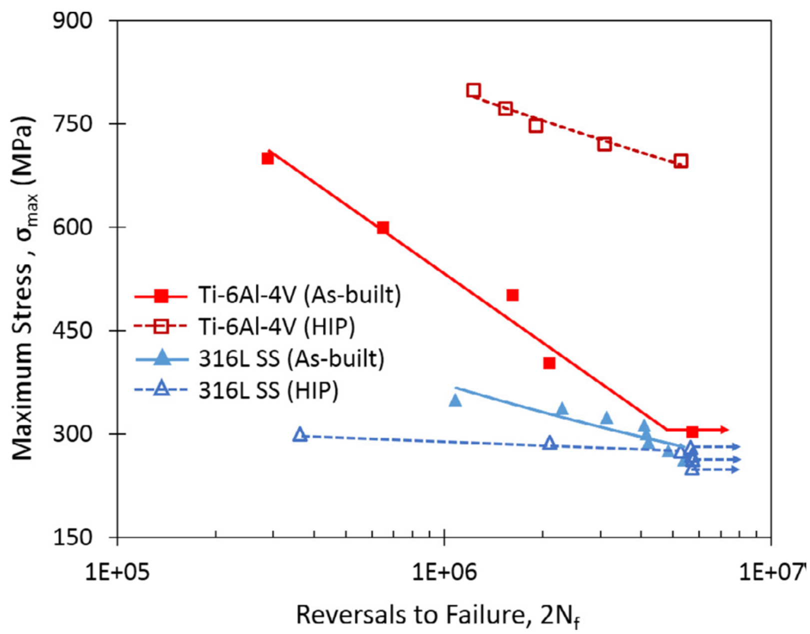


**Figure 43. Hot isostatic pressing (HIP) effects on LPBF 316L[129]. HIP substantially improves Ti-6Al-4V through porosity reduction, but in the 316L samples, porosity was already low in the as-built state; HIP instead annealed the material and reduced the YS, decreasing low-cycle fatigue performance.**

There are less studies investigating the effects of HIP on LP-DED or LW-DED 316L than those addressing the effects of HIP on LPBF; however, analysis of the effects observed in LPBF can be useful, as there is a fair degree of similarity in the microstructural features observed. As shown in Figure 43, in LPBF HIP substantially improved fatigue performance in Ti-6Al-4V samples with the closure of porosity; however, for samples of 316L that were already dense, the reduction in YS from annealing effects outweighed any reduction in porosity. The difference in YS and UTS between as-fabricated and HIP treated samples from grain size cannot be directly correlated because of the often-significant effects of phase transformations and precipitation. However, Young's modulus is usually negligibly affected by HIP. Porosity and internal cracks are typically reduced by an order of magnitude in volume. Treatment times as short as 4 minutes have been shown to reduce porosity just as significantly as treatments lasting 3–4 hours [130], suggesting that lengthy treatments to reduce porosity may not be necessary.

Studies in which HIP was followed by heat treatment reported negligible variation in porosity compared to those with no heat treatment [131], indicating that HIP largely dissolved the gas such that porosity reduction is permanent. Elongation at failure has been reported to improve by 30–200% with HIP; however, ductility may not improve for cases in which highly brittle phases are formed as a result of the

HIP temperature profile. Fatigue resistance increases with HIP as a result of the reduced internal crack nucleation sites, but the thermal effects on grain size and phase formation for each alloy system make comparisons difficult.

By themselves, heat treatments to re-austenitize the material can be completed. However, suitable temperatures must be used to dissolve the high-temperature oxides present in powder-based AM. Residual ferrite can be post-processed to austenite using solution heat treatments between 850 and 1,250°C [132], [133].

Susan conducted tests at 900°C for two hours and 1,200°C for two hours to recrystallize 316L AM material. The metallographs presented in Figure 44 show a largely unchanged microstructure when heat treated to 900°C, thus preventing recrystallization of the material. Susan compared the hardness response to heat treatment of LP-DED (LENS), LPBF, and forged material as plotted in Figure 45. Forged material of approximately equal grain size recovers ductility at lower temperature (~900°C) compared to the AM material. The oxides present in the AM material impede its ability to reduce strength through grain boundary pinning. Higher temperatures are needed for stress relaxation and grain growth [93][76].

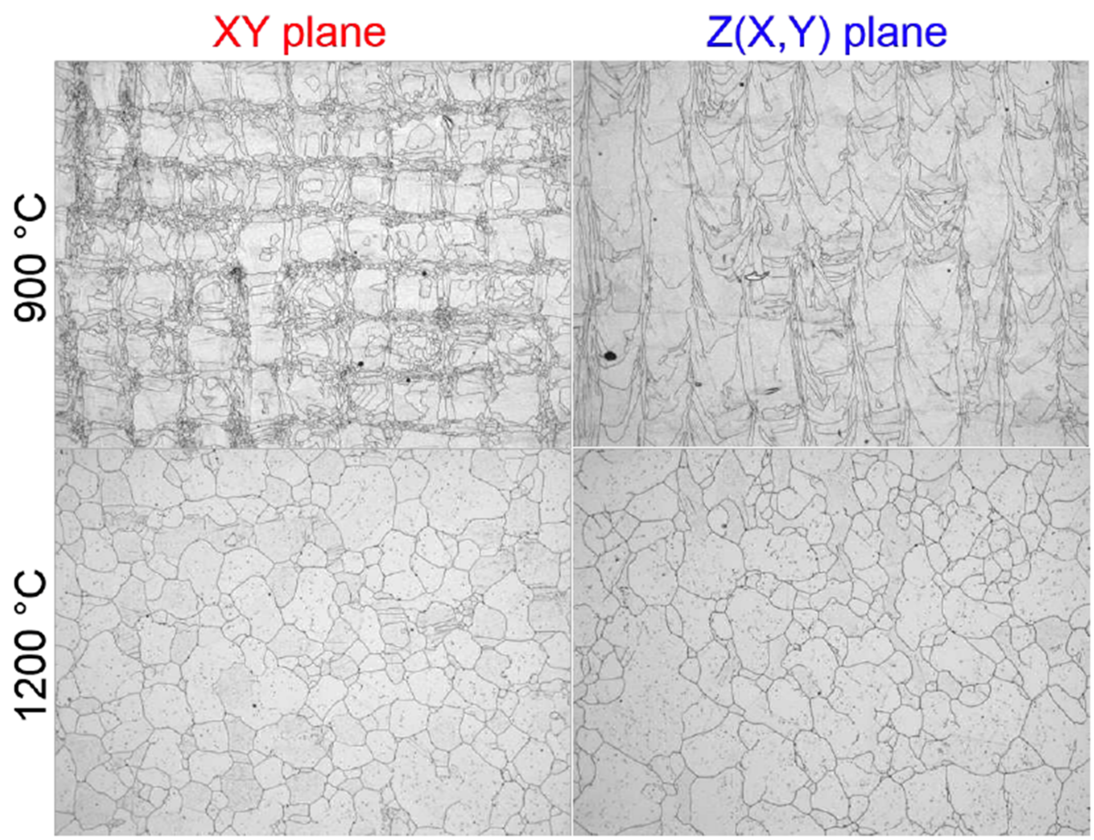


**Figure 44. Heat treatment of LPBF 316L at 900 and 1,200°C for 2 hours** [93].

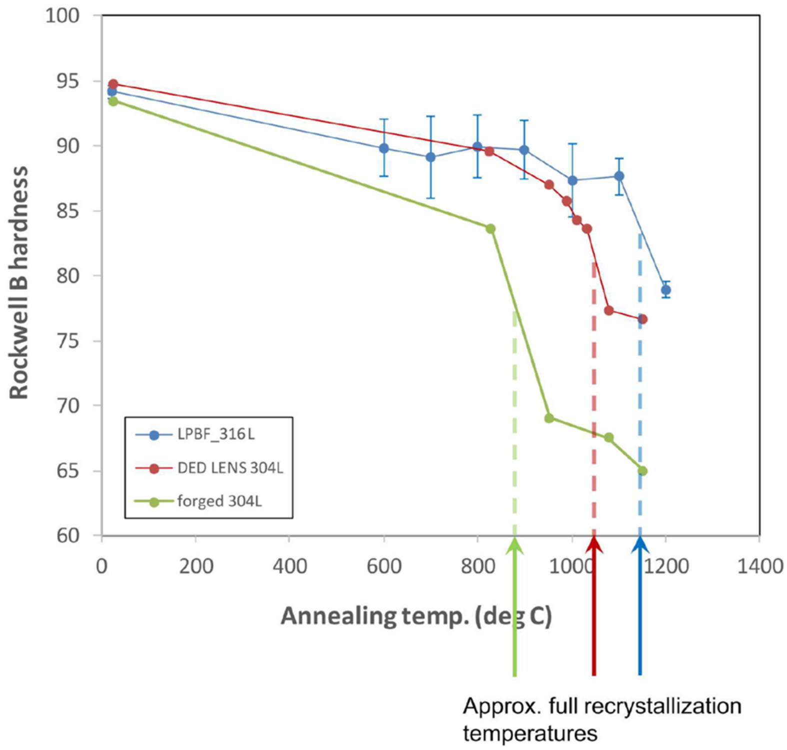


**Figure 45. Heat treatment hardness response of LP-DED, LPBF, and wrought material** [93].

# 3. GAP ANALYSIS

Additive manufacturing (AM) is a technology transitioning from laboratory experiments to industrial mass production of components. Many components will be required to conform to a quality assurance / quality control (QA/QC) process to ensure a minimum confidence level in component performance. However, as L-DED is transitioning to industrial usage, it is being noted that many pertinent standards are underdeveloped or do not exist. Best practices and standard operating procedures for machine calibration and process control must also be developed. This section discusses the gaps between existing requirements and the requirements necessary for statistically repeatable, predictable performance.

## 3.1 PREFABRICATION

### 3.1.1 Approaches to Control of Process - Geometry Interactions

L-DED is fundamentally a welding process. As such, it is sensitive to geometry in the same way as traditional welding: differences in geometry affect the amount of thermal dissipation available to the melt pool, which in turn affect the microstructure and properties of the final part. Just as no successful weld would be possible if the same settings were used for thin plate as for heavy castings, an L-DED fabrication process that does not adapt its settings to account for geometry will not produce satisfactory results. Therefore, it becomes critically important to understand and control the response of the process to different geometries, as the founding intent of AM is to create a process capable of manufacturing any shape needed.

For instance, when manufacturing a component with variable cross section thicknesses, such as that shown in Figure 46, a single slice will contain more or less area than other slices. The variable slice area translates to the variable linear laser path length and the variable time required to complete deposition of one slice. This in turn translates to more or less time for heat to dissipate from the top surface, which alters the temperature for the next layer. Because the process is an energy equilibrium, a hotter top surface will result in larger melt pool sizes and departure from nominal processing conditions [81]. Various approaches to this issue are discussed below.

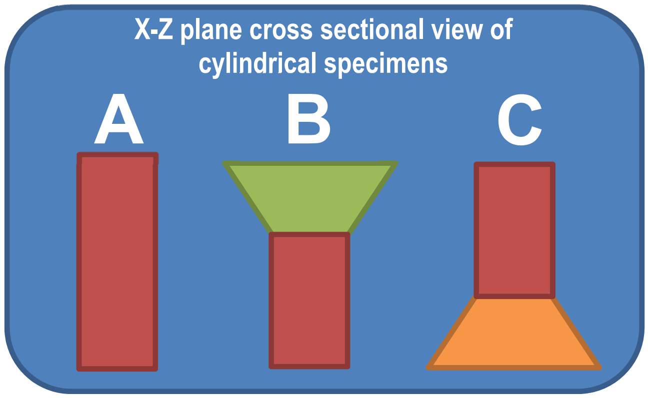


**Figure 46. Illustration of the effect of a changing cross sectional area** [12].

#### 3.1.1.1 Invariant parameter selection

For both LP-DED and LW-DED, if the material system has a broad enough processing window, then a single parameter set that works for both thick and thin geometries can be used. This approach can work for austenitic stainless steels, as their high ductility and low secondary phase formation allows for pore- and crack-free deposition under a relatively broad range of conditions. Differences in geometry will still express themselves in the microstructure and the properties of the component as a function of geometry, but depending on the application, such variance can be within tolerance levels.

A second related strategy is to assign different processing parameter sets manually or programmatically to different regions of the component. This is done based on the experience of the operator and information from prior deposition of similar geometries. An example of this is the use of a somewhat higher laser power at the beginning of the deposition when the deposited layer is in close contact with the substrate, which acts as a heat sink.

An invariant parameter selection strategy can produce components that conform to tolerances. However, using such a strategy requires the user to re-qualify the process for each new geometry produced, incurring additional delays to ensure that the microstructure and properties meet requirements. As the advantage of the AM process is to produce one-off or short-run components, any additional process qualification required when changing geometry would pose a serious cost in time and resources. Therefore, much research has been devoted to investigating other methods capable of intelligently adapting processing to compensate for geometric variations.

#### 3.1.1.2 Simulation of geometry effects

The problem of interactions with variable geometry can also be approached through the use of various modeling tools; many numeric schemes have been constructed to simulate heat transfer in AM. In principle, these tools would provide a predictive way to tune processing parameters specific to the geometry being produced, and several studies have shown success in this regard. However, in practice, simulation efforts are somewhat limited by several factors. Any error in thermophysical properties of the alloy being used will directly contribute to error in simulation results. This issue is further compounded by the pervasive issue of properties not being reported as a function of temperature. FEA and finite volume method (FVM) simulations introduce numerical inaccuracies that scale with the size of the element. For simulations of AM in which large, highly transient gradients exist close to the melt pool, a very fine element size is required. This makes highly accurate simulation of entire component depositions computationally infeasible. Adaptive meshing that dynamically splits and merges elements is one tool of many being used to speed computation, but there is always an essential tradeoff between simulation resolution and scale.

Despite the challenges facing quantitative simulation of L-DED, it is an area of intense academic and industrial study, and many advancements are being made annually. Although the details of the landscape of simulation efforts lie outside the scope of the current review, it is expected that the power, accuracy, speed, and usability of numeric tools specifically tailored to AM will continue to improve at a rapid rate. Predictive simulation of thermal history permits more thorough exploration of process parameters tuned for specific geometric features.

#### 3.1.1.3 Process control for geometric effect compensation

The final approach to compensation for geometric effects is through live process feedback control. For instance, in many LP-DED and LW-DED systems, it is common to image the melt pool either coaxially through laser optics using a beam splitter or with a camera mounted off-axis on the deposition head. The size and temperature of the melt pool can then be directly measured in real time with appropriate calibrations. This information can then be used to programmatically alter deposition parameters in situ. For fast-responding parameters such as laser power, this approach can effectively compensate for the perturbations in process equilibrium introduced from geometric effects.

Several factors present challenges with this approach. The combined latency between an imaging measurement, signal processing, and parameter modulation must be less than the time it takes for the process to exceed tolerable conditions. This is generally more practical for L-DED systems than for LPBF, as the melt pool moves at a slower speed. However, in the case of LP-DED, geometric features such as corners and laser starts/stops are generally too rapid to process effectively because of the generally higher travel speeds compared to LW-DED. Longer lasting effects such as thermal build-up can be compensated for by turning down laser power or pausing between layers for cooling.

Generally, process control can only compensate for a signal that is measurable in situ. Melt pool size, shape, and part temperature are optically identifiable, but other effects such as residual stress, porosity, and microstructure are not directly measurable. Several efforts have recently been implemented to associate more easily measurable signals, such as acoustic or photoemissions, to a non-measurable signal using convolutional neural networks [134], [135]. While such studies have shown preliminary success, it remains to be seen if these tools will generalize for different material systems and deposition geometries.

### 3.1.2 Software and File Preparation

Toolpath generation or *slicing* for LP-DED and LW-DED can be significantly more complicated than for LPBF. In addition to the effects highlighted in the accompanying LPBF report [22], L-DED has several additional degrees of freedom that currently do not have streamlined software solutions. Furthermore, L-DED systems are available in many different kinematic arrangements with widely varying motion control systems that require unique code syntaxes and commands for hardware support. Methods for site-specific modifications to process parameters require tight integration with the machine controller [136]. In the following subsections, gaps associated with 5+ axis slicing, toolpath generation, and parameter localization are discussed.

#### 3.1.2.1 5+ axis slicing

In LP-DED, no powder bed exists to support overhanging structures; instead, overhanging geometry must either rely on surface tension to hold bead weight, or overhanging geometries must be programmed using the additional degrees of freedom provided by multiaxis machines.

As discussed in Section 2.1, several commercial software packages designed for programming subtractive CNC operations have been adapted for additive toolpath generation. The software operation typically comprises defining a desired CAD geometry, defining the substrate, and loading machine models and process parameters into the software. The desired geometry is then sectioned into 2D slices. The 2D slice surface is then filled with 1D toolpath vectors, often defined as a *contour* and *rastering infill*. In addition to the XYZ position of the toolpath vector, the angle of deposition must be defined, which is an additional two degrees of freedom.

Programming to take full advantage of the additional degrees of freedom constitutes a major unaddressed challenge to CAM for L-DED AM. The challenge can be divided into two parts: calculation of the ideal deposition angle vector, and definition of slicing surfaces and slice order.

In typical 3-axis deposition, the deposition angle is always along the slice plane normal. As shown in Figure 47, this can result in large overhangs for a desired geometry, so the deposition angle can be adjusted to lie parallel to the CAD face plane to avoid overhanging geometry. As the toolpath vector also lies parallel to this surface, a local coordinate system can be defined. Using this coordinate system, additional tilt of the toolpath—in either the leading/lagging direction, or inward/outward across the CAD face—can be readily defined.

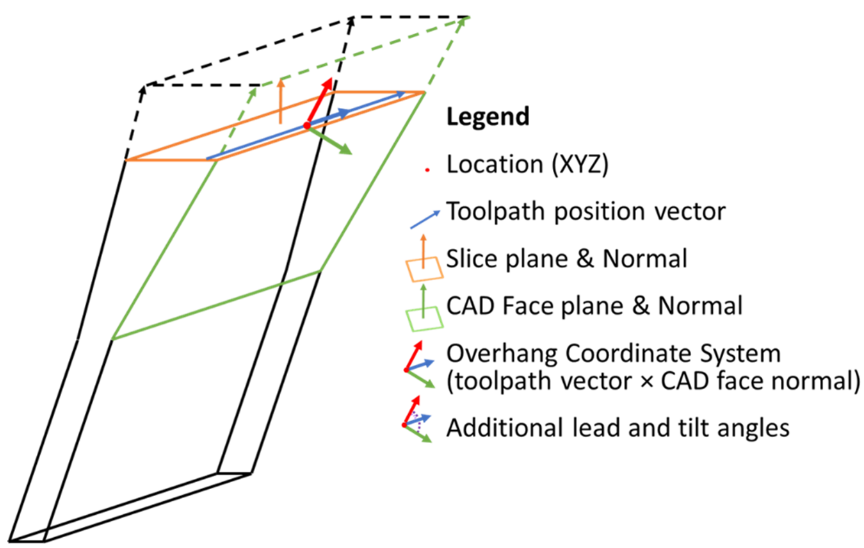


**Figure 47. Coordinate system definition for contour deposition using 5-axis motion to eliminate overhanging geometries.**

While current CAM packages are mathematically straightforward, they optimized for subtractive tooling and are programmed quite differently. Subtractive toolpaths can be used for generating the contours for 5× L-DED toolpaths, but several constraints and considerations complicate this approach. First, subtractive toolpaths can have variable amounts of overlap, allowing them to expand and contract the spacing between layers to match the geometry. AM toolpaths typically cannot do this because the processing conditions are optimized to lay down a specific thickness of material with each pass. This particularly becomes an issue when programming additive toolpaths that avoid overhangs, as shown in

Figure 47. In subtractive machining, this is accomplished by using the isocurve U/V surface texture coordinates of the geometry to define toolpath direction vectors which, depending on the CAD approach used, are not necessarily uniformly spaced. Second, subtractive tooling does not have the same dependencies on directionality as AM, as the melt pool shape is defined by many dynamic phenomena such as surface tension, viscosity, liquid metal wettability, and heat transfer. The specific contact angle and shape of the melt pool can change significantly, depending on the deposition angle. Most L-DED AM research has only addressed three axes, so this represents a significant gap in current research literature.

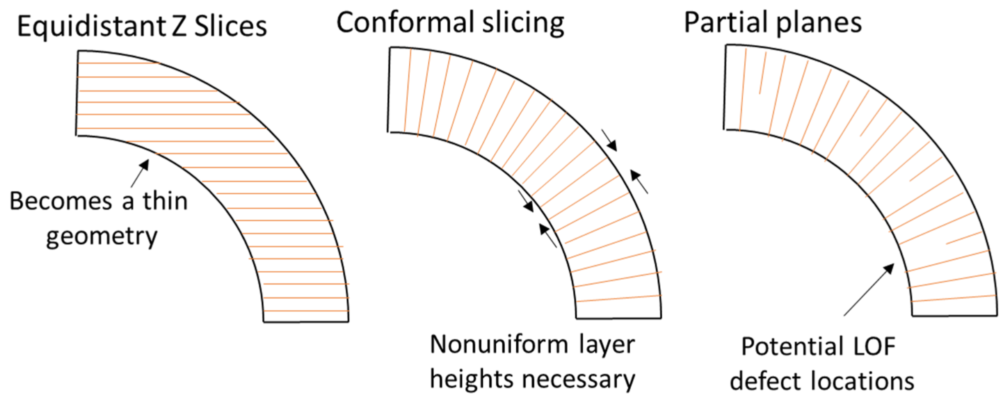


**Figure 48. Three-slice layer spacing strategies and the specific drawbacks of each.**

Definition of slice surfaces in 5+ axis deposition also becomes complicated for L-DED. Figure 48 shows three different approaches to a simple curved geometry. in the equidistant Z slices example on the left, the slices could be treated as equidistant planes along a common build direction, allowing toolpath orientation to be changed to avoid deposition of highly overhanging geometries. This works reasonably well at first, but as the geometry continues to curve, the slice plane eventually cuts the geometry in such a way that deposited material will be very thin, and the layer height in the tools orientation will become too large to actually deposit material in the manner intended. In the second strategy, depicted in the center image, uses the ISO contours of the part that can be defined so that each slice follows the U/V surface coordinates of the part. If the geometry is such that these contours form closed loops, then deposition can occur along a set of nonuniformly spaced layers. This avoids the thin geometry problem and maintains deposition nearer to the ideal L-DED setup, as each layer now has thicker and thinner portions, so either more or less material must be deposited to achieve the intended geometry. This could possibly be accomplished by varying feedstock flow rates through pre-planned parameter scheduling, through a form of layer height control [137], [138], or through deposition head speed, but this introduces material dependence and further complications such as modulation latency, numerical control (NC) code sampling rates, and others. In the third strategy shown on the right, the part is divided into individual segments, each of which has internally uniform layer spacing. However, this would introduce “half planes” at the junctions between these segments, so care must be taken to select processing parameters that can deposit over a somewhat nonuniform top surface in order to avoid lack of fusion porosity at these irregularities.

Although 5+ axis deposition allows much greater flexibility in the range of geometries that can be printed using L-DED, it is not capable of printing everything. Figure 49 shows a simple arch geometry. If the deposition angle and slice angle are varied to avoid overhangs, then the tool will eventually interfere with the other side of the arch. This is true regardless of the order of slice deposition. Instead, some amount of inward tilt is required of the tool, which produces an effective overhang deposit. Therefore, optimization of the L-DED processing parameters remains crucial for depositing on overhanging geometries, even for 5× machine designs.

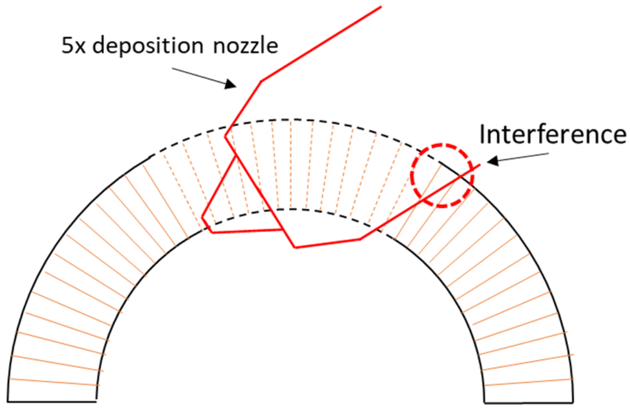


**Figure 49. Schematic demonstrating a fundamental limitation of 5+ axis deposition:**;interference between the deposition head and the component prevents deposition of a simple arch geometry without inducing some degree of overhung features.

#### 3.1.2.2 Toolpath generation – simulation integration

In LP-DED, LW-DED, and in metal AM in general, there is an unavoidable coupling between the toolpath selection, the generated heat transfer gradients and solidification direction, and the resultant microstructure. Numerous computer simulation tools have been proven to quantitatively predict many aspects of L-DED process behavior [139]. FEA models can readily simulate general heat transfer from a scanning heat source [140] which can be approximated with modified analytical expressions [28] [100] based on the famous Rosenthal welding solution [142]. Fluid flow within the melt pool, its dependence on thermocapillary convection [143]–[145], and the effects of wettability [35], [146] have been researched intensely by too many studies to name here.

Although individual facets of L-DED have been successfully simulated, there is a fundamental tradeoff between the number of simplifications made, the accuracy of the model, and the computational speed of the simulation. This problem is confounded by the very high degree of dimensionality of the process parameter space available. Simple choices of laser power, scan speed, and powder feed rate can all be spatially and temporally varied over an infinite number of different scan strategies. Currently, physics simulation software is not integrated with the CAM packages used to generate toolpaths and machine code for running the process. The software requires licenses and expertise in both domains to effectively design and simulate a build. Furthermore, as of this writing, no software for L-DED actively optimizes the toolpath structure to achieve effects simulated with physics-based FEA. Currently, the need for a holistic software solution to unify CAM and deposition simulation represents a gap in L-DED capabilities.

## 3.2 DURING FABRICATION

In L-DED AM, a growing body of research dedicated to effective process control has been generated; however, a consensus on strategies and best practices has not been achieved due to a number of technical challenges. First, the L-DED process relies on the molten weld pool as its fundamental building block, which in turn is influenced by a number of inextricable physical phenomena such as mass and thermal transport, surface tension, laser-matter interaction, and chemical inhomogeneity.

Effective process control depends on establishing useful, timely information feedback loops. Every control schema must measure the system state, predict the process response to a set of available actions, and execute the best predicted available action. In L-DED AM, the inextricability of many of the physical processes present have made it common practice to only control inputs to the process, evaluate the results of deposition through inspection and metallography, and select the parameter set that yielded the most desirable result, as diagrammed in Figure 50. This effectively puts the staff and personnel required to perform these inspections into the control loop. While this may be effective one-off development for static production processes, in L-DED AM, there is tight coupling between the geometry of the printed component and the process performance, and the geometry varies with nearly every produced part. Consequently, a great deal of human effort is spent in characterization to run this control loop.

For example, one would not use a box furnace by sending a fixed voltage through the heating coils. Variability in the furnace loading, power mains, and environmental effects such as room ventilation and humidity will all ensure that the furnace does not reach a fixed temperature. Instead, it is completely standard to use a thermocouple and proportional–integral–derivative (PID) control loop to prevent this variability from affecting the furnace temperature.

Therefore the inherent induced variability from geometric, feedstock, and environmental effects makes it ineffective to treat control in L-DED as an open-loop black box with fixed inputs and outputs. Instead, feedback control offers the chance to isolate system elements and dampen process variability instead of allowing it to propagate through to the final product. Some of the available information loops researched in L-DED are illustrated in Figure 50. Such control loops do not and cannot replace the need for traditional metallographic, mechanical, and other evaluations. Instead, they serve to buffer input variability and can reduce the overall effort required in testing deposited components.

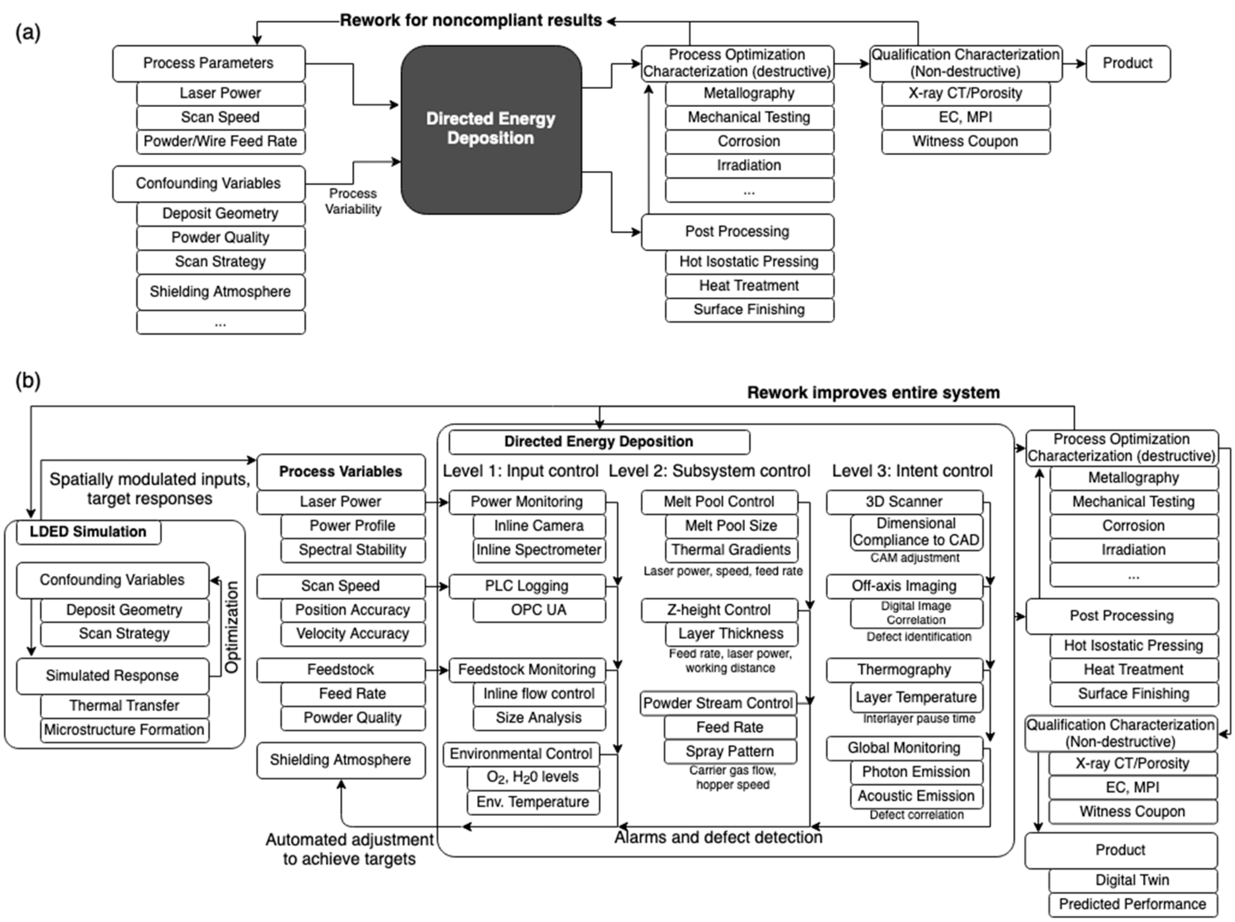


**Figure 50. (a) Open-loop black box approach to control in L-DED AM, and (b) example control-oriented approach to L-DED AM that integrates some common simulation and monitoring tools developed in the**

**literature.** As diagrammed, controls do not replace destructive and nondestructive characterization, but they do allow for more rapid development iterations to achieve a product worth qualifying.

## 3.3 POST FABRICATION

Post-fabrication requirements and processes for L-DED components are more nuanced than those for equivalent conventional components because L-DED material properties are affected by spatial orientation and interactions between the scan strategy and component geometry. Heat treatments, joining and welding practices, and characterization appropriate for the application must be performed.

Because of the geometric effects on microstructure and properties, characterization should be sampled from the portions of the final component where the properties are critical. Often, this is not possible because the sample specimen geometry requirements cannot fit within the volume of the intended printed component. Therefore, a more common practice is to sample from other geometry portions or to simultaneously print witness coupons. Although these methods allow for more experimental representation than what would otherwise be possible, they cannot account for geometrically induced effects and will only be representative of a process that is well-tuned for insensitivity to these effects.

### 3.3.1 Heat Treatment and Hot Isostatic Pressing (HIP)

Heat treatment is used for L-DED 316L to ensure residual stress relief and microsegregation homogenization. HIP, which uses both temperature and pressure, can serve as a heat treatment while also reducing internal porosity. The literature [79], [121], [147], [148] suggests that these processes differ for L-DED–manufactured 316L in several important ways, as discussed in Section 2.3 above. This section highlights several knowledge gaps in the current understanding.

It must be reiterated that microstructure produced during L-DED can vary significantly, depending on the machine, process parameters, and geometry, even within 316L. Heat treatment is intended to induce favorable alterations to a microstructure that enhance properties; however, since the starting microstructure is not necessarily uniform, even across the same component, the optimal temperature and time to induce that alteration may also be nonuniform. As such, any developed heat treatment and consequent properties are specific to the process that generated the original microstructure. The current knowledge gap is focused on the following question: *how can a heat treatment be specified in a robust manner that is also responsive to the uniqueness baked into an AM part?*

To demonstrate this knowledge gap, an example is provided here. All L-DED components possess some degree of nano-scale oxide precipitation. These oxides pin dislocation motion and affect the temperature at which stress relief occurs [149]. The size, frequency, and distribution of these precipitates depend on several processing factors which are not entirely understood. These could include powder feedstock oxidation levels, build chamber oxygen concentration, laser–surface interaction and potential element vaporization, specific powder feedstock chemistry within the envelope of 316L tolerances, and the presence of oxygen bonding elements, to name a few. Therefore, can a single heat treatment be prescribed that works for all L-DED 316L–fabricated components? It is unclear if the sensitivity of the system is too high for this to be effective or if a heat treatment plan that considers the as-built microstructure can be used instead.

As discussed in Section 2.3, there is rich interaction between the L-DED process, the obtained microstructure, and the resultant properties of the material. Heat treatments add yet another dimension of processing that requires further experimentation. While some studies have been performed exploring this issue, for many properties, there simply is not much data on heat treatment response because of the large design space.

### 3.3.2 Surface Finishing

As discussed in Sections 2.3.7.3 and 2.3.7.4, which address fatigue and corrosion properties, the surface finish can severely limit performance for applications dependent on these properties. The natural surface roughness has a length scale commensurate with the size of layers deposited, as well as the size of powder used. Components can be finished using a large variety of traditional processes such as subtractive machining, sandblasting, peening, media tumbling, chemical and electrochemical etching, to list a few. The considerations that must be made for finishing operations are as follows:

1. Does the operation maintain the dimensional tolerances required?

2. Does the treatment chemically or microstructurally modify the underlying material?

3. Does the treatment induce changes to the residual stress state of the deposited material?

4. Does the process introduce further opportunity for formation of surface flaws or cracking?

5. Will the qualification characterization include material after all finishing processing?

Satisfying the requirements of a particular application depends on optimizing and qualifying each processing step, which draws on knowledge from the respective finishing field, as well as an understanding of the properties of L-DED manufactured material.

### 3.3.3 Joining and Welding

As compared to PBF AM, the LP-DED and LW-DED processes have a higher degree of flexibility in relation to joining options. This stems from its strong similarity to laser welding and cladding; indeed, L-DED itself should be classified as a joining technique. Generally, LP-DED melt pool sizes tend to be smaller than laser welding (~0.5–2 mm) to provide a finer minimum feature size; however, LW-DED has essentially the same process scaling as laser welding, and the metallurgy and solidification behaviors for either powder or wire L-DED and conventional welding are quite similar, and publications frequently directly draw from welding research. The discussion in Section 2.3 on microstructure and properties lays a foundation for understanding the welding behavior of L-DED 316L.

Specific studies on the use of LP-DED for repair applications [150] or direct deposition on PBF components [151] have shown that L-DED can be performed successfully with a high degree of functional strength for a large variety of high-value applications such as drive shafts, piston seals, mold and die, and even gas turbine blades. Generally, the HAZ is significantly smaller for LP-DED than that of traditional arc welding because of its more precise heat input. This allows for tighter control of material properties in the heat-affected zone in the joined material.

Partitioning of elements during welding can lead to alloy depletion. The joining of AM components (LW-DED, LP-DED, LPBF) may result in slightly different crack susceptibilities as a result of successive element segregation and inherited residual stresses not typical of wrought material. Increased oxygen content, as discussed in Section 2.3.4, can be problematic during welding. The solubility of gas in stainless steel varies with temperature and metallurgical phase, so gas evolution may depend upon weld conditions. For example, EBW performed in vacuum may increase the amount of gas evolved out of the melt, with the potential for entrapping gas pores. Joining procedures for AM materials may require further development to avoid porosity formation.

LP-DED also has a long literature history of successful weldment to different alloy systems in the form of functionally graded materials (FGMs), a unique feature which is cited as one of the primary advantages of the LP-DED process over PBF [152]. Instead of abutting two components of different alloys to one another and using a single weld pass to meld them, LP-DED allows for differential mixing of multiple powder compositions into the melt pool, resulting in a smaller compositional difference between the melt pool and the supporting material. This provides for flattening compositional gradients over larger spatial distances, thus reducing diffusive driving forces and material property mismatches.

While enough success stories in the literature regarding L-DED joining are available to motivate and guide process development [153], [154], a major knowledge gap remains in qualification. Quality standards for AM practices in general are still under development, as discussed in Section 3.7, and by extension, standards for welding of L-DED components have yet to be established.

#### 3.3.4 Characterization and Inspection

Consistent, repeatable characterization of LP-DED and LW-DED manufactured material poses a particular challenge because many of the results are sensitive to microstructure and porosity, which are typically nonhomogeneous through the deposited specimen. As such, wide scatter in reported values can be observed, as individual studies that have different processing parameters may fail to report all relevant information such as the laser power profile, fail to characterize convoluting factors such as porosity content, or fail to replicate experiments to measure the variance in values. Despite the number of publications in the L-DED field of 316L, the large combinatorial space of processing parameters and relevant properties has substantial gaps. Accordingly, values reported in literature should be viewed as a best-case scenario of a well optimized process, with the recognition that few studies contain enough unique data to evaluate the real statistical distribution of the properties they measure.

##### 3.3.4.1 Nondestructive testing

Nondestructive post-process testing of LP-DED and LW-DED components is a critical aspect of certification for NPP applications, and it primarily consists of porosity detection and geometric measurement. Final porosity and geometry testing should occur after all post-processing treatments, to include HIP treatments, heat treatments, and precision machining. However, the geometric complexity of AM components and the frequent mixture of fine details with bulk structures add significant challenges to accurate measurement. Work on nondestructive testing of metal AM components has been published [155], [156] and is an active area of research given the commercial interest in fabricating critical components that require inspection and certification.

Porosity in a final component must be characterized with techniques that are sensitive to the size range and type that will impact mechanical properties, particularly fatigue strength. Existing standards for porosity, such as ASTM E186-15 for cast steel walls, may provide useful reference. Porosity can be characterized by average material density, number of pores, pore location, pore size distribution, and pore morphology. Comparing a component's actual density against theoretical density is the simplest characterization and can be achieved by the Archimedes principle [157]. Measurement of other aspects of porosity depend on the resolution desired, material properties (such as x-ray absorbance), and geometric considerations. Computed tomography (CT) is capable of pore resolution to 10 μm [158], and work has been published on CT pore measurement in laser welds [159], [160]. Synchrotron radiation microtomography [161] has been used to detect pores with a resolution of 1.3 × 1.3 × 1.3 μm, but the measurement area was small at 1.3 × 1.3 × 10 mm. Although CT and synchrotron radiation microtomography are highly accurate, both methods are capital-intensive and may be unnecessary if a HIP post-processing treatment is standard for a component. In such a case, using the Archimedes principle to determine overall porosity, along with another method to detect large pores, may be faster and more cost effective.

Grain size and orientation can be characterized on the component's surface via microscopy-based techniques such as EBSD [162]. Data on the internal microstructure can only be obtained through destructive methods. However, sacrificial startup specimens could be fabricated under the same processing conditions with the same feedstock, thereby offering a measure of assurance.

#### 3.3.4.2 Destructive testing

Destructive testing of LP-DED and LW-DED components typically comes at a higher relative cost than for other production processes. Because L-DED is typically applied for low-volume production runs, to destructively sample from a component, additional components must be produced purely for testing. In the worst case, for a one-off component, this will at minimum double the material, machine, and labor required. Therefore, the practice of printing witness coupons simultaneously with the component has become more common. While this approach is useful for identifying long-lasting layer scale problems such as a partially clogged powder nozzle, a fogged laser optic, or loss of shielding gas, this method is ineffective at identifying issues arising from local or scan-induced defects.

#### 3.3.4.3 File and data management

Integral to the entire production chain, there is a critical need for detailed, comprehensive information management systems, from design, file preparation, slicing, through in-situ data collection and ex-situ characterization. The quality of an L-DED component is provable only through effective record keeping and documentation of all the critical sources of variability such as feedstock properties and the chamber environment. In particular, in-situ data are only measurable once, during fabrication. Therefore, it is highly important that all generated data be managed according to a consistent, detailed, and if possible, completely automated plan. Ideally, data generated will abide by the "FAIR" principles: *findable*, *accessible*, *interoperable*, and *reusable*. For the success of the technology, it is critical that further standardization efforts not only focus on establishing the physical methodological infrastructure, but also on establishing data format standards that follow these principles.

## 3.4 TECHNICAL GAP ANALYSIS

The importance of each topic is rated according to its potential impact on material properties and does not correspond to a specific material property or failure mode. For example, contamination management is rated as highly important because contamination may adversely affect SCC resistance, ductility, or the as-fabricated microstructure in unpredictable ways. Feedstock contamination would be an adverse influence, regardless of whether a component experienced radiation or was in a corrosive environment.

**Table 6. L-DED fabrication gaps**

| Importance | Topic | |
|---|---|---|
| ***High*** | ***Geometry-scan strategy interactions*** | |
| | Related section | 3.1.1 |
| | Ranking rationale | Potential to result in incorrect geometry, adversely affect material properties, or produce manufacturing defects |
| | Discussion | Even more so than in LPBF, geometry-scan strategy interactions may significantly change the meltpool solidification rate and thermal profile. Heat frequently accumulates faster than it dissipates in deposited components, which leads to layer-wise alterations in auto-quenching behavior, cooling rate, solidification microstructure, and material properties. In particular, it causes geometric variation to drive process conditions away from the state for which they were optimized, thus ensuring that a single set of process conditions will not behave uniformly for different geometric features. Simulation and/or feedback control compensation is required, but a universal approach to the problem has not yet emerged. |
| ***High*** | ***Inspection of fabricated components*** | |
| | Related section | 3.3.4 |
| | Ranking rationale | The advantages of L-DED to fabricate components with as-built internal features can make inspection of the component features more difficult. |
| | Discussion | Internal features or hollow bodies of the part cannot always be inspected by conventional means, particularly when inspection would interrupt the build process. Some NDE methods such as UT, CT, and radiography may allow for the inspection of some features, however, are not typically relied upon for dimensional inspection. Standards and procedures need to be developed to standardize procedures for inspection and acceptance criteria. |
| ***High*** | ***Software and file control*** | |
| | Related section | 2.1.2, 3.1.2, 3.3.4.3 |
| | Ranking rationale | Significant potential to alter material properties, porosity, and geometric accuracy |
| | Discussion | The scan strategy used to fabricate a component and the software controlling the L-DED machine has an extremely important role in geometric accuracy, warping, material properties, and the probability of successfully completing a build. It is critically important that the exact same file, CAD software version, and software settings be used to fabricate replicates of a given qualified component. As a result, cybersecurity, database traceability, managing software updates, and similar items are highly important to ensuring end-use component quality. |

**Table 6. L-DED fabrication gaps (continued)**

| Importance | Topic | |
|---|---|---|
| ***High*** | ***Material property sampling methodology*** | |
| | Related sections | 3.1.1.3 |
| | Ranking rationale | Risk of overestimating material properties or underestimating variability |
| | Discussion | Heterogeneous L-DED microstructures and material properties have been documented in literature and are functions of the scan strategy, feedstock, component geometry, and L-DED machine. Heterogeneity in material properties should be assumed until sufficient empirical evidence is presented to prove otherwise. The sampling methodology for quantifying the mean, variance, skew, and kurtosis of L-DED material properties as a function of position and orientation is significantly more involved than in conventional materials. Establishing standard methods to guarantee representative homogeneous sampling would ensure that the effort expended on generating L-DED data provides quality data to consumers. |
| ***High*** | ***Data management*** | |
| | Related section | 3.3.4.3 |
| | Ranking rationale | Significant business risk of data loss |
| | Discussion | Data generated during the L-DED process have been shown to be an irreplaceable source of information for defect detection. Management, storage, retrieval, and analysis of the data is critical for accelerating process optimization and ensuring that fewer resources are expended evaluating infeasible designs. This is particularly important for L-DED because of the high degree of design space available and the inability of a single parameter set to produce consistent results across different geometries. Data mismanagement, incompatibility, or inaccessibility across project and corporate lines can effectively annihilate the original purpose of generating the data. The need to incorporate L-DED data streams into a findable, accessible, interoperable, and reusable (FAIR) framework constitutes a current major gap. |
| ***High*** | ***Planned and unplanned build interruptions*** | |
| | Related section | 3.2 |
| | Ranking rationale | Possible adverse effect on material properties or component geometry |
| | Discussion | Build interruptions may affect the thermal distribution within the build chamber by cooling, which may result in non-negligible component warping prior to restarting the build. For large L-DED components, process pauses are sometimes unavoidable, as the powder feedstock hoppers or wire spools must be refilled or process consumables, such as wire-feeder tips must be changed out. Depending on the cause of the interruption, several adverse events may occur. For example, exhaustion of inert gas may result in oxidation of multiple layers, electrical power outages may require recalibration of the laser optics, and laser overheating may result in build failure. Furthermore, build interruptions impact component thermal history and can interrupt process parameter schedules or invalidate previously run simulations. This is one of the reasons that real-time sensing and control is so valuable in L-DED. |

**Table 6. L-DED fabrication gaps (continued)**

| Importance | Topic | |
|---|---|---|
| ***Low*** | ***Contamination management for LP-DED*** | |
| | Related section | 2.1.1 |
| | Ranking rationale | Significant potential to alter material properties; however, for critical applications, it is possible to use virgin powder in LP-DED |
| | Discussion | Contamination of feedstock powder is a serious concern, as it may adversely affect material properties. Contamination can typically be reduced to acceptable levels by maintaining general cleanliness and dedicating LP-DED machines to specific alloys, or by changing out feedstock-conveying tubes and components. Lack of contamination may be documented in parallel with quantifying powder characteristics. The authors recommend sampling from the sprayed powder stream prior to each build and storing said powder sample for the lifespan of related components in case further feedstock analysis is warranted. It is not recommended that powder be reused without being recharacterized. |
| ***Medium*** | ***L-DED environmental sensor data*** | |
| | Related section | 3.2 |
| | Ranking rationale | May detect layer-wise component defects |
| | Discussion | Data from environmental sensors in the L-DED machine (e.g., oxygen and humidity sensors), do not provide information as spatially specific as in-situ monitoring, but the L-DED machine data are typically more accurate, and the underlying technologies are thoroughly documented. Events during fabrication that are captured by environmental sensors are likely to affect entire layers. The authors recommend analysis of environmental sensor data for all builds; determination of what environmental data are relevant to 316L in NPP applications must be empirically resolved as data become available. |
| ***High – LP-DED*** <br> ***Medium – LW-DED*** | ***Feedstock characterization*** | |
| | Related section | 2.1.1 |
| | Ranking rationale | Affects powder deposition performance through mass capture efficiency (for LP-DED), melt pool shape, and process stability |
| | Discussion | Powder feedstock characterization includes size distribution, morphology, internal porosity, and flowability. Said characteristics affect the drag coefficients, trajectories, and overall focus of powder streams. This in turn alters the number of powder particles interacting with the melt pool, the quantity shielding the melt pool from the laser, and the statistics of interaction time with the laser before impacting the melt. Additionally, morphology and oxidation of powder influences the interaction of particles with the melt pool's surface. There are fewer variables associated with wire feedstock, and wire has a longer history of established conformance testing, but nevertheless, feedstock issues for either LP-DED or LW-DED can yield variability in porosity content of deposited components in ways that are not fully understood. Detailed characterization and control are critical in removing powder variability as a factor in deposition performance. |

**Table 6. L-DED fabrication gaps (continued)**

| Importance | Topic | |
|---|---|---|
| ***Medium*** | ***L-DED machine calibration*** | |
| | Related section | 2.2.1 |
| | Ranking rationale | Potential to alter material properties and geometric accuracy |
| | Discussion | L-DED machines must be calibrated to operate at specified parameters (e.g., laser power, spot size) so that they can repeatably fabricate components, particularly when using the same scan strategy for multiple machines. It is unclear at this time how precisely machines must be calibrated. |
| ***Medium*** | ***Residual stress – warping, cracking, and delamination*** | |
| | Related section | 2.1.3, 2.1.4, 3.3.3 |
| | Ranking rationale | Potential for geometric inaccuracy and catastrophic part failure prior to service |
| | Discussion | All L-DED components experience significant as-fabricated residual stress which must be removed via post-processing heat treatments. Residual stress is not problematic if an appropriate heat treatment is applied prior to service; however, high residual stress can result in geometric inaccuracy which may result in component rejection. High residual stress may also result in cracking and delamination, but these events are not commonly associated with 316L and typically can be visually detected. |
| ***High*** | ***In-situ monitoring and feedback*** | |
| | Related section | 3.1.1, 3.2 |
| | Ranking rationale | In-situ monitoring provides opportunities for monitoring quality and feedback control. However, failures in in-situ inspection methods pose the risk of admitting defective components or steering the process poorly, adversely affecting material properties |
| | Discussion | Feedback controls are typically used to improve stability of the process to ensure the desired result. The feedback signals of essential variables can be collected through data acquisition and analyzed either for in-situ corrections (feedback control) or through a post process analysis method. In-situ monitoring with feedback control may affect material properties, and if the relationship between the controlled parameter, microstructure, and properties is not sufficiently developed, then it may induce undesirable variability in performance. However, unlike for LPBF, successful deposition frequently requires some form of feedback control due to the larger thermal variations induced from geometric effects as discussed in Section 3.1.1. This is frequently accomplished by melt pool size control or layer height control. In-situ monitoring without feedback control is analogous to a traditional data acquisition system that can be processed automatically or manually to identify suspect regions for targeted inspection of components. Reliance on in-situ methods introduces the risk of false negatives if used for qualification. It is highly recommended that L-DED standardization efforts focus on establishing the methodological practices necessary for certifying a control process instead of prescriptively requiring a certain set of unchanging process parameters. |

**Table 6. L-DED fabrication gaps (continued)**

| Importance | | Topic |
|---|---|---|
| ***High*** | | ***Porosity measurement*** |
| | Related section | 2.1.1.2, 2.3.6 |
| | Ranking rationale | Porosity's direct, adverse effects on multiple material properties |
| | Discussion | Because porosity is known to adversely affect fatigue life, SCC, and IASCC, the detection and quantification of porosity in the feedstock powder and fabricated component are important aspects of QC methodology. Porosity in the powder feedstock can indicate issues in the powder fabrication process, and it can contain higher-than-expected levels of gas that may later be entrapped in the build. High porosity levels (>1% volume) adversely affect ductility in 316L. The Archimedes method may be used to determine bulk porosity by determining the average density, and CT may be used to locate pores >10µm diameter. |
| ***Application-Specific*** | | ***L-DED design considerations*** |
| | Related section | 2.1.3 |
| | Ranking rationale | Potential for creating stress concentrators and heterogeneous microstructures |
| | Discussion | The greatest strength of L-DED is the geometric freedom to create simplified assemblies and organic shapes and to optimize load paths. However, design reviews must be conducted to prevent unintentional defects. For example, if a conventional component with a machined through-hole is replaced with an L-DED component, then the hole path in the L-DED component may be made serpentine, nonuniform in diameter, or similarly nonconventional to optimize pressure head losses, for example. However, a non–line-of-sight hole will prevent milling to improve surface roughness, and the overhang limitation of L-DED may result in diamond- or triangular-shaped holes, which will create significant stress concentrations. Designs must also consider and allow for the inspectability of such features. These design byproducts do not prevent the use of L-DED components, but special consideration must be given to designs in light of the limitations of the L-DED process. |
| ***High*** | | ***Surface roughness*** |
| | Related section | 2.1.3, 2.3.7.3, 2.3.7.4 |
| | Ranking rationale | Significant impact on deposited part performance |
| | Discussion | The layer-by-layer nature of the build in LP-DED and LW-DED results in a rough surface finish, which is a concern. LP-DED has additional roughness caused by unmelted powder particles that adhere to the surfaces of the component. The rough surfaces of LP-DED and LW-DED builds have been shown to degrade fatigue, corrosion, and SCC performance, and they also cause components to fail dimensional tolerances. Therefore, it is frequently necessary to finish as-built surfaces. Complicated geometries frequently cannot be finished using line-of-sight methods such as traditional machining. This limitation has spurred research in hybrid approaches. |

**Table 6. L-DED fabrication gaps (continued)**

| Importance | Topic | |
|---|---|---|
| ***Low*** | ***Powder reuse management*** | |
| | Related section | 2.1.1.1 |
| | Ranking rationale | Significant potential to alter material properties; however, powder reuse is not strictly necessary in LP-DED; ranking assumes that powder reuse is not allowed |
| | Discussion | Collecting, sieving, and reusing powder can cut material costs substantially. However, contamination of feedstock powder is a serious concern, as contamination may adversely and unpredictably affect material properties. Contamination can occur from the residual powders of other alloys, from abraded material from the chamber and powder-conveying apparatuses, or from interaction with heat sources that causes partial vaporization or oxidation. Unlike in the LPBF process, LP-DED can achieve powder utilizations exceeding 90% for large melt pool sizes, with lower efficiencies for higher resolution melt pools. Because powder reuse can induce significant variability, and material costs often comprise a relatively small fraction of total costs and can further burden characterization and qualification testing, it is recommended that powder not be reused for safety-critical components without further characterization. |

The following material property and performance gap analysis is written with the conventionally manufactured version of the alloy as a comparison. Ranking is assessed based on whether the L-DED version of the alloy exceeds the conventionally manufactured material properties and the frequency of a given failure mode. For example, the tensile properties of L-DED 316L are assessed as low importance because L-DED YS and UTS are typically higher than in conventionally manufactured 316L. Additionally, mechanical overloading is not a common failure mechanism in NPP applications.

**Table 7. Material property and performance gaps**

| Importance | | Topic |
|---|---|---|
| ***High*** | | ***Heterogeneity*** |
| | Related section | 2.3.7, 3.3.4 |
| | Ranking rationale | Significant risk of overestimating material properties |
| | Discussion | *Microstructural heterogeneity* refers to 3D nonuniformity in the microstructure of a component and is not to be confused with anisotropy. *Anisotropy* refers to whether material properties are uniform in all directions, as is common in conventional metallic materials, or they may be transversely isotropic, as is common in columnar microstructures. Simple blocky geometries are less likely to suffer from heterogeneity; however, such geometries do not take advantage of the geometric flexibility afforded by L-DED. Heterogeneity may appear in multiple forms singularly or in groups. Examples include (1) a component with equiaxed grains is heterogeneous if the grain size varies significantly from one region to another within a component, (2) a component exhibiting columnar grains in one region while being equiaxed in a different region, or (3) a component in which porosity varies significantly with respect to pore size, counts per volume, pore morphology, or volume percent. In all three examples, the average material properties change as a function of location within a component. Heterogeneity may affect a single material property, or it may affect multiple properties simultaneously. At a minimum, it is necessary to characterize the minimum property values within a heterogeneous component. Depending on component application and requirements for a failure modes and effects analysis, it may be necessary to quantify the heterogeneity of a component in four-dimensional space (X, Y, Z, orientation). |
| ***High*** | | ***Irradiation-assisted degradation*** |
| | Related section | 2.3.8 |
| | Ranking rationale | Irradiation embrittlement and void formation are potential concerns in NPP applications, but it is unclear at this time at what rate L-DED 316L ages relative to conventional 316L. |
| | Discussion | Irradiation embrittlement, and loss of fracture toughness, in particular, is a concern in NPP applications. Current studies point to reduced irradiation-induced defects in L-DED components; however, understanding is limited, and research is ongoing. |
| ***High*** | | ***SCC and IASCC*** |
| | Related section | 2.3.7.4, 2.3.8 |
| | Ranking rationale | SCC and IASCC are two potentially significant failure modes in NPP applications |
| | Discussion | Preliminary studies indicate that LPBF 316L may offer significantly higher SCC and IASCC resistance relative to conventional 316L given appropriate processing parameters and post-processing treatments. Porosity, grain size, and Si oxide inclusions have been identified as highly correlated to crack growth rates. However, few studies have reported irradiation properties for L-DED, and the mechanistic understanding of how L-DEDs improve IASCC resistance is still being sought. |

**Table 7. Material property and performance gaps (continued)**

| Importance | Topic | |
|---|---|---|
| ***High*** | ***Fatigue*** | |
| | Related section | 2.3.7.3 |
| | Ranking rationale | Fatigue failure is abrupt, and L-DED 316L has been documented to have lower high-cycle fatigue life (corroded and uncorroded) relative to conventional 316L |
| | Discussion | The fatigue strength of L-DED 316L strongly depends on the post-processing heat treatment, load path, and component porosity. Low-cycle fatigue life has been reported as comparable to that of conventional 316L, but high-cycle fatigue life is reduced relative to conventional 316L. Surface roughness adversely affects fatigue life in a manner similar to that seen in conventional 316L. Stress-relieved L-DED 316L shows anisotropic fatigue strength and preferential crack growth directions due to the columnar microstructure. |
| ***High*** | ***Fracture toughness*** | |
| | Related section | 2.3.7.2 |
| | Ranking rationale | L-DED 316L fracture toughness has been reported to be ~98 to ~46% of forged 316L toughness, but effects from porosity and heat treatment have not been isolated |
| | Discussion | The fracture toughness of L-DED 316L has not been reported over a wide range of porosity and post-processing heat treatments. This limits the ability to draw conclusions. Studies of LPBF suggest that metal AM has the capacity to achieve highly fracture-resistant states given the appropriate processing parameters and post-processing treatments, but demonstration of the steps required to ensure a high level of performance for L-DED have not been established. |
| ***Medium*** | ***Corrosion Resistance*** | |
| | Related Section | 2.3.7.4 |
| | Ranking rationale | Relatively little literature is available on the corrosion properties of L-DED 316L; stainless is typically used specifically for its corrosion resistance |
| | Discussion | As in welding of 316 and 316L, microstructures are drastically different than for forged vs. cast material. A higher propensity for scavenging oxygen or other contaminants can yield additional precipitation, which is known to alter corrosive properties. Additionally, the cellular dendritic microstructure in L-DED has a higher compositional variation than for LPBF, which may affect corrosion resistance. |
| ***Medium*** | ***Weldability*** | |
| | Related section | 3.3.3 |
| | Ranking rationale | Available literature suggests producing a defect-free weld on L-DED 316L is achievable; existing standards and qualification procedures are applicable |
| | Discussion | Existing studies have indicated that the welding behavior (penetration depth, weld cross section, solidified microstructure) of L-DED 316L differs from that of conventional 316L. Limited published information is available on the results of traditional joining methods being used on L-DED components. L-DED components are known to have high oxygen contents, high residual stresses, and microstructural segregated elements, each of which may affect the acceptance of traditional welds using L-DED base materials. Optimal pre- and post-heat treatments are not characterized at this time; nor is the phase and chemical composition distribution of L-DED 316L welds. |

**Table 7. Material property and performance gaps (continued)**

| Importance | Topic | |
|---|---|---|
| ***Low*** | ***Tensile properties*** | |
| | Related section | 2.3.7.1 |
| | Ranking rationale | Tensile properties of L-DED 316L are typically comparable or superior to those of conventional 316L. Mechanical overloading is also not a common failure mode in NPP applications |
| | Discussion | YS and UTS of L-DED 316L is typically similar or superior to conventional 316L because of grain size refinement, depending on post-processing heat treatments. The uniform elongation of L-DED 316L is approximately 50–60%, but this may be reduced by high (>1%) levels of porosity. |

## 3.5 CODES AND STANDARDS GAP ANALYSIS

### 3.5.1 Overview of Codes and Standards Relevant to L-DED

At the time of this document's publication, the list of organizations that have contributed to developing standards and specifications for AM is extensive. The most comprehensive review of standardization efforts was compiled by America Makes & ANSI Additive Manufacturing Standardization Collaborative (AMSC) in their landmark document, the *Standardization Roadmap for Additive Manufacturing* [163]. In this document, the works developed by many organizations are collated, including: ASTM International, the International Organization for Standardization (ISO), the American Welding Society (AWS), the Institute for Electronic and Electronics Engineers (IEEE), the American Society of Mechanical Engineers (ASME), the Association for the Advancement of Medical Instrumentation (AAMI), the Medical Imaging & Technology Alliance (MITA), Digital Imaging and Communications in Medicine (DICOM) of the National Electrical Manufacturers Association (NEMA), the Association Connecting Electronics Industries (IPC), the Metal Powder Industries Federation (MPIF), the MTConnect Institute (MTConnect), and SAE International. ANSI also maintains an AM webstore for standards [164], and America Makes and ANSI maintain a web portal for tracking standards development related to the 93 identified gaps in the standardization roadmap report [165].

The technical scope of the AMSC standardization roadmap ranges broadly, from general AM standards, to specific processes, to specific materials, down to specific applications. The hierarchy of standards is outlined in Figure 51.

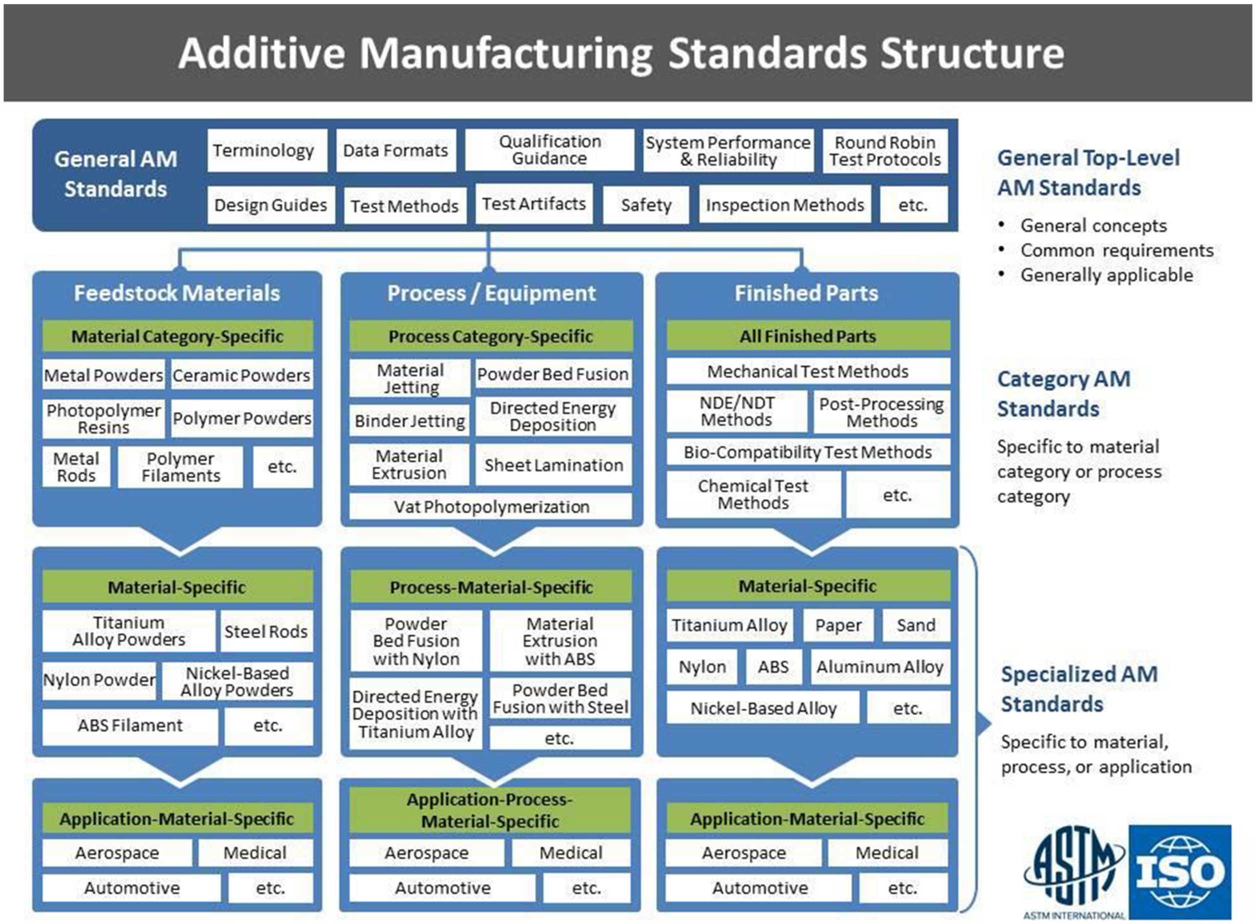


**Figure 51. AM standards organized by hierarchical specificity as outlined by ASTM and ISO** [163].

According to this specificity hierarchy, the standards relevant to AM in general—L-DED, its feedstock material, and associated qualification and specifications—are summarized in Table 8 through Table 15. Additionally, Table 16 lists standards developed for LPBF that currently have no L-DED equivalent. Standards published by organizations not typically referenced in US procurement documents (e.g., ASTM, ISO, AWS, or NASA) are italicized and in red print. Such standards are included for completeness and as potential starting points in developing NPP applicable standards. To the authors' knowledge, no codes or standards exist on joining and welding L-DED components.

**Table 8. AM general top-level codes and standards**

| Topic | Standard | Full name | Status |
|---|---|---|---|
| Terminology | ISO/ASTM 52900:2015 | Additive manufacturing – General principles – Terminology | Existing |
| | ISO / ASTM 52921 – 13(2019) | Standard Terminology for Additive Manufacturing—Coordinate Systems and Test Methodologies | Existing |
| Design | ISO/ASTM 52910:2018 | Additive manufacturing — Design — Requirements, guidelines and recommendations | Existing |
| Software requirements | ISO/ASTM 52915: 2016 | Specification for additive manufacturing file format (AMF) Version 1.2 | Existing |
| Geometry capability assessment | ISO/ASTM 52902: 2019 | Additive manufacturing — Test artifacts — Geometric capability assessment of additive manufacturing systems | Existing |

**Table 9. L-DED process and machine codes and standards**

| Topic | Standard | Full name | Status |
|---|---|---|---|
| Process control | AWS D20.1M | Specification for Fabrication of Metal Components using Additive Manufacturing | Existing |
| Laser power measurement | *JSA JIS C 6180* | *Measuring methods for laser output power* | Existing |
| | *SAC GB/T 6360-95* | *Specification for laser radiation power and energy measuring equipment* | Existing |
| | *GOST 25811* | *Means measuring laser output average power – Types – Basic parameters – Measuring methods* | Existing |
| Laser spot size measurement | ISO 11146-1 | Lasers and laser-related equipment — Test methods for laser beam widths, divergence angles and beam propagation ratios — Part 1: Stigmatic and simple astigmatic beams | Existing |
| | *SAC GB/T 13741-92* | *Testing method of beam diameter of laser radiation* | Existing |
| Laser power distribution measurement | ISO 13694 | Optics and photonics — Lasers and laser-related equipment — Test methods for laser beam power (energy) density distribution | Existing |
| Process gases | ANSI/AWS A5.32M | Specification for Welding Shielding Gases | Existing |
| Functional Grading | ISO/ASTM TR 52912:2020 | Additive manufacturing — Design — Functionally graded additive manufacturing | Existing |
| Laser dimensional control measurement | No existing standards | | — |
| Atmosphere specifications | No existing standards | | — |
| Feedback monitoring | ASTM WK62181 | New Guide for Standard Guide for In-Situ Monitoring (IPM) of Metal Additively Manufactured Aerospace Parts | Draft |

**Table 10. Powder metal feedstock relevant codes and standards**

| Topic | Standard | Full name | Status |
|---|---|---|---|
| Characterization | ASTM E2589 | Standard Terminology Relating to Nonsieving Methods of Powder Characterization | Existing |
| | ASTM B822 | Standard Test Method for Particle Size Distribution of Metal Powders and Related Compounds by Light Scattering | Existing |
| | ISO/ASTM 52907:2019 | Additive manufacturing — Feedstock materials — Methods to characterize metal powders | Existing |
| | ASTM F3049 – 14 | Standard Guide for Characterizing Properties of Metal Powders Used for Additive Manufacturing Processes | Existing |
| Internal porosity specifications | | No existing standards | — |
| Powder geometry specifications | | No existing standards | — |
| 316L phase specifications | | No existing standards | — |
| Reuse specifications | | No existing standards | — |

**Table 11. Powder sieving system codes and standards**

| Topic | Standard | Full name | Status |
|---|---|---|---|
| Terminology | ASTM E1638 | Standard Terminology Relating to Sieves, Sieving Methods, and Screening Media | Existing |
| Mesh specifications | ASTM E2016 | Standard Specification for Industrial Woven Wire Cloth | Existing |
| | ASTM E11 | Standard Specification for Woven Wire Test Sieve Cloth and Test Sieves | Existing |
| | ISO 3310-1 | Test sieves — Technical requirements and testing — Part 1: Test sieves of metal wire cloth | Existing |
| Initial testing methods | ASTM E2427 | Standard Test Method for Acceptance by Performance Testing for Sieves | Existing |
| Atmosphere specifications | | No existing standards | — |
| Mesh inspection specifications | | No existing standards | — |

**Table 12. Wire feedstock relevant codes and standards**

| Topic | Standard | Full name | Status |
|---|---|---|---|
| Characterization | AWS A5.4/A5.4M | Specification for Stainless Steel Electrodes for Shielded Metal Arc Welding | Existing |
| | AWS A5.9/A5.9M | Welding Consumables-Wire Electrodes, Strip Electrodes, Wires, and Rods for Arc Welding of Stainless and Heat Resisting Steels- Classification | Existing |
| | ISO 14343 | Welding consumables - Wire electrodes, strip electrodes, wires and rods for arc welding of stainless and heat resisting steels | Existing |
| | ASTM E353 | Standard Test Methods for Chemical Analysis of Stainless, Heat-Resisting, Maraging, and Other Similar Chromium-Nickel-Iron Alloys | Existing |

**Table 13. NDE codes and standards**

| Topic | Standard | Full name | Status |
|---|---|---|---|
| CT inspection specifications | ISO 15708-4 | Non-destructive testing — Radiation methods for computed tomography — Parts 1 to 4 | Existing |
| Weld inspection methods | DIN EN ISO 17635 | Non-destructive testing of welds – General rules for metallic materials | Existing |

**Table 14. Destructive testing material properties codes and standards**

| Topic | Standard | Full name | Status |
|---|---|---|---|
| Tensile testing methods | ASTM F3122 | Standard Guide for Evaluating Mechanical Properties of Metal Materials Made via Additive Manufacturing Processes | Existing |
| Reporting requirements | ASTM F2971 | Standard Practice for Reporting Data for Test Specimens Prepared by Additive Manufacturing | Existing |
| Recommended purchasing requirements | ISO / ASTM52901 - 16 | Standard Guide for Additive Manufacturing – General Principles – Requirements for Purchased AM Parts | Existing |

**Table 15. L-DED post-processing codes and standards**

| Topic | Standard | Full name | Status |
|---|---|---|---|
| Heat treatment | No existing standards | | — |
| Welding | No existing standards | | — |

**Table 16. LPBF specific standards currently without L-DED equivalents**

| Topic | Standard | Full name | Status |
|---|---|---|---|
| Design | ISO/ASTM52911-1: 2019 | Additive manufacturing — Design — Part 1: Laser-based powder bed fusion of metals | Existing |
| 316L chemical composition specifications | ASTM F3184-16 | Standard Specification for Additive Manufacturing Stainless Steel Alloy (UNS S31603) with Powder Bed Fusion | Existing |
| Process control | MSFC-SPEC-3717 | Specification for Control and Qualification of Laser Powder Bed Fusion Metallurgical Processes | Existing |
| | ASTM/ISO 52904:2019 | Additive manufacturing — Process characteristics and performance — Practice for metal powder bed fusion process to meet critical applications | Existing |
| Material property evaluation specifications | MSFC-STD-3716 | Standard for Additively Manufactured Spaceflight Hardware by Laser Powder Bed Fusion in Metals | Existing |
| 316L tensile specifications | ASTM F3184 – 16 | Standard Specification for Additive Manufacturing Stainless Steel Alloy (UNS S31603) with Powder Bed Fusion | Existing |
| Heat treatments | ASTM F3301 - 18a | Standard for Additive Manufacturing – Post Processing Methods – Standard Specification for Thermal Post-Processing Metal Parts Made Via Powder Bed Fusion | Existing |

### 3.5.2 Analysis of Existing Codes and Standards

A substantial effort is required to create codes and standards for AM processes to be used in industry. America Makes and ANSI have created a roadmap that helps identify, task, and track the development of these codes [165]. Standards for AM and L-DED are under active development by many organizations; however, substantive procedures are still being developed. Some of the subject areas in which significant codes and standards gaps are needed to implement AM (LW-DED, LP-DED, LPBF) include powder characterization (including internal porosity and geometry), porosity measurement (powder and components), surface finishing, inspection of fabricated components, procedures to quantify microstructural heterogeneity, acceptable chemical composition ranges, and pre- and post-welding heat treatment requirements.

At the time of this document's publication, ASTM has collaborated extensively with ISO in the creation of joint standards and specifications for AM processes, terminologies, and component requirements. However, many AM-specific standards do not contain relevant original technical specifications; rather, they simply reference existing technical specification documents for conventionally fabricated materials, provide generic background information or terminology, or provide recommendations for procurement specifications. For example, ASTM F3184 specifies, "Processing shall be conducted in accordance with applicable standards or as agreed upon by the component supplier and purchaser"; "Condition and finish of the components shall be agreed upon by the component supplier and purchaser"; and "Inspection criteria shall be agreed upon by the component supplier and purchaser." Further refinement of existing technical specifications for AM is needed, particularly for unique, demanding applications such as NPP environments. For example, ASTM F3184–16 for LPBF 316L specifies an acceptable maximum Si content of 1.00 wt%. As discussed in Sections 2.2.1 and 2.3.8, the Si content of 316L used in NPP SCC-susceptible environments may need to be reduced to a range of 0.05 to 0.1 wt% to prevent Si oxide inclusions in the microstructure.

AWS has adapted their prior standard, AWS B2.1/B2.1M, for use with AM to include LPBF and L-DED techniques in their D20.1/D20.1M document entitled "Specification for Fabrication of Metal Components Using Additive Manufacturing." The document outlines several substantive procedures worthy of note. First, a flow diagram and procedures are provided for qualifying AM machines, processes, and operators to three classes: A, B, and C. Second, they establish a list of process changes that trigger requalification of the machine or process. Finally, they explicitly state the statistical requirements for the 95/95 lower bound tolerance for tensile testing.

While AWS D20.1 is more definitive than other standards, several criticisms can be made. First, the document suggests the use of witness tensile specimens in a standard qualification build. While these coupons are useful in the initial optimization of machine parameters, they cannot account for the variation induced by geometric variation. The danger of this is illustrated in Figure 52. Witness coupon testing treats the entire build as a homogeneous unit with homogeneous properties; sampling from the thick portions of the deposition is attractive for specimen considerations, but it will not represent the material properties of the thin overhanging flange, which will have a different thermal history, cooling rate, and consequent grain structure and strength.

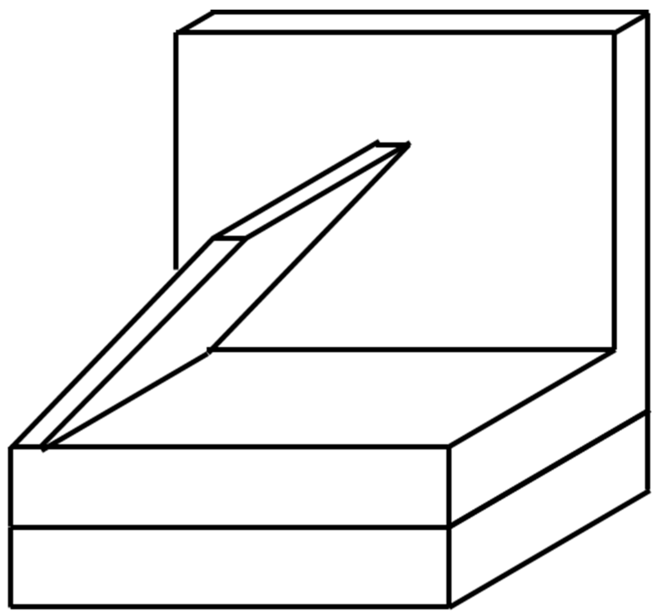

**Figure 52. A simple counterexample geometry that could be qualified to AWS D20.1 using tensile samples from thick sections but would systemically fail in thin sections, demonstrating that sampling strategies that do not account for geometry will fail to control performance.**

A second criticism of AWS D20.1 is that it requires recertification of the procedure for every change made to the build model. This is a highly conservative way to handle qualification, as it removes geometry variation as a factor to consider during qualification. However, this approach entirely frustrates the primary advantage of AM—geometric flexibility.

Clearly, the requirements and capabilities of AM break the subtractive standards model, in that *geometry matters*, and properties and microstructure cannot be extricated from the geometry and scan strategy. However, unlike other processes that may produce metallurgically nonhomogeneous results, AM and L-DED boast an unprecedented amount of localized, in-situ measurement data, because a part is printed millimeter by millimeter over the course of hours. This additional information can be leveraged to bypass geometric effects entirely, as illustrated in Figure 53.

Instead of a traditional qualification routine which locks a material + process + product to achieve a fixed performance, in AM, the qualification process would demonstrate that a particular in-situ measurement (color) guarantees performance at a certain level. Therefore, this allows the process to vary the geometry while still maintaining qualification. The role of a standards document, therefore, would not be to prescribe specific manufacturing conditions, but instead it would be to list the test requirements to demonstrate that sufficient process space has been sampled to establish a robust link between voxel-level information and performance.

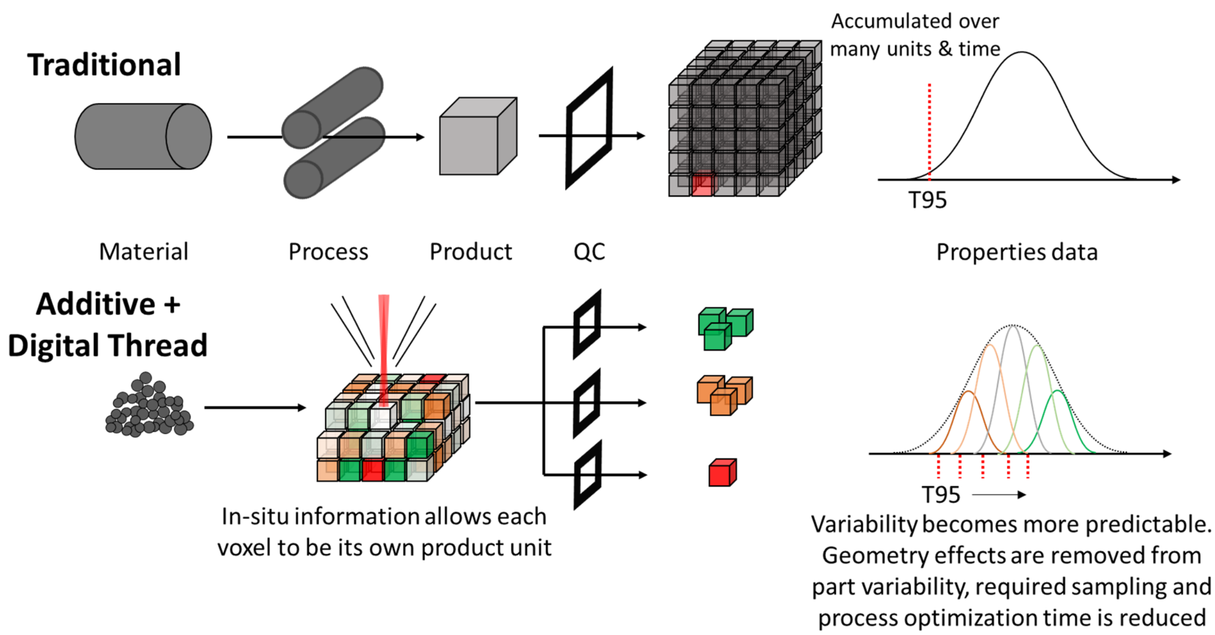


**Figure 53. How additional localized information for AM can be leveraged to isolate and predict geometric and stochastic effects, allowing for tighter control over property variability.**

While such a schema is attractive, it has yet to be demonstrated in practice. It must be conclusively demonstrated that the additional information collected contains enough information to account for and predict variability from sources such as geometry effects. For some properties of interest, there simply may not be enough relevance between externally observable signals to adequately predict performance. Therefore, AM standards could serve to codify how this link is established in a robust manner so that it is not focused either on the details of the component produced or on the specifics of information collection. Instead, the focus would be on the validation techniques required to demonstrate the capabilities and limitations of the monitoring methods. As a concrete example, instead of specifying a required wall thickness or a yield strength, a standard could allow for an arbitrary measurement method accompanied by a specific statistical testing regimen that includes a varied set of geometries and process conditions coupled to measurements of the metallurgical property specified. This would create a pipeline for a company to demonstrate the sensitivity and precision of new methods and claim a statistical confidence in their performance commensurate with the amount of testing and characterization they have invested, which would be limited to the bounds of the geometries and conditions over which they have tested.

# 4. CONCLUSIONS

Conventional subtractive manufacturing starts with an ingot of homogeneous and isotropic material and shapes it into the desired object with constraints on tooling paths and lines of sight. L-DED adds feedstock powder or wire to a laser weld in a programmed pattern to build a desired shape. In conventional machining manufacturing, design considerations and QC primarily revolve around testing statistically significant quantities of specimens sourced from the same ingot as a component, with the reasonable assumption that the material properties are homogeneous. In L-DED, the role of QC must necessarily expand to quantifying and controlling variability in the fabricated component's microstructure, and therefore its material properties, as microstructure varies as a function of the geometric design.

Effective process design and QC depend on a foundation of understanding built through literature review and analytical studies. Comparatively, much more research has been invested in LPBF than L-DED. Many relationships are still not understood well between the L-DED process, the microstructure, and the key properties such as fracture toughness, corrosion resistance, interaction with heat treatment, and in particular, irradiation effects. Existing exploratory studies strongly suggest that L-DED manufactured 316L will be capable of meeting requirements for NPP applications.

While progress has been made in demonstrating repeatable manufacturing processes and codifying requirements in standards, several technical gaps in the literature, as well as codes and standards gaps, should be addressed prior to the use of L-DED components in NPP applications. Major technical gaps include software and file control, sampling methodologies for determining material properties, procedures for planned and unplanned build interruptions, understanding of geometry-scan strategy interactions, and establishment of standard feedback controls. Major gaps in codes and standards include the areas of powder characterization, porosity measurement (powder and components), surface finishing, inspection of fabricated components, procedures to quantify microstructural heterogeneity, acceptable chemical composition ranges, and pre- and post-welding heat treatment requirements. If not addressed, each identified gap has the potential to adversely affect material properties.

Fabricating components for NPP applications with L-DED will require that the above gaps be addressed. However, L-DED offers significant advantages over conventional manufacturing, such as reduced lead times, reduced component inventory, potentially superior material properties, improved geometries, simplified assemblies, and the ability to reproduce practically any so-called "obsolete" component that was obtained from a vendor that has since gone out of business. Further technical advantages of L-DED include the ability to program different alloy mixtures and process parameters within the same component for embedded functionalization, as well as ready integration with CNC machining for a hybrid manufacturing approach.

# 5. REFERENCES


[1] "Standard for Additively Manufactured Spaceflight Hardware by Laser Powder Bed Fusion in Metals." National Aeronautics and Space Administration, Oct. 18, 2017.

[2] "AWS D20.1/D20.1M - Specification for Fabrication of Metal Components Using Additive Manufacturing." American Welding Society, Dec. 17, 2018, Accessed Oct. 12, 2020 [online] . Available: https://pubs.aws.org/p/1915/d201d201m2019-specification-for-fabrication-of-metal-components-using-additive-manufacturing.

[3] T. Zacharia, "Statement of Thomas Zacharia Director , Oak Ridge National Laboratory Hearing on the Future of Nuclear Power : Advanced Reactors," Oak Ridge National Laboratory, 2019, pp. 1–9.

[4] Nuclear Energy Institute, "Roadmap for Regulatory Acceptance of Advanced Manufacturing Methods in the Nuclear Energy Industry," 2019.

[5] "Boeing 787." https://www.reuters.com/article/us-norsk-boeing-idUSKBN17C264 (accessed Mar. 18, 2019).

[6] "GE Fuel Nozzel." https://www.ge.com/reports/epiphany-disruption-ge-additive-chief-explains-3d-printing-will-upend-manufacturing/ (accessed Mar. 18, 2019).

[7] D. Herzog, V. Seyda, E. Wycisk, and C. Emmelmann, "Additive Manufacturing of Metals," *Acta Materialia*, vol. 117, pp. 371–392, 2016, doi: 10.1016/j.actamat.2016.07.019.

[8] W. E. Frazier, "Metal Additive Manufacturing: A Review," *Journal of Materials Engineering and Performance*, vol. 23, no. 6, pp. 1917–1928, 2014, doi: 10.1007/s11665-014-0958-z.

[9] D. I. Wimpenny, P. M. Pandey, and L. J. Kumar, Eds., *Advances in 3D Printing and Additive Manufacturing Technologies*. Springer US, 2017.

[10] G. Allaire, C. Dapogny, R. Estevez, A. Faure, and G. Michailidis, "Structural Optimization under Overhang Constraints Imposed by Additive Manufacturing Technologies," *Journal of Computational Physics*, vol. 351, pp. 295–328, 2017, doi: 10.1016/j.jcp.2017.09.041.

[11] Y. Zhang et al., "Additive Manufacturing of Metallic Materials: A Review," *Journal of Materials Engineering and Performance*, vol. 27, no. 1, pp. 1–13, 2018, doi: 10.1007/s11665-017-2747-y.

[12] J. Simpson et al., "Considerations for Application of Additive Manufacturing to Nuclear Reactor Core Components," ORNL/TM-2019/1190, 1564201, May 2019. doi: 10.2172/1564201.

[13] S. K. Kennedy, A. M. Dalley, and G. J. Kotyk, "Additive Manufacturing: Assessing Metal Powder Quality Through Characterizing Feedstock and Contaminants," *Journal of Materials Engineering and Performance*, vol. 28, pp. 728–740, 2019, doi: 10.1007/s11665-018-3841-5.

[14] A. Santomaso, P. Lazzaro, and P. Canu, "Powder Flowability and Density Ratios: The Impact of Granules Packing," *Chemical Engineering Science*, vol. 58, pp. 2857–2874, 2003, doi: 10.1016/S0009-2509(03)00137-4.

[15] A. T. Sutton, C. S. Kriewall, M. C. Leu, and J. W. Newkirk, "Powder Characterisation Techniques and Effects of Powder Characteristics on Part Properties in Powder-Bed Fusion Processes," *Virtual and Physical Prototyping*, vol. 12, no. 1, pp. 3–29, 2016, doi: 10.1080/17452759.2016.1250605.

[16] "Welding Consumables - Part 4 - TWI." https://www.twi-global.com/technical-knowledge/job-knowledge/welding-consumables-part-4-085 (accessed Jun. 07, 2021).

[17] A. G. Demir, "Micro Laser Metal Wire Deposition for Additive Manufacturing of Thin-Walled Structures," *Optics and Lasers in Engineering*, vol. 100, pp. 9–17, Jan. 2018, doi: 10.1016/j.optlaseng.2017.07.003.

[18] W. J. Sames, F. A. List, S. Pannala, R. R. Dehoff, and S. S. Babu, "The Metallurgy and Processing Science of Metal Additive Manufacturing," *International Materials Reviews*, vol. 61, no. 5, pp. 315–360, 2016, doi: 10.1080/09506608.2015.1116649.

[19] J. Lei, J. Xie, S. Zhou, H. Song, X. Song, and X. Zhou, "Comparative Study on Microstructure and Corrosion Performance of 316 Stainless Steel Prepared by Laser Melting Deposition with Ring-

Shaped Beam and Gaussian Beam," *Optics and Laser Technology*, vol. 111, pp. 271–283, 2019, doi: 10.1016/j.optlastec.2018.09.057.
[20] A. Klassen, T. Scharowsky, and C. Körner, "Evaporation Model for Beam Based Additive Manufacturing Using Free Surface Lattice Boltzmann Methods," *Journal of Physics D: Applied Physics*, vol. 47, 2014, doi: 10.1088/0022-3727/47/27/275303.
[21] A. Klassen, V. E. Forster, and C. Körner, "A Multi-Component Evaporation Model for Beam Melting Processes," *Modelling and Simulation in Materials Science and Engineering*, vol. 25, 2017, doi: 10.1088/1361-651X/aa5289.
[22] J. Simpson and R. Dehoff, "Review of Advanced Manufacturing Techniques and Qualification Processes for Light Water Reactors - Laser Powder Bed Fusion Additive Manufacturing." [Online]. Available: https://www.nrc.gov/docs/ML2035/ML20351A217.pdf
[23] J. I. Arrizubieta, I. Tabernero, J. E. Ruiz, A. Lamikiz, S. Martinez, and E. Ukar, "Continuous Coaxial Nozzle Design for LMD based on Numerical Simulation," *Physics Procedia*, vol. 56, pp. 429–438, Jan. 2014, doi: 10.1016/j.phpro.2014.08.146.
[24] M. Renderos, F. Girot, A. Lamikiz, A. Torregaray, and N. Saintier, "Ni Based Powder Reconditioning and Reuse for LMD Process," *Physics Procedia*, vol. 83, pp. 769–777, Jan. 2016, doi: 10.1016/j.phpro.2016.08.079.
[25] K. L. Terrassa, J. C. Haley, B. E. MacDonald, and J. M. Schoenung, "Reuse of Powder Feedstock for Directed Energy Deposition," *Powder Technology*, vol. 338, pp. 819–829, Oct. 2018, doi: 10.1016/j.powtec.2018.07.065.
[26] M. J. Heiden et al., "Evolution of 316L Stainless Steel Feedstock Due to Laser Powder Bed Fusion Process," *Additive Manufacturing*, vol. 25, no. July 2018, pp. 84–103, 2019, doi: 10.1016/j.addma.2018.10.019.
[27] W. J. Sames, F. Medina, W. H. Peter, S. S. Babu, and R. R. Dehoff, "Effect of Process Control and Powder Quality on Inconel 718 Produced Using Electron Beam Melting," *8th International Symposium on Superalloy 718 and Derivatives*, pp. 409–423, 2014, doi: 10.1002/9781119016854.ch32.
[28] H. Qi, M. Azer, and A. Ritter, "Studies of Standard Heat Treatment Effects on Microstructure and Mechanical Properties of Laser Net Shape Manufactured INCONEL 718," *Metallurgical and Materials Transactions A: Physical Metallurgy and Materials Science*, vol. 40A, pp. 2410–2422, 2009, doi: 10.1007/s11661-009-9949-3.
[29] X. Zhao, J. Chen, X. Lin, and W. Huang, "Study on Microstructure and Mechanical Properties of Laser Rapid Forming Inconel 718," *Materials Science and Engineering A*, vol. 478, no. 1–2, pp. 119–124, 2008, doi: 10.1016/j.msea.2007.05.079.
[30] P. Balu, P. Leggett, S. Hamid, and R. Kovacevic, "Multi-Response Optimization of Laser-based Powder Deposition of Multi-track Single Layer Hastelloy C-276," *Mater. Manuf. Process.*, vol. 28, no. 2, pp. 173–182, Feb. 2013, doi: 10.1080/10426914.2012.677908.
[31] J. C. Haley, B. Zheng, U. S. Bertoli, A. D. Dupuy, J. M. Schoenung, and E. J. Lavernia, "Working Distance Passive Stability in Laser Directed Energy Deposition Additive Manufacturing," *Materials and Design*, 2019, doi: 10.1016/j.matdes.2018.11.021.
[32] J. Volpp, "Behavior of Powder Particles on Melt Pool Surfaces," *Int J Adv Manuf Technol*, vol. 102, no. 5–8, pp. 2201–2210, Jun. 2019, doi: 10.1007/s00170-018-03261-1.
[33] J. C. Haley, J. M. Schoenung, and E. J. Lavernia, "Observations of Particle-Melt Pool Impact Events in Directed Energy Deposition," *Additive Manufacturing*, vol. 22, pp. 368–374, Aug. 2018, doi: 10.1016/j.addma.2018.04.028.
[34] F. Zhang et al., "Interaction between Powder Particle and Gas-Liquid Interface of the Melt Pool during laser Solid Forming Process," *Optics and Lasers in Engineering*, vol. 129, p. 106065, Jun. 2020, doi: 10.1016/j.optlaseng.2020.106065.
[35] J. C. Haley, J. M. Schoenung, and E. J. Lavernia, "Modelling Particle Impact on the Melt Pool and Wettability Effects in Laser Directed Energy Deposition Additive Manufacturing," *Materials Science and Engineering: A*, vol. 761, p. 138052, Jul. 2019, doi: 10.1016/j.msea.2019.138052.

[36] A. Heralić, A.-K. Christiansson, K. Hurtig, M. Ottosson, and B. Lennartson, “Control Design for Automation of Robotized Laser Metal-wire Deposition,” *IFAC Proceedings Volumes*, vol. 41, no. 2, pp. 14785–14791, 2008, doi: 10.3182/20080706-5-KR-1001.02503.

[37] A. R. Nassar et al., “Sensing for Directed Energy Deposition and Powder Bed Fusion Additive Manufacturing at Penn State University,” in *Laser 3D Manufacturing III*, 2016, vol. 9738, p. 97380R.

[38] B. T. Gibson et al., “Melt Pool Size Control through Multiple Closed-Loop Modalities in Laser-Wire Directed Energy Deposition of Ti-6Al-4V,” *Additive Manufacturing*, vol. 32, p. 100993, Mar. 2020, doi: 10.1016/j.addma.2019.100993.

[39] B. T. Gibson et al., “Accelerating Large-Format Metal Additive Manufacturing: How Controls R&D Is Driving Speed, Scale, and Efficiency,” in *Volume 2A: Advanced Manufacturing*, Virtual, Online, Nov. 2020, p. V02AT02A038. doi: 10.1115/IMECE2020-23322.

[40] J. Barnes, A. Kingsbury, and E. Bono, “Does low cost titanium powder yield low cost titanium parts,” 2016.

[41] A. R. Nassar and E. W. Reutzel, “Beyond Layer-by-Layer Additive Manufacturing – Voxel-Wise Directed Energy Deposition.” Accessed: Jul. 22, 2020. [Online]. Available: http://utw10945.utweb.utexas.edu/sites/default/files/2015/2015-22-Nassar.pdf

[42] R. R. Dehoff et al., “Site Specific Control of Crystallographic Grain Orientation through Electron Beam Additive Manufacturing,” *Materials Science and Technology*, vol. 31, no. 8, pp. 931–938, 2015, doi: 10.1179/1743284714y.0000000734.

[43] J. L. Dávila, P. I. Neto, P. Y. Noritomi, R. T. Coelho, and J. V. L. da Silva, “Hybrid Manufacturing: a Review of the Synergy between Directed Energy Deposition and Subtractive Processes,” *Int J Adv Manuf Technol*, vol. 110, no. 11, pp. 3377–3390, Oct. 2020, doi: 10.1007/s00170-020-06062-7.

[44] P. Edwards and M. Ramulu, “Fatigue Performance Evaluation of Selective Laser Melted Ti-6Al-4V,” *Materials Science and Engineering A*, vol. 598, pp. 327–337, 2014, doi: 10.1016/j.msea.2014.01.041.

[45] Z. Wang, K. Guan, M. Gao, X. Li, X. Chen, and X. Zeng, “The Microstructure and Mechanical Properties of Deposited-IN718 by Selective Laser Melting,” *Journal of Alloys and Compounds*, vol. 513, pp. 518–523, 2012, doi: 10.1016/j.jallcom.2011.10.107.

[46] L. M. Sochalski-Kolbus et al., “Comparison of Residual Stresses in Inconel 718 Simple Parts Made by Electron Beam Melting and Direct Laser Metal Sintering,” *Metallurgical and Materials Transactions A: Physical Metallurgy and Materials Science*, vol. 46A, pp. 1419–1432, 2015, doi: 10.1007/s11661-014-2722-2.

[47] K. N. Amato et al., “Microstructures and Mechanical Behavior of Inconel 718 Fabricated by Selective Laser Melting,” *Acta Materialia*, vol. 60, pp. 2229–2239, 2012, doi: 10.1016/j.actamat.2011.12.032.

[48] T. D. Ngo, A. Kashani, G. Imbalzano, K. T. Q. Nguyen, and D. Hui, “Additive Manufacturing (3D printing): A Review of Materials, Methods, Applications and Challenges,” *Composites Part B: Engineering*, vol. 143, pp. 172–196, 2018, doi: 10.1016/j.compositesb.2018.02.012.

[49] D. D. Gu, W. Meiners, K. Wissenbach, and R. Poprawe, “Laser Additive Manufacturing of Ceramic Components: Materials, Processes, and Mechanisms,” *International Materials Reviews*, vol. 57, no. 3, pp. 133–164, 2012, doi: 10.1016/B978-0-08-100433-3.00006-3.

[50] Y. Hu et al., “Laser Deposition-Additive Manufacturing of In Situ TiB Reinforced Titanium Matrix Composites: TiB Growth and Part Performance,” *International Journal of Advanced Manufacturing Technology*, vol. 93, pp. 3409–3418, 2017, doi: 10.1007/s00170-017-0769-0.

[51] J. Vaithilingam, S. Kilsby, R. D. Goodridge, S. D. R. Christie, S. Edmondson, and R. J. M. Hague, “Functionalisation of Ti6Al4V Components Fabricated Using Selective Laser Melting with a Bioactive Compound,” *Materials Science and Engineering C*, vol. 46, pp. 52–61, 2015, doi: 10.1016/j.msec.2014.10.015.

[52] H. Attar, M. Calin, L. C. Zhang, S. Scudino, and J. Eckert, “Manufacture by Selective Laser Melting and Mechanical Behavior of commercially Pure Titanium,” *Materials Science and Engineering A*, vol. 593, pp. 170–177, 2014, doi: 10.1016/j.msea.2013.11.038.
[53] I. Yadroitsev, L. Thivillon, P. Bertrand, and I. Smurov, “Strategy of Manufacturing Components with Designed Internal Structure by Selective Laser Melting of Metallic Powder,” *Applied Surface Science*, vol. 254, pp. 980–983, 2007, doi: 10.1016/j.apsusc.2007.08.046.
[54] C. Körner, H. Helmer, A. Bauereiß, and R. F. Singer, “Tailoring the Grain Structure of IN718 during Selective Electron Beam Melting,” *MATEC Web of Conferences*, vol. 14, 2014, doi: 10.1051/matecconf/20141408001.
[55] I. Rosenthal, A. Stern, and N. Frage, “Strain Rate Sensitivity and Fracture Mechanism of AlSi10Mg Parts Produced by Selective Laser Melting,” *Materials Science and Engineering A*, vol. 682, pp. 509–517, 2017, doi: 10.1016/j.msea.2016.11.070.
[56] P. Vora, K. Mumtaz, I. Todd, and N. Hopkinson, “AlSi12 In-Situ Alloy Formation and Residual Stress Reduction Using Anchorless Selective Laser Melting,” *Additive Manufacturing*, vol. 7, pp. 12–19, 2015, doi: 10.1016/j.addma.2015.06.003.
[57] Y. H. Xiong, J. E. Smugeresky, and J. M. Schoenung, “The Influence of Working Distance on Laser Deposited WC-Co,” *J. Mater. Process. Technol.*, vol. 209, no. 10, pp. 4935–4941, Jun. 2009, doi: 10.1016/j.jmatprotec.2009.01.016.
[58] H. D. Carlton, A. Haboub, G. F. Gallegos, D. Y. Parkinson, and A. A. MacDowell, “Damage Evolution and Failure Mechanisms in Additively Manufactured Stainless Steel,” *Materials Science and Engineering A*, vol. 651, pp. 406–414, 2016, doi: 10.1016/j.msea.2015.10.073.
[59] J. Mazumder, J. Choi, K. Nagarathnam, J. Koch, and D. Hetzner, “The Direct Metal Deposition of H13 Tool Steel for 3-D Components,” *JOM*, vol. 49, no. 5, pp. 55–60, 1997.
[60] L. E. Murr et al., “Microstructures and Properties of 17-4 PH Stainless Steel Fabricated by Selective Laser Melting,” *Journal of Materials Research and Technology*, vol. 1, no. 3, pp. 167–177, 2012, doi: 10.1016/S2238-7854(12)70029-7.
[61] G. Casalino, S. L. Campanelli, N. Contuzzi, and A. D. Ludovico, “Experimental Investigation and Statistical Optimisation of the Selective Laser Melting Process of a Maraging Steel,” *Optics and Laser Technology*, vol. 65, pp. 151–158, 2015, doi: 10.1016/j.optlastec.2014.07.021.
[62] J. S. Zuback and T. DebRoy, “The Hardness of Additively Manufactured Alloys,” *Materials*, vol. 11, p. 2070, 2018, doi: 10.3390/ma11112070.
[63] S. Magar, N. K. Khedkar, and S. Kumar, “Review of the Effect of Built Orientation on Mechanical Properties of Metal-Plastic Composite Parts Fabricated by Additive Manufacturing Technique,” *Materials Today: Proceedings*, vol. 5, pp. 3926–3935, 2018, doi: 10.1016/j.matpr.2017.11.649.
[64] Y. Kok et al., “Anisotropy and Heterogeneity of Microstructure and Mechanical Properties in Metal Additive Manufacturing: A Critical Review,” *Materials and Design*, vol. 139, pp. 565–586, 2018, doi: 10.1016/j.matdes.2017.11.021.
[65] M. M, R. J, and F. D, *Handbook of Laser Materials Processing*. Orlando, USA: Magnolia Publishing Inc, 2001.
[66] J. Haley, “Long and Short Time Scale Mass Capture Mechanisms in Laser Directed Energy Deposition Additive Manufacturing,” UC Irvine.
[67] N. Coniglio and C. E. Cross, “Initiation and Growth Mechanisms for Weld Solidification Cracking,” *International Materials Reviews*, vol. 58, no. 7, pp. 375–397, Sep. 2013, doi: 10.1179/1743280413Y.0000000020.
[68] H. Bhadeshia and R. Honeycombe, *Steels: Microstructure and Properties*. Butterworth-Heinemann, 2017.
[69] J. W. Elmer, “The Influence of Cooling Rate on the Microstructure of Stainless Steel Alloys,” Lawrence Livermore National Lab., CA (USA), 1988.
[70] V. Kujanpaa, N. Suutala, T. Takalo, and T. Moisio, “Correlation between Solidification Cracking and Microstructure in Austenitic and Austenitic-Ferritic Stainless Steel Welds,” *Welding Research International*, vol. 9, no. 2, pp. 55–75, 1979.

[71] J. C. Lippold, “Solidification Behavior and Cracking Susceptibility of Pulsed-Laser Welds in Austenitic Stainless Steels,” *Welding Journal Including Welding Research Supplement*, vol. 73, no. 6, p. 129s, 1994.
[72] S. Fukumoto and W. Kurz, “Solidification Phase and Microstructure Selection Maps for Fe-Cr-Ni Alloys,” *ISIJ international*, vol. 39, no. 12, pp. 1270–1279, 1999.
[73] T. R. Smith, J. D. Sugar, C. San Marchi, and J. M. Schoenung, “Strengthening Mechanisms in Directed Energy Deposited Austenitic Stainless Steel,” *Acta Materialia*, vol. 164, pp. 728–740, Feb. 2019, doi: 10.1016/j.actamat.2018.11.021.
[74] J. C. Lippold and D. J. Kotecki, *Welding Metallurgy and Weldability of Stainless Steels*. 2005.
[75] T. J. Lienert and J. C. Lippold, “Improved Weldability Diagram for Pulsed Laser Welded Austenitic Stainless Steels,” *Science and Technology of Welding and Joining*, vol. 8, no. 1, pp. 1–9, 2003.
[76] D. M. Wilson, “Metallurgical and Mechanical Property Characterization of Additively Manufactured 304L Stainless Steel,” Text, Colorado School of Mines, 2018. Accessed: Jun. 07, 2021. [Online]. Available: https://mountainscholar.org/handle/11124/173079
[77] J. C. Lippold, “Solidification Behavior and Cracking Susceptibility of Pulsed-Laser Welds in Austenitic Stainless Steels,” p. 11.
[78] T. DebRoy et al., “Additive Manufacturing of Metallic Components – Process, Structure and Properties,” *Progress in Materials Science*, vol. 92, no. Supplement C, pp. 112–224, Mar. 2018, doi: 10.1016/j.pmatsci.2017.10.001.
[79] A. Yadollahi, N. Shamsaei, S. M. Thompson, and D. W. Seely, “Effects of Process Time Interval and Heat Treatment on the Mechanical and Microstructural Properties of Direct Laser Deposited 316L Stainless Steel,” *Mater. Sci. Eng. A-Struct. Mater. Prop. Microstruct. Process.*, vol. 644, pp. 171–183, Sep. 2015, doi: 10.1016/j.msea.2015.07.056.
[80] B. Zheng et al., “On the Evolution of Microstructure and Defect Control in 316L SS Components Fabricated via Directed Energy Deposition,” *Materials Science and Engineering: A*, vol. 764, p. 138243, Sep. 2019, doi: 10.1016/j.msea.2019.138243.
[81] V. D. Manvatkar et al., “Estimation of Melt Pool Dimensions, Thermal Cycle, and Hardness Distribution in the Laser-Engineered Net Shaping Process of Austenitic Stainless Steel,” *Metallurgical and Materials Transactions A*, vol. 42A, no. 13, pp. 4080–4087, 2011.
[82] K. Zhang, S. Wang, W. Liu, and X. Shang, “Characterization of Stainless Steel Parts by Laser Metal Deposition Shaping,” *Materials & Design*, vol. 55, pp. 104–119, Mar. 2014, doi: 10.1016/j.matdes.2013.09.006.
[83] U. Scipioni Bertoli, B. E. MacDonald, and J. M. Schoenung, “Stability of Cellular Microstructure in Laser Powder Bed Fusion of 316L Stainless Steel,” *Materials Science and Engineering: A*, vol. 739, pp. 109–117, Jan. 2019, doi: 10.1016/j.msea.2018.10.051.
[84] S. Katayama and A. Matsunawa, “Solidification Microstructure of Laser Welded Stainless Steels,” in *International Congress on Applications of Lasers & Electro-Optics*, Boston, Massachusetts, USA, 1984, pp. 60–67. doi: 10.2351/1.5057623.
[85] Paul. Lacombe et al., *Stainless Steels*. Les Ulis, France: Les Editions de Physique, 1993.
[86] A. Aversa et al., “The role of Directed Energy Deposition atmosphere mode on the microstructure and mechanical properties of 316L samples,” *Additive Manufacturing*, vol. 34, p. 101274, Aug. 2020, doi: 10.1016/j.addma.2020.101274.
[87] A. A276, *Standard Specification for Stainless Steel Bars and Shapes*. ASTM International West Conshohocken, Pa., 2010.
[88] M. Z. Gao, B. Ludwig, and T. A. Palmer, “Impact of Atomization Gas on Characteristics of Austenitic Stainless Steel Powder Feedstocks for Additive Manufacturing,” *Powder Technology*, vol. 383, pp. 30–42, 2021.
[89] T. R. Smith, J. D. Sugar, C. San Marchi, and J. M. Schoenung, “Strengthening Mechanisms in Directed Energy Deposited Austenitic Stainless Steel,” *Acta Materialia*, vol. 164, pp. 728–740, Feb. 2019, doi: 10.1016/j.actamat.2018.11.021.

[90] D.-R. Eo, S.-H. Park, and J.-W. Cho, “Inclusion Evolution in Additive Manufactured 316L Stainless Steel by laser Metal Deposition Process,” *Materials & Design*, vol. 155, pp. 212–219, Oct. 2018, doi: 10.1016/j.matdes.2018.06.001.

[91] D.-R. Eo, S.-H. Park, and J.-W. Cho, “Inclusion Evolution in Additive Manufactured 316L Stainless Steel by Laser Metal Deposition Process,” *Materials & Design*, vol. 155, pp. 212–219, Oct. 2018, doi: 10.1016/j.matdes.2018.06.001.

[92] X. Lou, P. L. Andresen, and R. B. Rebak, “Oxide Inclusions in Laser Additive Manufactured Stainless Steel and Their Effects on Impact Toughness and Stress Corrosion Cracking Behavior,” *Journal of Nuclear Materials*, vol. 499, pp. 182–190, Feb. 2018, doi: 10.1016/j.jnucmat.2017.11.036.

[93] D. F. Susan, D. Kammler, M. A. Rodriguez, J. R. Michael, Z. Ghanbari, and C. A. Profazi, “The Effects of Annealing Treatments on AM 316L Stainless Steel,” Sandia National Lab.(SNL-NM), Albuquerque, NM (United States), 2018.

[94] Y. M. Wang et al., “Additively Manufactured Hierarchical Stainless Steels with High Strength and Ductility,” *Nature Materials*, Oct. 2017, [Online]. Available: http://dx.doi.org/10.1038/nmat5021

[95] H. Yin, M. Song, P. Deng, L. Li, B. C. Prorok, and X. Lou, “Thermal Stability and Microstructural Evolution of Additively Manufactured 316L Stainless Steel by Laser Powder Bed Fusion at 500–800°C,” *Additive Manufacturing*, vol. 41, p. 101981, May 2021, doi: 10.1016/j.addma.2021.101981.

[96] S. Webster, K. Ehmann, and J. Cao, “Energy Density Comparison via Highspeed, In-situ Imaging of Directed Energy Deposition,” *Procedia Manufacturing*, vol. 48, pp. 691–696, Jan. 2020, doi: 10.1016/j.promfg.2020.05.101.

[97] J. Li et al., “Microstructure and Performance Optimisation of Stainless Steel Formed by Laser Additive Manufacturing,” *Materials Science and Technology (United Kingdom)*, vol. 32, no. 12, pp. 1223–1230, 2016, doi: 10.1080/02670836.2015.1114774.

[98] Z. Wang, T. A. Palmer, and A. M. Beese, “Effect of Processing Parameters on Microstructure and Tensile Properties of Austenitic Stainless Steel 304L Made by Directed Energy Deposition Additive Manufacturing,” *Acta Materialia*, vol. 110, pp. 226–235, 2016, doi: 10.1016/j.actamat.2016.03.019.

[99] A. Röttger, K. Geenen, M. Windmann, F. Binner, and W. Theisen, “Comparison of Microstructure and Mechanical Properties of 316 L Austenitic Steel Processed by Selective Laser Melting with Hot-Isostatic Pressed and Cast Material,” *Materials Science and Engineering A*, vol. 678, pp. 365–376, 2016, doi: 10.1016/j.msea.2016.10.012.

[100] M. Ziętala et al., “The Microstructure, Mechanical Properties and Corrosion Resistance of 316 L Stainless Steel Fabricated Using Laser Engineered Net Shaping,” *Materials Science and Engineering A*, vol. 677, pp. 1–10, 2016, doi: 10.1016/j.msea.2016.09.028.

[101] K. Zhang, S. Wang, W. Liu, and X. Shang, “Characterization of Stainless Steel Parts by Laser Metal Deposition Shaping,” *Materials and Design*, vol. 55, pp. 104–119, 2014, doi: 10.1016/j.matdes.2013.09.006.

[102] C. S. Hamza Hassn Alsalla and L. Hao, “Effect of Build Orientation on the Surface Quality, Microstructure and Mechanical Properties of Selective Laser Melting 316L Stainless Steel,” 2016.

[103] A. Mertens, S. Reginster, Q. Contrepois, T. Dormal, O. Lemaire, and J. Lecomte-Beckers, “Microstructures and Mechanical Properties of Stainless Steel AISI 316L Processed by Selective Laser Melting,” *Materials Science Forum*, vol. 783–786, pp. 898–903, 2014, doi: 10.4028/www.scientific.net/msf.783-786.898.

[104] A. Mertens et al., “Mechanical Properties of Alloy Ti–6Al–4V and of Stainless Steel 316L Processed by Selective Laser Melting: Influence of Out-Of-Equilibrium Microstructures,” *Powder Metallurgy*, vol. 57, no. 3, pp. 184–189, 2014, doi: 10.1179/1743290114Y.0000000092.

[105] J. Yu, M. Rombouts, and G. Maes, “Cracking Behavior and Mechanical Properties of Austenitic Stainless Steel Parts Produced by Laser Metal Deposition,” *Materials and Design*, p. 8, 2013.

[106] F42 Committee, "Specification for Additive Manufacturing Stainless Steel Alloy (UNS S31603) with Powder Bed Fusion," ASTM International. doi: 10.1520/F3184-16.
[107] A01 Committee, "Specification for Stainless Steel Bars and Shapes," ASTM International. doi: 10.1520/A0276_A0276M-17.
[108] Z. Wang, T. A. Palmer, and A. M. Beese, "Effect of Processing Parameters on Microstructure and Tensile Properties of Austenitic Stainless Steel 304L Made by Directed Energy Deposition Additive Manufacturing," *Acta Materialia*, vol. 110, pp. 226–235, May 2016, doi: 10.1016/j.actamat.2016.03.019.
[109] C.-H. Shiau et al., "Deformation Behavior and Irradiation Tolerance of 316 L Stainless Steel Fabricated by Direct Energy Deposition," *Materials & Design*, vol. 204, p. 109644, Jun. 2021, doi: 10.1016/j.matdes.2021.109644.
[110] M. Akbari and R. Kovacevic, "An Investigation on Mechanical and Microstructural Properties of 316LSi Parts Fabricated by a Robotized Laser/Wire Direct Metal Deposition System," *Additive Manufacturing*, vol. 23, pp. 487–497, 2018.
[111] D. Kono, A. Maruhashi, I. Yamaji, Y. Oda, and M. Mori, "Effects of Cladding Path on Workpiece Geometry and Impact Toughness in Directed Energy Deposition of 316L Stainless Steel," *CIRP Annals*, vol. 67, no. 1, pp. 233–236, Jan. 2018, doi: 10.1016/j.cirp.2018.04.087.
[112] A. J. Cooper, N. I. Cooper, J. Dhers, and A. H. Sherry, "Effect of Oxygen Content upon the Microstructural and Mechanical Properties of Type 316L Austenitic Stainless Steel Manufactured by Hot Isostatic Pressing," *Metall and Mat Trans A*, vol. 47, no. 9, pp. 4467–4475, Sep. 2016, doi: 10.1007/s11661-016-3612-6.
[113] A. McWilliams, M. Morgan, and P. Korinko, "Hydrogen Effects on Fracture Toughness of Additively Manufactured Type 304L Stainless Steel," in *Volume 6A: Materials and Fabrication*, San Antonio, Texas, USA, Jul. 2019, p. V06AT06A005. doi: 10.1115/PVP2019-93709.
[114] J. J. Lewandowski and M. Seifi, "Metal Additive Manufacturing: A Review of Mechanical Properties," *Annual Review of Materials Research*, vol. 46, no. 1, pp. 151–186, 2016, doi: 10.1146/annurev-matsci-070115-032024.
[115] A. Fatemi, R. Molaei, S. Sharifimehr, N. Phan, and N. Shamsaei, "Multiaxial Fatigue Behavior of Wrought and Additive Manufactured Ti-6Al-4V Including Surface Finish Effect," *International Journal of Fatigue*, vol. 100, pp. 347–366, Jul. 2017, doi: 10.1016/j.ijfatigue.2017.03.044.
[116] A. B. Spierings, T. L. Starr, and K. Wegener, "Fatigue Performance of Additive Manufactured Metallic Parts," *Rapid Prototyping Journal*, vol. 19, no. 2, pp. 88–94, 2013, doi: 10.1108/13552541311302932.
[117] K. Xu et al., "In Situ Observation for the Fatigue Crack Growth Mechanism of 316L Stainless Steel Fabricated by Laser Engineered Net Shaping," *International Journal of Fatigue*, vol. 130, p. 105272, Jan. 2020, doi: 10.1016/j.ijfatigue.2019.105272.
[118] T. R. Smith, J. D. Sugar, J. M. Schoenung, and C. San Marchi, "Relationship between Manufacturing Defects and Fatigue Properties of Additive Manufactured Austenitic Stainless Steel," *Materials Science and Engineering: A*, vol. 765, p. 138268, Sep. 2019, doi: 10.1016/j.msea.2019.138268.
[119] B. Blinn et al., "Process-Influenced Fatigue Behavior of AISI 316L Manufactured by Powder- and Wire-Based Laser Direct Energy Deposition," *Materials Science and Engineering: A*, vol. 818, p. 141383, Jun. 2021, doi: 10.1016/j.msea.2021.141383.
[120] T. G. Gooch, "Corrosion Behavior of Welded Stainless Steel," *Welding Journal*, vol. 75, no. 5, May 1996, Accessed: Jun. 22, 2021. [Online]. Available: https://www.osti.gov/biblio/248119
[121] J. A. Stull, M. A. Hill, T. J. Lienert, J. Tokash, K. R. Bohn, and D. E. Hooks, "Corrosion Characteristics of Laser-Engineered Net Shaping Additively-Manufactured 316L Stainless Steel," *JOM*, vol. 70, no. 11, pp. 2677–2683, Nov. 2018, doi: 10.1007/s11837-018-3123-6.
[122] M. A. Melia, H.-D. A. Nguyen, J. M. Rodelas, and E. J. Schindelholz, "Corrosion Properties of 304L Stainless Steel Made by Directed Energy Deposition Additive Manufacturing," *Corrosion Science*, vol. 152, pp. 20–30, May 2019, doi: 10.1016/j.corsci.2019.02.029.

[123] X. Chen, B. Chen, X. Cheng, G. Li, and Z. Huang, “Microstructure and Properties of Hybrid Additive Manufacturing 316L Component by Directed Energy Deposition and Laser Remelting,” *J. Iron Steel Res. Int.*, vol. 27, no. 7, pp. 842–848, Jul. 2020, doi: 10.1007/s42243-020-00396-y.
[124] J. A. Stull, M. A. Hill, T. J. Lienert, J. Tokash, K. R. Bohn, and D. E. Hooks, “Corrosion Characteristics of Laser-Engineered Net Shaping Additively-Manufactured 316L Stainless Steel,” *JOM*, vol. 70, no. 11, pp. 2677–2683, Nov. 2018, doi: 10.1007/s11837-018-3123-6.
[125] NRC: Package ML20351A292 - Impending Publication of TLR, "Review of Advanced Manufacturing Techniques and Qualification Processes for LWRs - Laser Powder Bed Fusion Additive Manufacturing" and Technical Context Document, "NRC Technical Assessment of Additive Manufacturing.” https://www.nrc.gov/docs/ML2035/ML20351A292.html (accessed Sep. 23, 2021).
[126] M. McMurtrey et al., “Investigation of the Irradiation Effects in Additively Manufactured 316L Steel Resulting in Decreased Irradiation Assisted Stress Corrosion Cracking Susceptibility,” *Journal of Nuclear Materials*, vol. 545, p. 152739, Mar. 2021, doi: 10.1016/j.jnucmat.2020.152739.
[127] X. Gong, T. Anderson, and K. Chou, “Review on Powder-Based Electron Beam Additive Manufacturing Technology,” 2012. doi: 10.1115/ISFA2012-7256.
[128] L. N. Carter, M. M. Attallah, and R. C. Reed, “Laser Powder Bed Fabrication of Nickel-Base Superalloys: Influence of Parameters; Characterisation, Quantification and Mitigation of Cracking,” in *Superalloys 2012: 12th International Symposium on Superalloys*, 2012, pp. 577–586.
[129] A. Yadollahi and N. Shamsaei, “Additive Manufacturing of Fatigue Resistant Materials: Challenges and Opportunities,” *International Journal of Fatigue*, vol. 98, pp. 14–31, May 2017, doi: 10.1016/j.ijfatigue.2017.01.001.
[130] B. Ruttert, M. Ramsperger, L. Mujica Roncery, I. Lopez-Galilea, C. Körner, and W. Theisen, “Impact of Hot Isostatic Pressing on Microstructures of CMSX-4 Ni-Base Superalloy Fabricated by Selective Electron Beam Melting,” *Materials and Design*, vol. 110, pp. 720–727, 2016, doi: 10.1016/j.matdes.2016.08.041.
[131] A. R. Balachandramurthi, J. Moverare, S. Mahade, and R. Pederson, “Additive Manufacturing of Alloy 718 via Electron Beam Melting: Effect of Post-Treatment on the Microstructure and the Mechanical Properties,” *Materials*, vol. 12, 2018, doi: 10.3390/ma12010068.
[132] R. G. Thomas and D. Yapp, “The Effect of Heat Treatment on Type 316 Stainless Steel Weld Metal,” 1978.
[133] R. L. Plaut, C. Herrera, D. M. Escriba, P. R. Rios, and A. F. Padilha, “A Short Review on Wrought Austenitic Stainless Steels at High Temperatures: Processing, Microstructure, Properties and Performance,” *Materials Research*, vol. 10, no. 4, pp. 453–460, 2007, doi: 10.1590/S1516-14392007000400021.
[134] S. A. Shevchik, G. Masinelli, C. Kenel, C. Leinenbach, and K. Wasmer, “Deep Learning for In Situ and Real-Time Quality Monitoring in Additive Manufacturing Using Acoustic Emission,” *IEEE Transactions on Industrial Informatics*, vol. 15, no. 9, pp. 5194–5203, Sep. 2019, doi: 10.1109/TII.2019.2910524.
[135] M. Montazeri, A. R. Nassar, A. J. Dunbar, and P. Rao, “In-Process Monitoring of Porosity in Additive Manufacturing Using Optical Emission Spectroscopy,” *IISE Transactions*, vol. 52, no. 5, pp. 500–515, May 2020, doi: 10.1080/24725854.2019.1659525.
[136] B. T. Gibson, B. S. Richardson, T. W. Sundermann, and L. J. Love, “Beyond the Toolpath: Site-Specific Melt Pool Size Control Enables Printing of Extra-Toolpath Geometry in Laser-Wire Directed Energy Deposition,” 2019.
[137] A. Heralić, A.-K. Christiansson, and B. Lennartson, “Height Control of Laser Metal-Wire Deposition Based on Iterative Learning Control and 3D Scanning,” *Optics and Lasers in Engineering*, vol. 50, no. 9, pp. 1230–1241, 2012.

[138] M. Borish, B. K. Post, A. Roschli, P. C. Chesser, L. J. Love, and K. T. Gaul, "Defect Identification and Mitigation via Visual Inspection in Large-Scale Additive Manufacturing," *JOM*, vol. 71, no. 3, pp. 893–899, 2019.
[139] A. J. Pinkerton, "Advances in the Modeling of Laser Direct Metal Deposition," *J. Laser Appl.*, vol. 27, p. 7, Feb. 2015, doi: 10.2351/1.4815992.
[140] V. Manvatkar, A. De, and T. DebRoy, "Heat Transfer and Material Flow during Laser Assisted Multi-Layer Additive Manufacturing," *J. Appl. Phys.*, vol. 116, no. 12, p. 124905, Sep. 2014, doi: 10.1063/1.4896751.
[141] P. Peyre, P. Aubry, R. Fabbro, R. Neveu, and A. Longuet, "Analytical and Numerical Modelling of the Direct Metal Deposition Laser Process," *J. Phys. D-Appl. Phys.*, vol. 41, no. 2, p. 025403, Jan. 2008, doi: 10.1088/0022-3727/41/2/025403.
[142] Daniel. Rosenthal, *The Theory of Moving Sources of Heat and Its Application to Metal Treatments*. Cambridge: ASME, 1946.
[143] Z. Gan, G. Yu, X. He, and S. Li, "Numerical Simulation of Thermal Behavior and Multicomponent Mass Transfer in Direct Laser Deposition of Co-Base Alloy on Steel," *International Journal of Heat and Mass Transfer*, vol. 104, pp. 28–38, Jan. 2017, doi: 10.1016/j.ijheatmasstransfer.2016.08.049.
[144] Z. Gan, G. Yu, X. He, and S. Li, "Surface-Active Element Transport and Its Effect on Liquid Metal Flow in Laser-Assisted Additive Manufacturing," *International Communications in Heat and Mass Transfer*, vol. 86, pp. 206–214, Aug. 2017, doi: 10.1016/j.icheatmasstransfer.2017.06.007.
[145] Y. Wang, Q. Shi, and H. L. Tsai, "Modeling of the Effects of Surface-Active Elements on Flow Patterns and Weld Penetration," *Metall. Mater. Trans. B-Proc. Metall. Mater. Proc. Sci.*, vol. 32, no. 1, pp. 145–161, Feb. 2001, doi: 10.1007/s11663-001-0017-7.
[146] W. Pei, W. Zhengying, C. Zhen, L. Junfeng, Z. Shuzhe, and D. Jun, "Numerical Simulation and Parametric Analysis of Selective Laser Melting Process of AlSi10Mg Powder," *Appl. Phys. A*, vol. 123, no. 8, p. 540, Aug. 2017, doi: 10.1007/s00339-017-1143-7.
[147] K. Benarji, Y. Ravi Kumar, A. N. Jinoop, C. P. Paul, and K. S. Bindra, "Effect of Heat-Treatment on the Microstructure, Mechanical Properties and Corrosion Behaviour of SS 316 Structures Built by Laser Directed Energy Deposition Based Additive Manufacturing," *Met. Mater. Int.*, Aug. 2020, doi: 10.1007/s12540-020-00838-y.
[148] A. Aversa, G. Piscopo, A. Salmi, and M. Lombardi, "Effect of Heat Treatments on Residual Stress and Properties of AISI 316L Steel Processed by Directed Energy Deposition," *J. of Materi Eng and Perform*, Sep. 2020, doi: 10.1007/s11665-020-05061-9.
[149] T. R. Smith, J. D. Sugar, J. M. Schoenung, and C. San Marchi, "Anomalous Annealing Response of Directed Energy Deposited Type 304L Austenitic Stainless Steel," *JOM*, vol. 70, no. 3, pp. 358–363, Mar. 2018, doi: 10.1007/s11837-017-2711-1.
[150] A. Saboori, A. Aversa, G. Marchese, S. Biamino, M. Lombardi, and P. Fino, "Application of Directed Energy Deposition-Based Additive Manufacturing in Repair," *Appl. Sci.-Basel*, vol. 9, no. 16, p. 3316, Aug. 2019, doi: 10.3390/app9163316.
[151] W. J. Oh, W. J. Lee, M. S. Kim, J. B. Jeon, and D. S. Shim, "Repairing Additive-Manufactured 316L Stainless Steel Using Direct Energy Deposition," *Optics & Laser Technology*, vol. 117, pp. 6–17, Sep. 2019, doi: 10.1016/j.optlastec.2019.04.012.
[152] M. Ansari, E. Jabari, and E. Toyserkani, "Opportunities and Challenges in Additive Manufacturing of Functionally Graded Metallic Materials via Powder-Fed Laser Directed Energy Deposition: A Review," *Journal of Materials Processing Technology*, vol. 294, p. 117117, Aug. 2021, doi: 10.1016/j.jmatprotec.2021.117117.
[153] M. Akbari and R. Kovacevic, "Joining of Elements Fabricated by a Robotized Laser/Wire Directed Energy Deposition Process by Using an Autogenous Laser Welding," *Int J Adv Manuf Technol*, vol. 100, no. 9, pp. 2971–2980, Feb. 2019, doi: 10.1007/s00170-018-2891-z.

[154] L. Simoneau, A. Bois-Brochu, and C. Blais, “Tensile Properties of Built and Rebuilt/Repaired Specimens of 316L Stainless Steel Using Directed Energy Deposition,” *J. of Materi Eng and Perform*, Sep. 2020, doi: 10.1007/s11665-020-05087-z.
[155] R. Jacob, R. Montgomery, J. Harrison, M. Komarasamy, H. Jiang, and K. Ross, “Survey of Pre-Service and In-Service Nondestructive Evaluation Techniques of AMT-Fabricated Components,” Pacific Northwest National Laboratory, PNNL-30759, Dec. 2020. [Online]. Available: https://adamswebsearch2.nrc.gov/webSearch2/main.jsp?AccessionNumber=ML20349A012
[156] L. W. Koester, H. Taheri, T. A. Bigelow, P. C. Collins, and L. J. Bond, “Nondestructive Testing for Metal Parts Fabricated Using Powder-Based Additive Manufacturing,” *Materials Evaluation*, no. April, 2018.
[157] J. A. Slotwinski, E. J. Garboczi, and K. M. Hebenstreit, “Porosity Measurements and Analysis for Metal Additive Manufacturing Process Control,” *Journal of Research of the National Institute of Standards and Technology*, vol. 119, p. 494, 2014, doi: 10.6028/jres.119.019.
[158] E. Girardin, C. Renghini, J. Dyson, V. Calbucci, F. Moroncini, and G. Albertini, “Characterization of Porosity in a Laser Sintered MMCp Using X-Ray Synchrotron Phase Contrast Microtomography,” *Materials Sciences and Applications*, vol. 02, no. 09, pp. 1322–1330, 2011, doi: 10.4236/msa.2011.29180.
[159] J. W. Elmer, J. Vaja, and H. D. Carlton, “The Effect of Reduced Pressure on Laser Keyhole Weld Porosity and Weld Geometry in Commercially Pure Titanium and Nickel,” *Welding Journal 94*, vol. 95, pp. 419–430, 2016.
[160] J. W. Elmer, J. Vaja, H. D. Carlton, and R. Pong, “The Effect of Ar and N2 Shielding Gas on Laser Weld Porosity in Steel, Stainless Steel, and Nickel,” *Welding Journal*, vol. 94, pp. 313–325, 2015.
[161] W. E. King et al., “Observation of Keyhole-Mode Laser Melting in laser Powder-Bed Fusion Additive Manufacturing,” *Journal of Materials Processing Technology*, vol. 214, pp. 2915–2925, 2014, doi: 10.1016/j.jmatprotec.2014.06.005.
[162] L. L. Parimi, G. Ravi, D. Clark, and M. M. Attallah, “Microstructural and Texture Development in Direct Laser Fabricated IN718,” *Materials Characterization*, vol. 89, pp. 102–111, 2014, doi: 10.1016/j.matchar.2013.12.012.
[163] “Standardization Roadmap for Additive Manufacturing.” America Makes & ANSI Additive Manufacturing Standardization Collaborative (AMSC), Jun. 2018. Accessed: Oct. 12, 2020. [Online]. Available: https://share.ansi.org/Shared%20Documents/Standards%20Activities/AMSC/AMSC_Roadmap_June_2018.pdf
[164] “ANSI Webstore Additive Manufacturing.” https://webstore.ansi.org/industry/additive-manufacturing (accessed Apr. 24, 2021).
[165] “America Makes & ANSI Additive Manufacturing Standardization Collaborative (AMSC).” https://www.ansi.org/portal/amsc/america-makes-and-ansi-amsc-overview (accessed Apr. 24, 2021).